MSc thesis May 2025

An Analytical Study of the Basic Characteristics of Urban Gusts in the Nanjing Area and Their Influencing Factors

Chen Xiang

UNIVERSITY OF HELSINKI

An Analytical Study of the Basic Characteristics of Urban Gusts in the Nanjing Area and Their Influencing Factors

Chen Xiang

30 ECTS thesis approved in partial fulfilment of a double Master degree in Atmospheric Sciences, from Nanjing University and University of Helsinki.

Academic supervisors:

Professor Liu Hongnian

Academic examiners:

Professor Tareq Hussein

University of Helsinki

Nanjing University

Nanjing, May 2025

学校代码：10284
分 类 号：P4
密　　级：公开
U　D　C：551.5
学　　号：502023380002



南京大學

硕士学位论文

论文题目 南京地区城市阵风基本特征及其影响因子的分析研究

作者姓名 陈翔

专业名称 大气科学

研究方向 大气物理学与大气环境

导师姓名 刘红年

2025 年 5 月 16 日

答辩委员会主席 张宁

评　　阅　　人 刘罡

王成刚

Tareq Hussein

论文答辩日期　　2025年　5月　16日

研究生签名：

导 师 签 名：



Nanjing University

Master's Dissertation

An Analytical Study of the Basic Characteristics of Urban Gusts in the Nanjing Area and Their Influencing Factors

By Chen Xiang

Major：Atmospheric Science

Advisor：Prof. Liu Hongnian

Nanjing-Helsinki Institute in Atmospheric and Earth System Sciences, Nanjing University

May，2025

南京大学研究生毕业论文中文摘要首页用纸

毕业论文题目： 南京地区城市阵风基本特征及其影响因子的分析研究

大气科学 专业 2023 级硕士生姓名： 陈翔

指导教师（姓名、职称）： 刘红年 教授

摘 要

阵风是在长时间风速序列中出现的短时间最大风速。尽管阵风持续时间短暂，但其危害与影响十分广泛，可能会对建筑物和电力设施等结构造成强烈冲击，甚至引发倒塌或断电事故。在交通领域也可能导致车辆失控或飞机颠簸，增加事故风险。随着我国城市化程度越来越高，城市中特有的阵风特征值得我们关注，因为阵风在风能工程、建筑安全、交通运输等领域具有重要意义，同时也会对城市区域的气象和环境产生深远影响。本研究为城市极端风灾预警及抗风工程设计提供了观测与模拟依据。

本研究围绕城市环境下的阵风特征及其影响因子展开，选取南京市作为典型研究区域。首先，基于南京大学地球系统区域过程综合观测站（SORPES 站）铁塔多层（3 m、25 m、50 m）的超声观测资料，对 2018 年冬夏两季的阵风进行了统计与特征分析。本文还建立了阵风参数化模块，并将之耦合进城市边界层数值模式（RBLM）中，比较分析了 6 种不同参数化方案。通过与观测资料的对比，筛选出最适用于南京城市环境的参数化方案。随后对 2018 年夏季个例开展敏感性实验，分析了动力学效应、热力学效应、城市地表类型对阵风的影响。

研究表明，南京的阵风在季节和高度上具有显著的定量分层特征。冬季近地面阵风受城市建筑密集和冷空气活动的共同作用，平均风速比夏季高约 0.5 m/s，阵风风速高约 0.87 m/s，阵风超过 10 m/s 的极端事件更多，阵风因子(GF)超过 2.5 的比例达到约 20%，振幅超过 7.5 m/s 的极端事件占比较高，持续时间长于夏季约 6-7 秒；夏季中高层则表现出阵风风速更高（约高 1 m/s），超过 10 m/s 的极端阵风事件占比明显增加，阵风的平均空间尺度比冬季增加约 80 m，尺度超过 500 m 的事件占比超过 20%，显示出大尺度环流

和局地热对流对高空阵风的显著作用。整体来看，季节性气象条件与高度对城市阵风参数的调制效应显著。

日内变化分析显示，冬季近地面阵风因子通常在 11-16 时达到约 2.5 左右的峰值，夏季则在早晚交通高峰时段（5-7时和 18时）显著升高；而高层的阵风因子相对稳定，但白天比夜晚高约 0.1-0.2，这是因为白天平均风速较高导致阵风相对于平均风速的增幅降低。高度增加后，夏季各高度间阵风幅值的同步性更强，散点拟合 R^2 多在 0.8 以上，冬季则不确定性较大，R^2 约为 0.58-0.85，但高层始终保持一定基准风值。总体来看，阵风随高度增长受大尺度环流、局地湍流以及建筑粗糙度等多重因素的综合影响。阵风参数相关性分析表明，平均风速和地表剪切作用始终是驱动城市阵风的重要因素，其中摩擦速度和湍流应力的相关系数高达 0.66-0.85。

在数值模拟方面，通过对比不同阵风参数化方案发现，ECMWF 方案在 RBLM 模式下对南京地区观测阵风的再现效果最好，为后续敏感性实验提供了可靠的技术支撑。建筑物对局地风场的调节作用显著：去除建筑后，阵风和平均风速分别提高约 0.2-1.0 m/s 和 0.35-0.4 m/s，但湍流强度和热岛效应相对减弱，城市中心气温和地表温度降低约 0.06-0.12℃。通过“无城市”情形减去“有城市无建筑”情形，分离出城市热力学效应对阵风的影响。热力学效应会增强阵风风速，去除热力学效应的影响后，城区阵风减小 0.8-1.6 m/s，平均风速则增强 0.9-1.8 m/s，阵风因子降幅达 0.9-1.8。同期中心区地表温度与近地层气温分别降低 3.5-5.0℃和 0.8-1.2℃，相对湿度上升 3–5.5 %，但湍流动能却在城市核心区局部升高 0.03–0.15 J/kg。城市热力学效应对阵风的增强作用大于动力学效应。若完全去除城市，城区阵风风速降低约 0.4-1.2 m/s，平均风速显著上升约 0.9-1.5 m/s，城市地区阵风因子显著降低约 1.0-1.8，展现出城市对局地风场和热环境的深刻调控作用。

关键词：城市边界层模式；RBLM；城市阵风；阵风参数化方案

南京大学研究生毕业论文英文摘要首页用纸

THESIS： An Analytical Study of the Basic Characteristics of Urban Gusts in the Nanjing Area and Their Influencing Factors
SPECIALIZATION: Atmospheric Science
POSTGRADUATE: Chen Xiang
MENTOR: Professor Liu Hongnian

Abstract

Gusts are short-duration peak wind speeds observed within long-term wind speed sequences. Despite their brief nature, gusts can have extensive and significant impacts, including severe structural damage to buildings and electrical infrastructure, potentially resulting in collapse or power outages. In transportation, gusts may cause vehicle control loss or aircraft turbulence, increasing accident risks. With China's increasing urbanization, it is critical to understand the specific characteristics of urban gusts, as they play a crucial role in wind energy engineering, building safety, and transportation safety, and profoundly affect urban meteorology and environmental conditions. This research provides observational and modeling foundations for early warnings of extreme urban wind disasters and the design of wind-resistant engineering measures.

This study examines the characteristics and influencing factors of gusts in urban environments, using Nanjing city as a representative study area. Initially, gust data collected from the multi-level ultrasonic anemometers (3 m, 25 m, and 50 m) installed at the Nanjing University Station for Observing Regional Processes of the Earth System (SORPES station) were analyzed statistically and characterized for winter and summer 2018. Additionally, a gust parameterization module was developed and integrated into the urban boundary layer numerical model (RBLM). Five different parameterization schemes were compared and evaluated against observational data, selecting the optimal scheme for the urban environment of Nanjing. Subsequently, sensitivity experiments were conducted for the summer 2018 case to evaluate the influence of dynamical effects, thermodynamic effects, and urban surface types on gusts.

Results indicate pronounced seasonal and altitudinal variations in Nanjing’s gust characteristics. In winter, gusts near the ground, influenced by dense urban structures and cold air events, exhibited average wind speeds approximately 0.5 m/s higher and gust speeds about 0.87

m/s higher than in summer. Extreme gust events exceeding 10 m/s occurred more frequently, gust factors (GF) surpassing 2.5 comprised about 20% of occurrences, and events with amplitudes exceeding 7.5 m/s had a higher proportion, lasting approximately 6–7 seconds longer than those in summer. Conversely, during summer, mid- to upper-level gust speeds were notably higher (about 1 m/s greater), the proportion of extreme gust events over 10 m/s significantly increased, and the average spatial scale of gusts was approximately 80 m greater compared to winter. Events with spatial scales over 500 m accounted for more than 20%, highlighting significant contributions from large-scale circulation and local thermal convection at higher altitudes. Overall, seasonal meteorological conditions and altitude substantially modulate urban gust parameters.

Diurnal analysis revealed that gust factors near the ground in winter typically peaked around 2.5 between 11:00 and 16:00, while in summer, peaks occurred notably during morning and evening traffic rush hours (5:00–7:00 and around 18:00). Gust factors at higher altitudes remained relatively stable but were about 0.1–0.2 higher during daytime than nighttime due to higher daytime mean wind speeds, which relatively reduced gust amplitude. With increased altitude, summer gust amplitude synchronization between different heights strengthened, with scatterplot fitting R^2 generally above 0.8, whereas winter data showed greater uncertainty ($R^2 \approx 0.58$–0.85), though a certain baseline wind speed persisted at higher altitudes. The comprehensive influence of large-scale circulation, local turbulence, and building roughness on gusts became more evident with increasing altitude. Correlation analysis of gust parameters identified mean wind speed and surface shear as critical drivers for urban gusts, with correlation coefficients between friction velocity, turbulence stress, and gust parameters ranging from 0.66 to 0.85.

Numerical simulations revealed that the ECMWF parameterization scheme provided the best reproduction of observed gusts in Nanjing under the RBLM framework, offering robust technical support for subsequent sensitivity analyses. Buildings significantly modulated local wind fields and thermal conditions: their removal increased gust and mean wind speeds by approximately 0.2–1.0 m/s and 0.35–0.4 m/s, respectively, while reducing turbulence intensity and the urban heat island effect, lowering urban center air and surface temperatures by approximately 0.06–0.12°C. By subtracting the “With City, No Buildings” scenario from the “No City” scenario, the isolated influence of urban thermodynamic effects on gusts and related meteorological variables was obtained. With the urban thermodynamic effect removed, gust wind speeds in the city center

decreased by 0.8–1.6 m/s, while mean wind speeds increased by 0.9–1.8 m/s and gust factors fell by 0.9–1.8. During the same period, surface temperatures and near-surface air temperatures in the central area declined by 3.5–5.0 °C and 0.8–1.2 °C, respectively; relative humidity rose by 3.0–5.5 %; however, turbulent kinetic energy locally increased by 0.03–0.15 J/kg in the urban core. Complete urban removal decreased urban gust speeds by about 0.4–1.2 m/s, significantly increased mean wind speeds by about 0.9–1.5 m/s, and notably reduced urban gust factors by approximately 1.0–1.8, highlighting the profound regulatory role of urban structures on local wind and thermal environments.

Key Words: Urban Boundary Layer Model; RBLM; Urban Gusts; Gust Parameterization Schemes

Contents

摘　要.....6
Abstract.....8
Contents.....11
1 Introduction.....13
1.1 Research Significance.....13
1.2 Domestic and International Research Progress.....14
1.2.1 Influence of Terrain on Gusts.....14
1.2.2 Influence of Urban Areas on Gusts.....16
1.3 Research Contents and Chapter Outline.....19
2 Numerical Model and Data Description.....22
2.1 Model Introduction.....22
2.1.1 Urban Boundary Layer Model.....22
2.1.2 Classification of Gust Simulation Schemes.....23
2.1.3 Gust Parameterization Schemes Introduction.....25
2.1.4 Gust Module for the Boundary Layer Model.....27
2.2 Data Description.....28
2.2.1 Source of Observational Data.....28
2.2.2 Definition of Gust Parameters.....30
3 Statistical Characteristics of Urban Gusts in Nanjing.....32
3.1 Statistical Analysis of Gust Characteristics.....32
3.1.1 Time Series Features and Basic Statistics of Gusts.....32
3.1.2 Wind Direction Characteristics.....37
3.1.3 Gust Parameter Cumulative Distribution Function Analysis.....40
3.1.4 Diurnal Variation of Gust Factor.....46
3.1.5 Inter-Level Relationships and Scatter Plot Fitting Analysis of Gusts.....48
3.2 Statistical Analysis of Gust Correlations.....51
3.2.1 Correlation Analysis of Gust Parameters at 3 m.....51

3.2.2 Correlation Analysis of Gust Parameters at 25 m 53
3.2.3 Correlation Analysis of Gust Parameters at 50 m 55
3.3 Summary of This Chapter..... 错误!未定义书签。
4 Numerical Simulation of Gusts and Analysis of Influencing Factors in Nanjing 58
4.1 Validation of the Gust Model and the Design of Sensitivity Experiments 58
4.2 Analysis and Discussion of Gust Simulation Results..... 61
4.2.1 Spatial Distribution Characteristics..... 61
4.2.2 Temporal Distribution Characteristics 64
4.3 Impact of Urban Environment on Gust Characteristics..... 68
4.3.1 Influence of Urban Building Dynamics on Gust Characteristics..... 68
4.3.2 The Impact of Urban Thermodynamic Effects on Gust Characteristics 76
4.3.3 Impact of Integrated Urban Effects on Gust Characteristics..... 83
4.4 Chapter Summary ..... 错误!未定义书签。
5 Conclusion and Outlook 90
5.1 Conclusions 90
5.2 Innovations of This Study..... 93
5.3 Outlook 93
References..... 95

1 Introduction

1.1 Research Significance

A gust is characterized by a short-duration maximum wind speed that emerges within a longer wind-speed time series. Typically lasting from a few seconds to a few minutes, gust wind speed, as defined by the World Meteorological Organization (WMO, 2014), refers specifically to the highest 3-second moving-average wind speed recorded within a 10-minute wind speed sequence. Such gust phenomena frequently occur when high-momentum air parcels reach the surface, which is typically observed in convective environments driven mainly by descending airflows interacting with strong convection, or in non-convective conditions dominated by turbulent vertical momentum exchange within the atmospheric boundary layer (Sheridan, 2011).

Cities, as the primary hubs for modern socioeconomic activities and population aggregation, exhibit unique meteorological characteristics and environmental impacts, directly influencing urban operational safety, energy utilization efficiency, and air quality. Gusts are critical not only in areas such as wind energy engineering, building safety, and transportation but also profoundly impact urban meteorology and environmental conditions, potentially causing structural damage to buildings, destruction of vegetation, and exacerbation of urban heat island effects (WMO, 2014; Beljaars, 1987; Suomi et al., 2013). Moreover, the destructive potential of urban gusts poses significant risks to human safety and property and is a critical factor in air pollution issues (Shi et al., 2022). In recent years, accelerated urbanization has significantly altered urban wind structures through modifications in surface morphology, building density and height, and anthropogenic heat emissions. These changes substantially affect near-surface wind structures, turbulence characteristics, and gust formation and development, introducing complex interactions and challenges (Oke, 1982; Zhao et al., 2013; Liao et al., 2015). Particularly, short-term extreme wind events—characterized by instantaneous wind speeds considerably exceeding the average wind speed—can rapidly amplify wind energy in a quadratic manner, posing severe challenges to buildings, transportation infrastructure, and urban safety. Additionally, localized meteorological phenomena triggered by gusts, such as turbulence enhancement and mixed-layer structural variations, directly influence pollutant transport and deposition processes, profoundly affecting urban environmental quality. A deeper understanding of gust characteristics and their impact on air pollution will thus enable better responses to gust-induced hazards, significantly reducing the

damage gusts may inflict on urban environments.

1.2 Domestic and International Research Progress

1.2.1 Influence of Terrain on Gusts

Terrain plays a significant regulatory role in the evolution of near-surface wind fields and gust characteristics, influencing not only the overall acceleration of airflow but also introducing complex changes in local thermal and turbulent structures. Natural terrains such as mountains, hills, and valleys frequently induce short-term high-intensity gusts through channeling effects that guide and accelerate airflow. For example, Wagenbrenner et al. (2016) observed substantial wind speed increases in narrow valleys and mountain passes. Studies by Clifton et al. (2014) and Barthelmie et al. (2016) further indicated that such localized accelerations offer potential benefits for wind energy development but pose structural challenges to buildings. Jubayer and Hangan (2018) also confirmed the close link between terrain-induced local wind variability and gust occurrence.

Among terrain-influenced mechanisms, thermal effects play a crucial role. Uneven heating of the surface due to variations in vegetation coverage and soil moisture creates significant local thermal gradients, inducing local thermal circulations (Rucker et al., 2008; Rotach and Zardi, 2007). These circulations are capable of generating specialized wind structures in valleys, hills, and urban fringe areas. For example, small-scale vortices often form along mountain ridges on the leeward side, correlating closely with frequent and intense gust events (Grubišić et al., 2008).

In recent years, significant progress has been made in understanding gust characteristics within complex terrains. Studies such as those by Letson et al. (2018) and Earl et al. (2017) used high-frequency observations to reveal substantial spatial and temporal heterogeneity of gusts, emphasizing the impact of terrain variability on gust scale and duration. Sheridan (2011) and Hasager et al. (2003) demonstrated enhanced local wind fluctuations under complex topographic conditions. More recent research by Letson et al. (2019) employed statistical analysis of multi-level gust parameters, uncovering decreasing wind coupling with height and providing detailed quantitative descriptions of relationships between surface attributes and gust parameters. Additionally, novel improvements in numerical modeling and parameterization schemes have further advanced the understanding of gust formation mechanisms in complex terrain.

Researchers have employed diverse methods—including high-frequency field observations, probabilistic statistical analyses, and numerical simulations—to reveal the intrinsic mechanisms of terrain impacts on gusts. For instance, Hu et al. (2018) used 18 Hz ultrasonic anemometers and vertically oriented Doppler lidars to collect simultaneous wind speed data from multiple observation towers. By constructing various probability distribution models, they comprehensively described gust intensity, rise time, duration, and spatial scales, providing empirical support for wind load calculations and engineering designs. Concurrently, Markowski and Dotzek (2011) explored terrain effects on downdraft structures within mesoscale convective systems, while Durran (1990) and Hertenstein and Kuettner (2005) elucidated nonlinear mechanisms involved in gust formation from mountain waves and supercritical flow breakdown.

Compared to natural terrains, urban environments represent more complex "artificial terrain" characteristics. The dense presence of high-rise buildings and irregular layouts significantly increases surface roughness, enhancing small-scale turbulence and resulting in frequent, unpredictable local gust occurrences (Liao et al., 2015). Buildings in urban areas not only alter the prevailing wind direction but also amplify wind speed fluctuations through localized wind channels and vortex formations, posing substantial challenges to wind-resistant design and disaster forecasting.

Although numerous high-resolution numerical models have been applied to complex terrain and urban gust studies, uncertainties persist in extreme gust predictions and model validations due to limited observational data and parameterization scheme constraints (Butler et al., 2015; Bechmann et al., 2011; Berg et al., 2011; Suomi and Vihma, 2018). Future studies involving denser observation networks, combined with innovative technologies such as drones and lidars, could address observational gaps of traditional meteorological towers and foster breakthroughs in numerical modeling to better understand gust formation and evolution.

In summary, terrain's impact on gusts is a complex issue involving the interplay of fluid dynamics, thermodynamics, and geographic information. Current research highlights local wind acceleration due to terrain-induced channeling, thermal circulations, and vortex formations in mountainous and hilly areas, and the disturbance of urban wind fields caused by high-rise buildings. Although existing studies provide foundational theories for wind energy development, structural engineering, and environmental safety, further explorations into extreme weather gust

predictions and parameterization improvements remain necessary. Future research should emphasize multi-scale and multi-technique integration, enhancing understanding of gust dynamics in complex terrains and urban environments, and providing more reliable scientific support for related fields (Letson et al., 2019).

1.2.2 Influence of Urban Areas on Gusts

The acceleration of global urbanization has significantly altered urban surface characteristics, profoundly influencing atmospheric boundary layer structures and thereby affecting local gust properties. Urban surfaces, characterized by tall buildings and large building clusters, exhibit significantly higher roughness compared to flat areas, resulting in a notable reduction in near-surface average wind speeds and a simultaneous increase in turbulence intensity (Wieringa, 1973; Roth, 2000). Empirical studies indicate that although the statistical gust coefficients are generally lower in urban environments compared to open areas, localized gust amplification is frequently observed around buildings, attributed primarily to local flow disturbances induced by building structures (Ashcroft, 1994). Street-canyon effects are particularly important in urban gust dynamics. Airflow constrained within narrow streets, known as the "channeling effect," significantly accelerates winds when large-scale winds align along street directions, generating strong gusts. Conversely, when winds cross street canyons, turbulent separation vortices often form at intersections and building corners, creating localized gust fluctuations (Murakami et al., 1979; Kanda et al., 2013). Additionally, buildings, roads, and other impermeable surfaces not only increase surface roughness but also modify surface heat flux and anthropogenic heat distribution (Oke, 1982; Zhao et al., 2013). Consequently, average near-surface wind speeds typically decrease, while gust strength and frequency may paradoxically increase due to enhanced turbulence mixing and local wind fluctuations (Liao et al., 2015; Wang et al., 2019).

Urbanization impacts gusts primarily through two mechanisms. The first is dynamic effects: complex building layouts and increased surface roughness amplify frictional effects on airflow, weakening mean wind fields while enhancing turbulence (Ryu et al., 2013; Wang et al., 2014). The second is thermal effects: urban heat islands and anthropogenic heat emissions alter the thermal structure of the urban boundary layer, particularly at night when slower heat dissipation increases atmospheric instability, further enhancing turbulence and facilitating gust generation

(Tao et al., 2017; Huszar et al., 2018).

Studies using numerical simulations and observational analysis suggest that despite an overall decline in wind speed with urbanization, localized gust intensities can still increase. Liu et al. (2023), in a case study of Nanjing, identified increased surface friction and enhanced boundary layer instability as primary factors intensifying urban gusts, whereas contributions from deep convection were limited. Different urban land-use types also modulate gust characteristics; densely built commercial and industrial areas are especially prone to intense local gust events due to differences in building arrangements and local thermal effects (Chen et al., 2009; Lin et al., 2008).

Due to complex urban wind conditions, traditional numerical weather prediction models struggle to capture instantaneous gust variability accurately (Brasseur, 2001; Suomi, 2017). Consequently, researchers have proposed various gust parameterization schemes, integrating factors such as mean wind speed, turbulence characteristics, and convection processes to more accurately simulate urban gusts (Gutierrez and Fovell, 2018; Sheridan, 2018; Kurbatova et al., 2018). Studies by Ao et al. (2022) and Zhang et al. (2018) highlight the need for refined modeling to better represent urban impacts on gust dynamics for improved urban meteorological forecasting and wind energy assessments.

Recent research extensively utilizes numerical simulations and wind tunnel experiments to investigate urban gusts, thereby informing urban design and wind environment evaluations. Computational fluid dynamics (CFD) modeling has emerged as an essential tool for studying airflow around buildings and gust structures. Blocken et al. (2012) developed a CFD framework for pedestrian-level wind environment evaluation, revealing highly uneven gust distributions around tall buildings, with instantaneous peak wind speeds exceeding twice the average wind speed at windward corners and downwind exits. Liu et al. (2017), employing Detached Eddy Simulation (DES), found that elevated buildings with open ground floors generated strong downdrafts and vortex shedding, intensifying gust peaks behind buildings. Similarly, wind tunnel experiments by Li et al. (2024) demonstrated complex gust distributions around irregularly elevated buildings, highlighting the need for optimized urban design to mitigate hazardous gust conditions.

Besides modeling and wind tunnel tests, full-scale measurements remain indispensable for

understanding urban gust dynamics. Rakib et al. (2020) conducted a 12-month rooftop wind experiment, documenting numerous gust events exceeding standard IEC definitions. Their findings indicated significantly higher frequencies of intense gusts in urban areas compared to open locations, resulting in increased fatigue loading and reduced wind turbine blade lifespan. Hirose et al. (2022) employed Particle Image Velocimetry (PIV) to analyze gust statistics at pedestrian height within simplified urban models, revealing significant variability in gust factors across urban blocks, particularly at intersections and behind buildings. Such studies contribute to refining empirical gust models and enhancing wind comfort assessment standards.

Urban gusts impact engineering and livability extensively. Structural engineering must account for urban wind fluctuations to prevent resonance and fatigue accumulation in flexible structures such as high-rise buildings and long bridges. Solari (2014) emphasized the need to extend traditional quasi-static wind load models to incorporate gust-induced effects. Additionally, excessive gusts can negatively affect pedestrian comfort and safety, prompting urban regulations requiring wind tunnel evaluations for high-rise developments (Blocken et al., 2012). Urban gusts also influence pollutant dispersion and thermal environments, representing a separate research domain.

Urban wind energy development is notably constrained by gust characteristics. Due to urban wind instability, small-scale wind turbines exhibit lower efficiency and shorter lifespan in urban environments. Studies by Toja-Silva et al. (2015) and Onol & Yesilyurt (2017) indicated significant performance fluctuations and early shutdowns for urban wind turbines, recommending adaptive control strategies for managing irregular wind speed variations.

In summary, research on the influence of urban underlying surfaces on gusts has established a comprehensive framework ranging from macro-scale roughness effects to micro-scale building flow effects. A substantial body of literature in authoritative journals indicates that urban areas reduce the near-surface average wind speed while intensifying local gust variability. The overall effects of roughness are reflected in the empirical gust factor (Wieringa, 1973; Wieringa, 1992), whereas the detailed effects of building features require precise characterization using wind tunnel experiments and CFD (Kawamura et al., 1988; Liu et al., 2017). Although the complexity of urban gusts poses challenges for forecasting and engineering applications, recent research advances have been remarkable: through high-resolution observations (Rakib et al., 2020), innovative

measurement techniques (such as lidar and infrared imaging), and advanced simulation methods (Blocken et al., 2012), researchers have gained a deeper understanding of the spatiotemporal distribution, formation mechanisms, and effects of urban gusts. These insights are gradually being applied to urban planning and building design to mitigate urban wind hazards and improve comfort, while also providing a scientific basis for wind energy utilization and natural ventilation design in urban environments.

1.3 Research Contents and Chapter Outline

Traditional numerical weather prediction models, when describing urban boundary layer processes, tend to focus on the mean wind field and large-scale turbulence parameters while neglecting the parameterization of gust phenomena. This oversight makes it difficult to fully capture how complex urban surfaces (such as buildings and anthropogenic heat) regulate the generation and evolution of gusts. Taking Nanjing as the study area, this work aims to reveal the characteristics of gusts under urban conditions in the Nanjing region and to explore the relationships between gusts and other meteorological as well as urban morphological factors.

This study is based on the urban boundary layer RBLM model and introduces a gust module incorporating various parameterization schemes. The observational data and the simulation results from these different schemes are systematically compared and validated in order to select the parameterization approach that best reflects reality. Subsequently, based on this optimal scheme, a series of sensitivity experiments will be conducted to thoroughly investigate the regulatory effects and mechanisms of factors such as buildings and anthropogenic heat on gusts. As a historic and culturally renowned city, as well as an important economic center in eastern China, Nanjing is characterized by a dense distribution of buildings and complex topography. Its gust characteristics and the interrelationships among various factors have not yet been studied in depth. Therefore, a comprehensive investigation of the basic gust characteristics in Nanjing and their intrinsic links with urban morphological factors is of significant theoretical and practical importance for enhancing the simulation capabilities of urban boundary layer models and improving urban weather forecasting.

This study mainly comprises the following three research components:

(1) Statistical Analysis of Gust Characteristics in Nanjing. Ultrasonic observational data

(recorded at 3 m, 25 m, and 50 m) from the SORPES station for January and August 2018 are utilized to statistically analyze the gust characteristics and their variation with height, examine the diurnal variation of gusts in Nanjing, and assess the influencing factors of urban gusts through correlation analysis.

(2) Construction of the Gust Module and Selection of the Parameterization Scheme. Based on the self-developed urban boundary layer RBLM model, a gust module is incorporated to compute the results from several different gust parameterization schemes. Detailed comparative analyses between the simulation results of each scheme and the observed gust data are conducted, ultimately determining the parameterization approach that best aligns with the actual observations.

(3) Sensitivity Experiments and Analysis of Influencing Factors. Building on the optimal parameterization scheme, a series of sensitivity experiments are carried out with a focus on investigating the effects of buildings, anthropogenic heat, and other factors on gust characteristics. Through systematic experimental analysis, the regulatory mechanisms and interactions among the various influencing factors on urban gust processes are explored in depth.

The thesis is organized as follows:

Chapter 1: Introduction – This chapter reviews the current state of research, both domestically and internationally, on the impacts of gusts on urban meteorology and environmental conditions, as well as the methodologies used in previous studies. It outlines the basic ideas, research methods, main contents, and innovative aspects of this study on the gust characteristics and influencing factors in Nanjing.

Chapter 2: Numerical Model and Data Description – This chapter provides a detailed introduction to the urban boundary layer RBLM model employed in this study, along with a framework diagram after the addition of the gust module, and an explanation of each gust parameterization scheme used. It also describes the gust-related observational data (3 m, 25 m, and 50 m data from the SORPES station for January and August 2018) and the data preprocessing methods, and defines the gust parameters applicable to this study based on statistical comparison methods.

Chapter 3: Statistical Characteristics of Urban Gusts in Nanjing – This chapter presents the statistical results of gusts in Nanjing and provides an in-depth analysis of the data to reveal the basic characteristics and influencing factors of gusts during both winter and summer.

Chapter 4: Numerical Simulation of Gusts and Analysis of Influencing Factors in Nanjing – This chapter first compares the simulation results of each gust parameterization scheme with the observed gust data for a summer case in Nanjing to select the scheme that best represents the actual conditions. Then, based on the optimal scheme, sensitivity experiments are conducted to study the effects of buildings, anthropogenic heat, and other factors on gusts, and a comprehensive analysis is provided on how these factors regulate the characteristics of urban gusts and interact with one another.

Chapter 5: Conclusion and Outlook – This chapter systematically summarizes the research contents and conclusions of the thesis, identifies the limitations of the study, and outlines prospects for future research on urban gusts and their influencing factors.

2 Numerical Model and Data Description

2.1 Model Introduction

2.1.1 Urban Boundary Layer Model

Developed in 2002, the urban boundary layer model RBLM is a three-dimensional, nonhydrostatic, high-resolution regional numerical weather prediction system that evolved from the ARPS (Advanced Regional Prediction System). It is specifically designed for simulating meteorological processes at urban and regional scales. Based on the Reynolds-averaged governing equations of atmospheric motion, RBLM encompasses the momentum, heat flux, scalar, and fully elastic continuity equations. While inheriting the advantages of ARPS, it meticulously incorporates the effects of underlying surface characteristics and anthropogenic factors on the boundary layer structure. The model is applicable to numerical prediction studies ranging from medium-β to medium-γ scales, or even smaller scales, and can provide essential meteorological data for pollutant dispersion and urban photochemical simulations. This, in turn, supports the forecasting and evaluation of wind fields and air pollutants over complex surfaces—such as cities, mountainous regions, and coastal–inland transition zones—and aids decision-makers in their work.

In subsequent improvements, Xu Min et al. (2002) introduced a building drag term into the momentum and turbulence kinetic energy equations to enhance the accuracy of urban meteorological simulations. He Xiaofeng et al. (2007, 2009) developed an urban canopy model (NJU-UCM-S) and coupled it with RBLM to refine the parameterization of land surface processes in urban areas. Yang et al. (2018) further advanced the urban tree canopy model and integrated it with the RBLM to investigate the impact of summer vegetation on meteorological conditions. In addition, Yan Zijin et al. (2024) made improvements specifically addressing the issues associated with shallow lakes in urban regions.

The RBLM is mainly divided into four modules:

Preprocessing Module: Responsible for handling terrain, vegetation, soil types, and basic urban geographic information, and converting these data into the format required for numerical forecasting.

Objective Analysis Module: Constructs a three-dimensional initial meteorological field using actual observational data and the BARNES objective analysis method.

Atmospheric Numerical Prediction Module: Executes the model integration process, which

includes processing of initial and boundary conditions, parameterization of turbulence and warm rain processes, radiation updates, integration of soil–vegetation processes, integration of atmospheric equations, pollutant transport and diffusion, as well as outputting historical files.

Postprocessing Module: Organizes and processes the historical files output by the forecasting module.

Its parameterization schemes include those for turbulence, the Kessler warm rain process, surface flux, and a two-layer soil–vegetation model, with additional parameterizations for building drag and anthropogenic heat emissions specifically introduced for the unique urban underlying surface.

In the original RBLM, the focus was primarily on calculating the mean wind field, with no dedicated module for computing gusts. To more accurately reflect the occurrence and evolution of gust phenomena in urban environments, this study has added a gust module to the existing RBLM framework. This module incorporates several established parameterization schemes to simulate gust characteristics, comprehensively taking into account the effects of building-induced resistance, local heat sources, and microscale disturbances, thereby capturing the spatiotemporal variability of gusts in urban areas. Similar to previous practices that improved urban meteorological simulations by incorporating urban building drag terms into the momentum and turbulent kinetic energy equations, this study integrates both dynamic effects and thermodynamic effects into the gust module, aiming to enhance the accuracy and practicality of gust simulations.

2.1.2 Classification of Gust Simulation Schemes

The formation of gusts in the atmospheric boundary layer involves complex turbulent processes and unsteady airflow, representing a significant manifestation of wind speed extremes. In recent years, various gust simulation methods have emerged based on fluid mechanics, turbulence theory, and statistical principles. According to the existing research findings, the main international gust simulation schemes can be broadly categorized into the following two groups:

(1) Parameterization Schemes Based on Physical Theories

These methods rely on a physical understanding of the turbulent processes in the atmospheric boundary layer. Common physical theories include the Monin-Obukhov similarity theory (M-O theory), which analyzes turbulence scales and uses the nondimensionalized variance of wind speed

to estimate gust intensity. Such methods typically parameterize the relationship between turbulence and gusts based on fundamental physical principles, employing empirical formulas—for example, relating wind speed variance to height and defining gusts by setting a threshold probability.

Among these approaches is the turbulence kinetic energy (TKE)-based method. This method assumes that gusts arise from deviations of instantaneous wind speeds from the mean wind speed, using the model output of TKE as a quantitative measure of wind speed fluctuations. A typical practice is to add the mean wind speed and a multiple of the turbulence standard deviation (or the square root of TKE), for instance, using a formula like $wge = U + 3\sqrt{q}$ (or a variant thereof) to estimate gust intensity. This method is theoretically robust and can effectively explain the generation of gusts under mechanical turbulence conditions, although it may have certain limitations under strong convective or non-uniform conditions. Another approach is the particle-sinking method based on the wind speed at the top of the boundary layer, which assumes that gusts are produced by the downward transport of higher-level wind speeds to the surface. By collecting wind speed information from the boundary layer top and employing the physical process of wind speed transport within the atmospheric layer, surface gusts can be estimated. This method is more applicable under convective conditions or in deep boundary layers but may be limited in non-convective, mechanically turbulent situations. Consequently, there are also hybrid parameterization methods. Given that any single method may have shortcomings under different meteorological conditions, some studies have proposed hybrid schemes. These approaches dynamically switch or weight the physical method and the boundary-layer-top method based on atmospheric stability indicators (such as the Richardson number) to better capture gust characteristics under various weather conditions. Such hybrid methods have demonstrated certain advantages in balancing detection probability with false alarm rates (Kurbatova et al., 2018).

(2) Statistical and Machine Learning Methods

With the improvement of data resources and computational capabilities, statistical methods and machine learning techniques have also been introduced into the field of gust forecasting. By conducting extreme value statistics, regression analysis, or training neural networks, support vector machines, and other machine learning models on historical observations and model output data, gust characteristics can be directly extracted from large datasets. Although these methods

offer high flexibility in dealing with nonlinear and complex wind fields, they rely heavily on ample, high-quality observational data and typically have weaker physical interpretability (Sheridan, 2018).

2.1.3 Gust Parameterization Schemes Introduction

In this study, we adopt a physics-based gust parameterization scheme. The main reason for this approach is that it is based on fundamental physical processes, such as atmospheric boundary layer turbulence and energy transfer, and employs Monin–Obukhov similarity theory and turbulent kinetic energy to characterize the mechanism of gust formation, which can intuitively reflect the influence of dynamic and thermodynamic factors on gusts in urban environments. Compared to statistical and machine learning methods, this approach does not depend on extensive historical data fitting but is rooted in basic atmospheric physics, offering good universality and interpretability. This provides a solid theoretical foundation for an in-depth investigation of urban gust characteristics and their influencing factors. The following are the gust parameterization schemes employed:

(1) The parameterization scheme used by the European Centre for Medium-Range Weather Forecasts (ECMWF) to generate gust wind speeds in its reanalysis dataset (ECMWF, 2021).

$$GWS_{10\mathrm{m}} = WS_{10m} + C_{\mathrm{ugn}} U_{*} f\left(\frac{z_{\mathrm{i}}}{L}\right) + C_{\mathrm{conv}} max(0, U_{850} - U_{950}) \tag{2.1}$$

where $GWS_{10\mathrm{m}}$ is the gust wind speed at 10 meters height, WS_{10m} is the mean wind speed at the same height, C_{ugn} a coefficient set to be 7.2, U_{*} the friction velocity, C_{conv} the convective mixing coefficient set to be 0.3, U_{850} and U_{950} the mean wind speed at the pressure level of 850-hPa and 950-hPa, respectively. The function

$$f(z_{\mathrm{i}}/L) = \begin{cases} \left(1 - \frac{0.5}{12}\frac{z_{\mathrm{i}}}{L}\right)^{\frac{1}{3}} & L < 0 \\ 1 & L > 0 \end{cases} \tag{2.2}$$

represents the effects of the atmospheric boundary-layer height and stratified stability. Here z_{i} is the convective boundary-layer height set to be 1000 meters above ground level. L is the Obukhov length.

(2) TKE (Born et al., 2012): This method uses turbulence kinetic energy (TKE) to represent the deviation of instantaneous wind speed from the mean. Its basic formula is:

$$wge = U + 3\sigma = U + 3\sqrt{q} \tag{2.3}$$

where U represents the mean wind speed, q is the turbulence kinetic energy (TKE), and assuming that the wind speed distribution follows a normal distribution, the gust increment is approximated by three times the standard deviation.

(3) TKE2 (Born et al., 2012): This method also employs turbulence kinetic energy (TKE), but it posits that the TKE output from the model can directly represent the maximum deviation of the instantaneous wind speed. Its formula is:

$$wge = U + \sqrt{2q} \tag{2.4}$$

Compared with the TKE method, the TKE2 method yields slightly different values, with an emphasis on estimating the maximum deviation.

(4) Schreur: This is an improvement to the TKE method as proposed by Schreur and Geertsema (2008). By introducing empirically fitted coefficients derived from observational data, it adjusts the wind speed fluctuations. Its expression is:

$$wge = U\left(1 + gr_\sigma \frac{\sqrt{2q}}{U}\right) \tag{2.5}$$

$$g = 1.42 + 0.3013 \ln\left(\frac{990}{Ut} - 4\right) \tag{2.6}$$

$$r_\sigma = \left(1 - 0.069 \exp\left(-2.3 \frac{Ut}{z}\right)\right) \exp\left(-2.3 \left(\frac{Ut}{z}\right)^{0.555}\right) \tag{2.7}$$

where g and r_σ are parameters determined from observational data, used to adjust the extent to which turbulence influences gusts. t = 3s is gust duration and z = 10m is height above ground.

(5) Nakamura: For deep convective conditions, this method not only considers the boundary layer height but also incorporates vertical motion and precipitation processes into the calculations. Its formulation involves integrating the temperature and precipitation mixing ratio within the boundary layer to capture the gust effects produced during convection (Nakamura et al., 1996).

$$wge = \sqrt{\alpha \int_0^H 2g\left(\frac{\Delta\theta}{\theta} + q_r\right) dz + \beta U(H)} \tag{2.8}$$

$$\alpha = 0.25 \text{ and } \beta = 0.85 \tag{2.9}$$

Where $\Delta\theta$ is the potential temperature deficit in the downdraught, θ is the potential temperature of the surroundings, H is boundary layer height, and q_r is rain mixing ratio, Nakamura et al. (1996) suggests $\alpha = 0.25$ and $\beta = 0.85$.

2.1.4 Gust Module for the Boundary Layer Model

At present, the RBLM model has undergone several improvements in the context of urban applications (Yang et al., 2015). To more accurately describe the characteristics and influencing mechanisms of gusts in urban areas, the traditional RBLM model, which has primarily focused on simulating the mean wind field and large-scale turbulence processes, has not independently computed the short-term extreme phenomenon of gusts. To better capture the generation and evolution of gusts within urban regions, an independent gust computation module has been added to the original RBLM framework in this study. This module operates independently within RBLM without bidirectional coupling with other external systems. It computes the 3-second moving average gust wind speed using various gust parameterization schemes based on physical theories (including those based on turbulence kinetic energy, the wind speed at the boundary layer top, and hybrid methods) and compares it with the 10-minute mean wind speed. This design not only retains the advantages of the original model in simulating overall atmospheric processes but also provides dedicated computational output for studying the characteristics of urban gusts and their relationships with factors such as buildings and the urban heat island effect. The schematic diagram of the new gust computation module is shown in Figure 2.1.

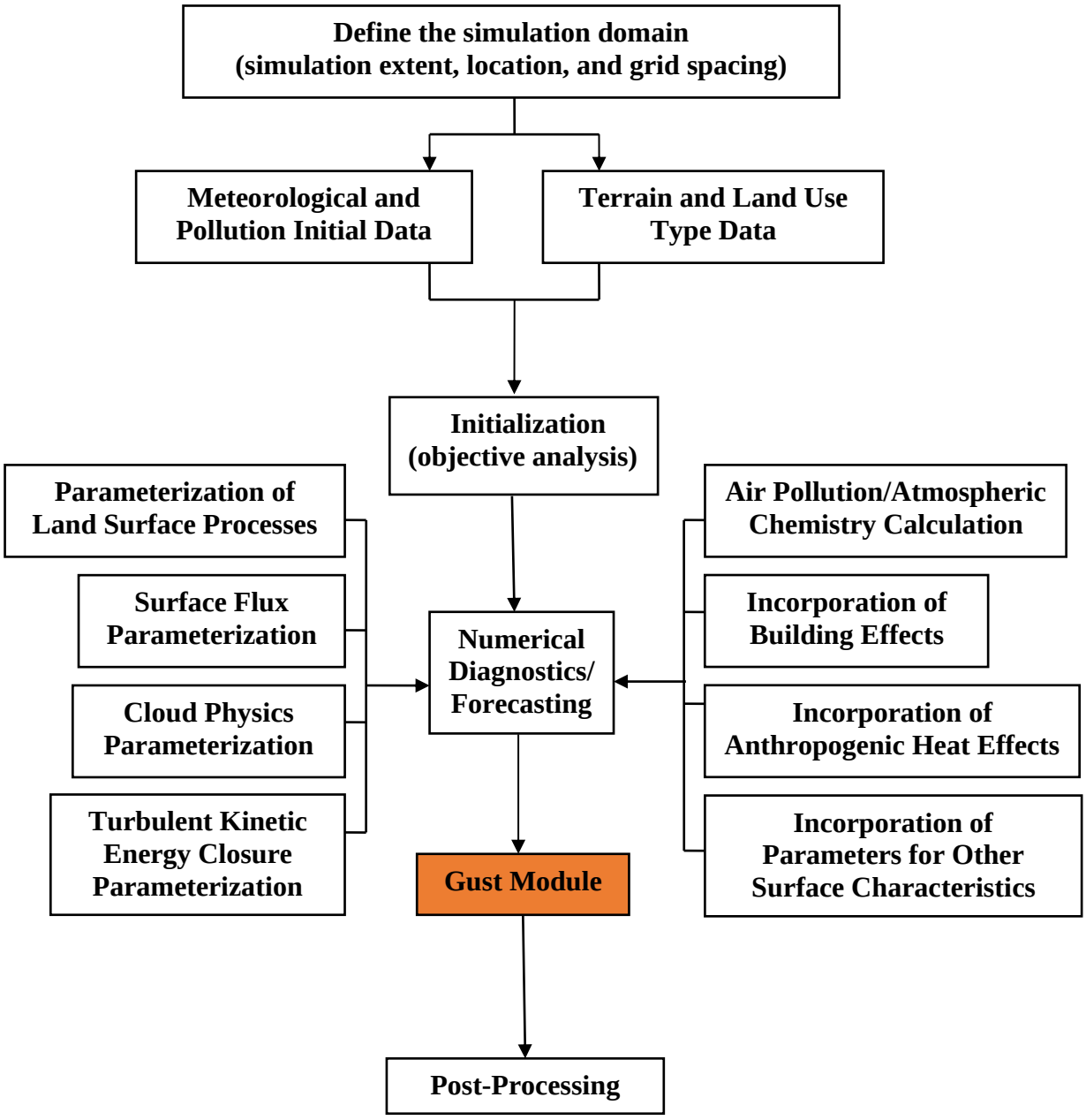

Figure 2.1 Schematic diagram of the RBLM model structure

2.2 Data Description

2.2.1 Source of Observational Data

The data used in this study were collected from the wind tower at the SORPES station of the Nanjing University Earth System Regional Process Observation Network, located within the

Xianlin campus of Nanjing University in the northeastern suburb of Nanjing, as shown in Figure 2.1. The underlying surface of the Xianlin campus and its surrounding areas is complex, comprising hilly terrains covered with vegetation, bare soil, green spaces, and built-up urban areas. The SORPES station is situated at the center of the campus on a flat area atop a small hill—in contrast to the campus roads and flat lands which have elevations of 10 to 14 meters, the hilltop reaches approximately 43 meters, making it about 30 meters higher than the average campus elevation.

Within this main flat area, a 30 m × 40 m observation field has been established and is equipped with a turbulence measurement system operating at a height of 2.6 m. Additionally, a 75-meter-high triangular observation tower has been constructed adjacent to the field, with turbulence measurement systems installed at 25 m and 50 m, respectively. These systems comprise an integrated three-dimensional ultrasonic anemometer and thermometer (used for rapid measurements of wind speed, temperature, and water vapor fluctuations) along with water vapor/CO_2 gas analyzers (CSAT3 and EC150, both manufactured by Campbell Scientific, USA), all sampling at a frequency of 10 Hz.

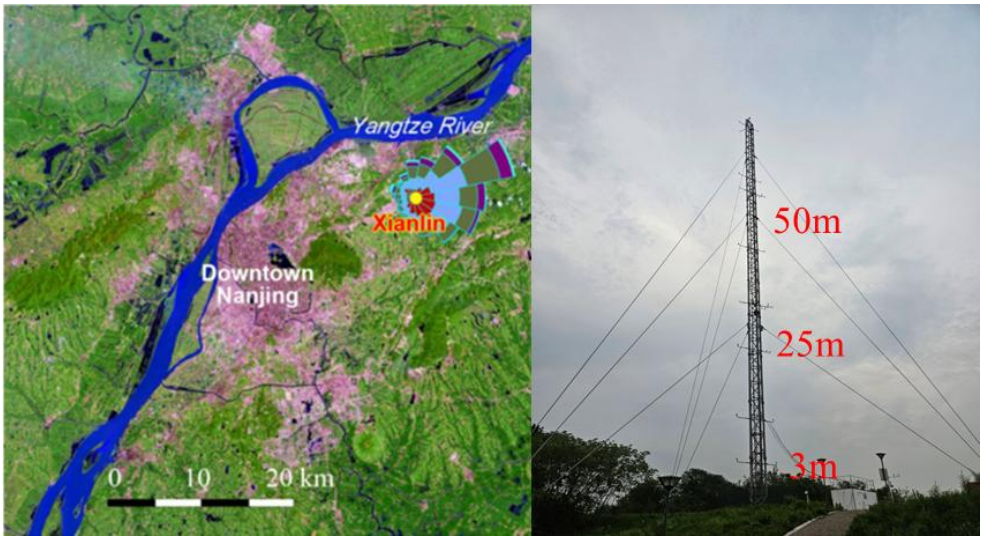

Figure 2.1 The location of the SORPES station (left) and the wind tower (right).

This study selected data from January and August 2018 for analysis, with January and August representing typical meteorological conditions for winter and summer, respectively, to comprehensively reveal the seasonal differences in urban gust characteristics. Furthermore, observational data from different heights (approximately 3 m, 25 m, and 50 m) were chosen to

examine the vertical distribution of urban gusts near the surface and at higher levels, as well as their potential variability. By comparing the gust data across these heights, this study systematically investigates how the vertical structure within the urban boundary layer influences the generation, evolution, and transmission of gusts, thereby providing a robust observational basis for optimizing the parameterization schemes in the gust module of subsequent numerical simulations.

2.2.2 Definition of Gust Parameters

In this study, we adopt the following definitions as used by Letson et al. (2018):

(1) 10-minute Mean Wind Speed (U_{mean}) [m/s]: Represents the average wind speed in the along-wind direction over a 10-minute period, serving as a fundamental index for assessing the strength of the background wind field.

(2) 10-minute Mean Wind Direction: The average wind direction calculated over the same time scale, used to describe the predominant wind flow.

(3) Gust (U_{gust}) [m/s]: Defined as the maximum along-wind speed computed using a 3-second moving average within a 10-minute period, reflecting the instantaneous intensity of short-term strong wind events.

(4) Gust amplitude (a_{agust}) [m/s]: The difference between the gust and the 10-minute mean wind speed, i.e., $a_{agust} = U_{gust} - U_{mean}$, which quantifies the enhancement of gusts relative to the background wind speed.

(5) Peak Factor (k_{peak}): Obtained by normalizing the 3-second gust increment with the standard deviation (σ) of the 10 Hz along-wind speed over the 10-minute period, i.e., $k_{peak} = a_{agust} / \sigma$, reflecting the relative intensity of gusts within the local turbulent environment.

(6) Gust Factor (GF): Defined as the ratio of the 3-second gust amplitude to the 10-minute mean wind speed, i.e., $GF = U_{gust} / U_{mean}$. This dimensionless parameter is commonly used to describe gust intensity.

(7) Rise Time (t_{rise}) [s]: The time interval from the last local minimum (below U_{mean}) before the onset of the gust to the occurrence of the gust peak, representing the time scale of gust generation.

(8) Lapse Time (t_{lapse}) [s]: The time difference from the occurrence of the gust peak to the

moment when the wind speed falls again below the local minimum of U_{mean}, used to characterize the gust dissipation process.

(9) Gust Duration (t_{gust}) [s]: Defined as the sum of the rise time and decay time, $t_{gust} = t_{rise} + t_{lapse}$ (or equivalently, $t_3 - t_1$), which reflects the total duration of a gust event.

(10) Gust Length Scale (L_{gust}) [m]: Estimated by integrating the 3-second moving average along-wind speed over the gust duration, serving as an estimate of the physical scale of the gust and revealing its spatial extent.

$$L_{\text{gust}} = \int_{t_1}^{t_3} u_3 \text{sd}t \tag{2.10}$$

(11) Turbulence Intensity (TI): Expressed as the ratio of the standard deviation of the 10 Hz along-wind speed to the corresponding 10-minute mean wind speed U_{mean}, it measures the level of local turbulent fluctuations. $Ti = \sigma / U_{mean}$.

3 Statistical Characteristics of Urban Gusts in Nanjing

3.1 Statistical Analysis of Gust Characteristics

3.1.1 Time Series Features and Basic Statistics of Gusts

In the previous chapter, we provided a detailed introduction to the sources and preprocessing methods of urban gust observational data in Nanjing, as well as the definitions of gust parameters and the basis for selecting statistical indicators. In this chapter, we systematically analyze the statistical characteristics of urban gusts in Nanjing—across different seasons and at various heights—using the aforementioned data and parameters. This analysis aims to explore the influence mechanisms of urban underlying surfaces and seasonal circulations on gust characteristics. The statistical results presented here will serve as empirical support for the subsequent parameterization validation and sensitivity experiments in the numerical simulations.

The behavior of hourly mean and gust wind speeds at a 3-meter height shows notable differences between winter and summer periods. Figure 3.1 displays two graphs showing the hourly mean wind speed (U_{mean}) and gust wind speed (U_{gust}) at a height of 3 meters for winter (January) and summer (August), respectively. From the winter curves, it is evident that the fluctuation range of U_{gust} is relatively small during mid-January, but there are noticeable increases in both early and late January. In August, the variations of U_{gust} (depicted in orange) and U_{mean} (in blue) are roughly similar, with a distinct peak emerging in mid-August; during this period, gust speeds can reach approximately 9–10 m/s, indicating enhanced local turbulent activity. Overall, the U_{mean} at 3 meters remains relatively stable, while U_{gust} notably exceeds the mean wind speed during periods of active convection or abrupt weather changes, reflecting the amplification effect of densely built-up urban areas on extreme wind speeds near the surface.

To compare wind behavior at different levels within the urban environment, the analysis was extended to a height of 25 meters. Figure 3.2 shows that at a height of 25 m, the overall trends of U_{mean} and U_{gust} in January and August are similar to those at 3 m. Notably, the January curve displays significant increases in U_{gust} at both the beginning and end of the month, suggesting the influence of weather systems such as cold air intrusions or low-level shear lines. The summer peak is even more pronounced; in mid-August, U_{gust} can reach approximately 17.5 m/s, indicating strong instantaneous wind speed fluctuations. Compared with the 3 m level, U_{mean} at 25 m is generally higher, and U_{gust} is more likely to escalate during periods of intensified convection or

turbulence, demonstrating that the mid-to-upper layers of the urban boundary layer are more susceptible to the combined effects of large-scale wind fields and local thermal processes, resulting in a significant amplification of gust speeds.

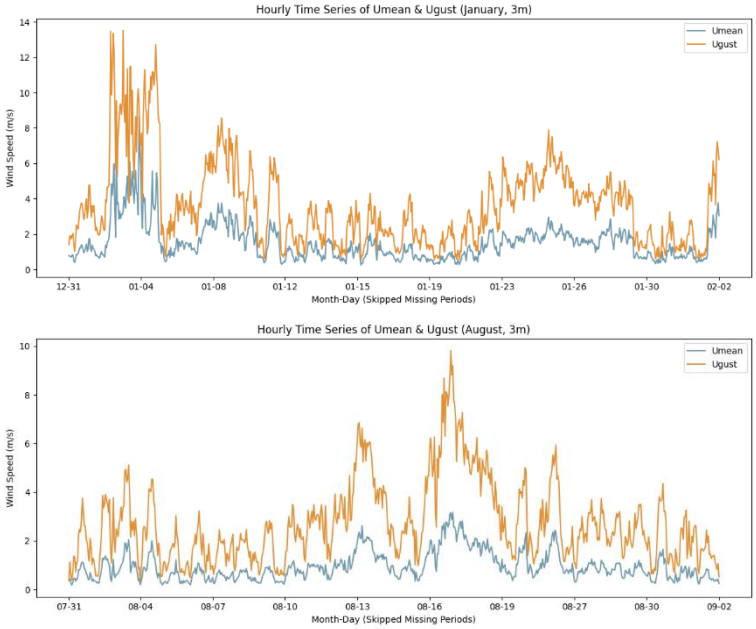

Figure 3.1 Time series of mean wind and gust at 3m height in January (top) and August (bottom) 2018

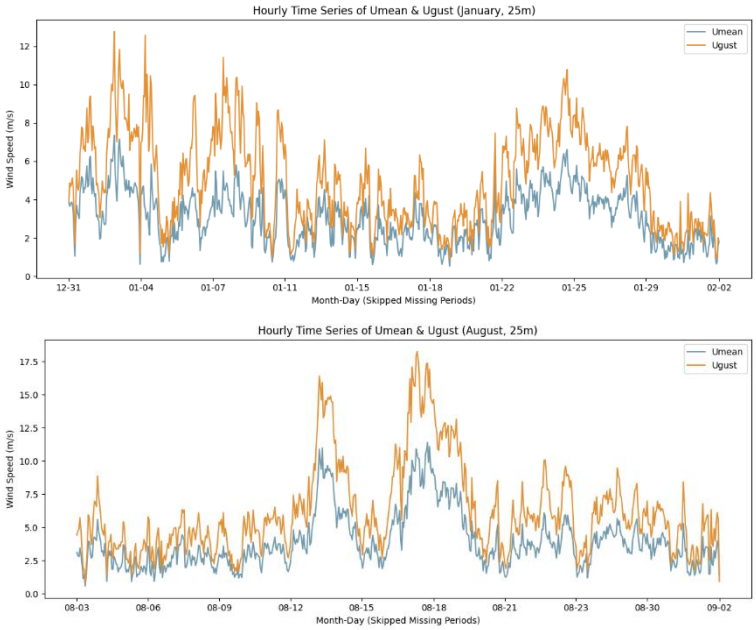

Figure 3.2 Time series of mean wind and gust at 25m height in January (top) and August (bottom) 2018

Finally, wind conditions at the 50-meter level were examined to complete the vertical profile

analysis within the urban environment. According to Figure 3.3, at a height of 50 m, during the January period, U_{gust} exceeds 10 m/s multiple times in early January, followed by a significant decline later on. This pattern suggests a coupling effect between winter cold air activity and the influence of the urban underlying surface. In August, the curve shows two peaks (around August 13–19), with the highest U_{gust} reaching nearly 18 m/s—far exceeding the corresponding U_{mean} during that period—which indicates that high-altitude wind shear or convective activity helps transport stronger momentum down to this height. Compared with the 25 m and 3 m levels, the extreme values of both U_{mean} and U_{gust} at 50 m are higher, demonstrating that in areas above the tops of tall buildings, the combination of local turbulence and the background wind speed makes gust events more sudden and intense.

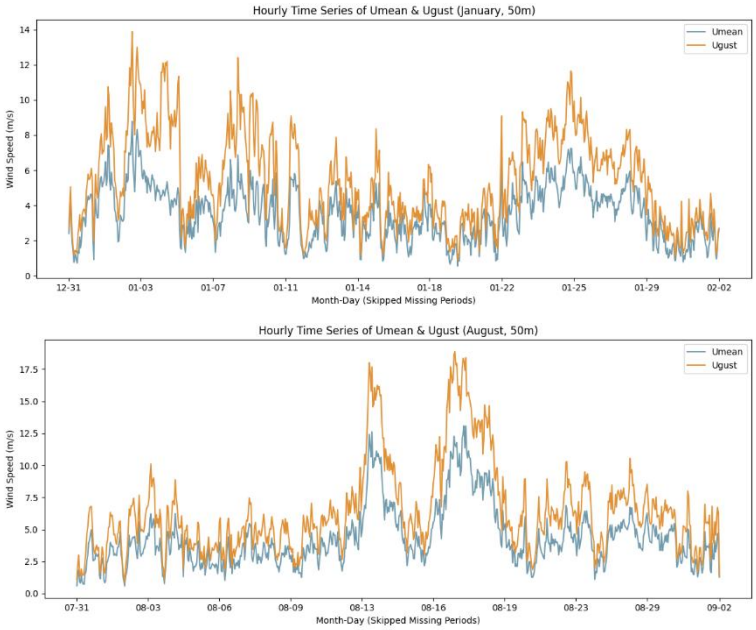

Figure 3.3 Time series of mean wind and gust at 50m height in January (top) and August (bottom) 2018

From the statistical table for the 3-meter level (Table 3.1), it is evident that there are significant differences in gust parameters between January and August. The average U_{gust} in January is 3.65 m/s, while in August it is only 2.78 m/s. Meanwhile, the U_{mean} values are 1.47 m/s in January and 0.97 m/s in August, indicating that near-surface gust speeds are relatively higher in winter, and their fluctuation range (as measured by the standard deviation) is also more pronounced. The gust factor in both seasons is close to 2, with January being higher than August, suggesting that in winter the amplification effect of gust intensity relative to the mean wind speed

is more significant. Notably, the L_{gust} data in January exhibit considerable variability, with a standard deviation much larger than the mean, reflecting a strong spatiotemporal heterogeneity in local gust scales. Overall, the 3-meter level data reveal clear seasonal differences, demonstrating that near-surface gust characteristics are more easily influenced by surface roughness and local turbulent disturbances.

Table 3.1 Basic gust statistics at 3m in January and August 2018

3m	January				August			
	mean	std	min	max	mean	std	min	max
U_{gust} (m/s)	3.65	2.54	0.39	19.36	2.78	1.74	0.24	13.45
U_{mean} (m/s)	1.47	0.93	0.16	8.72	0.97	0.61	0.13	3.56
GA (m/s)	2.18	1.77	0.10	17.15	1.81	1.18	0.09	9.90
Peak Factor	2.96	0.77	0.29	10.99	3.51	0.75	1.67	7.36
Gust Factor	2.47	0.65	1.15	10.95	2.90	0.60	1.33	6.38
TI	0.50	0.15	0.08	1.77	0.54	0.09	0.15	0.92
t_{rise} (s)	18.10	20.05	0.10	264.30	15.70	14.35	3.00	163.20
t_{lapse} (s)	22.16	21.39	0.10	287.80	18.07	15.35	0.30	192.40
t_{gust} (s)	40.26	34.50	3.20	354.40	33.76	23.84	3.50	256.10
L_{gust} (m)	82.87	272.58	0.67	2298.18	50.41	39.56	1.58	504.82

The statistical results at the 25-meter level show that the average U_{gust} values in January and August are 5.29 m/s and 6.51 m/s, respectively, while the corresponding U_{mean} values are 3.22 m/s and 4.12 m/s. The data indicate that wind speeds at the higher level (25 m) are noticeably greater than those near the surface (3 m), and the overall wind speed in summer is slightly higher than in winter—possibly due to the stronger influence of large-scale wind fields at higher altitudes. At this level, the January gust factor is slightly lower than at the near-surface layer, suggesting that in winter, the ratio of gust speed to mean wind speed decreases with height, whereas the opposite trend is observed in August. Furthermore, the higher average values of t_{rise} and t_{lapse} indicate that gust events at 25 m have longer rising and decaying phases compared to those near the surface, resulting in an increased gust duration (t_{gust}). The L_{gust} at 25 m also exhibits a larger scale, with the average value in August exceeding that in January, indicating that in summer the spatial extent of gusts in the upper urban wind field is relatively greater. At the 25-meter level, the combined effects of urban buildings, local thermal conditions, and the structure of the atmospheric boundary layer

collectively determine the generation and evolution of gusts.

Table 3.2 Basic gust statistics at 25m in January and August 2018

25m	January				August			
	mean	std	min	max	mean	std	min	max
U_{gust} (m/s)	5.29	2.53	0.42	19.29	6.51	3.59	0.76	19.78
U_{mean} (m/s)	3.21	1.42	0.16	8.20	4.12	2.22	0.42	13.00
GA (m/s)	2.07	1.37	0.11	15.24	2.39	1.49	0.14	8.68
Peak Factor	2.40	0.49	0.42	6.51	2.41	0.40	1.15	4.46
Gust Factor	1.66	0.35	1.07	5.08	1.59	0.21	1.06	3.60
TI	0.28	0.19	0.03	2.26	0.24	0.08	0.04	0.71
t_{rise} (s)	29.81	28.67	0.10	387.90	29.70	24.67	2.50	234.00
t_{lapse} (s)	36.87	31.44	0.10	319.40	38.17	28.78	0.30	253.70
t_{gust} (s)	66.68	47.19	3.20	409.70	67.88	40.57	3.20	315.10
L_{gust} (m)	266.51	224.80	0.27	2263.61	348.27	275.20	4.22	2791.16

Data from the 50-meter level further reflects the impact of increasing height on the wind field structure. In January, the average U_{gust} is 5.74 m/s and U_{mean} is 3.72 m/s, while in August they are 6.73 m/s and 4.53 m/s, respectively. Overall, the wind speeds at 50 m are higher than those at 25 m, and both seasons exhibit a clear increase in wind speeds. Meanwhile, the Gust Factor at 50 m is slightly lower than that at the lower levels, indicating that although wind speeds at higher altitudes are greater, the relative increase of gust speed over the mean wind speed becomes more moderate. Furthermore, the time-scale parameters—such as t_{rise}, t_{lapse}, and t_{gust}—show that gust events at 50 m have longer durations and extended rising and decaying phases, with t_{gust} reaching nearly 73 seconds in summer, indicating a longer-lasting gust event at higher levels. The average L_{gust} at 50 m is also significantly higher than the corresponding values at lower levels, reaching nearly 400 m in summer, which reflects a larger spatial extent of gusts at higher altitudes. These statistical results demonstrate that as height increases, the characteristics of gusts within the urban boundary layer gradually come under the control of large-scale wind fields and vertical wind shear, expanding both their temporal and spatial scales. At the same time, they reveal significant differences in the transmission of wind speeds and turbulent mixing processes among different height levels in urban areas.

Table 3.3 Basic gust statistics at 50m in January and August 2018

50m	January				August			
	mean	std	min	max	mean	std	min	max
U_{gust} (m/s)	5.74	2.73	0.46	15.82	6.73	3.72	0.45	19.98
U_{mean} (m/s)	3.72	1.60	0.30	9.88	4.53	2.47	0.28	14.91
GA (m/s)	2.02	1.42	0.11	9.64	2.20	1.40	0.10	9.81
Peak Factor	2.31	0.49	0.31	4.80	2.37	0.41	1.42	4.51
Gust Factor	1.55	0.32	1.04	4.51	1.50	0.22	1.07	3.98
TI	0.25	0.19	0.02	1.62	0.21	0.08	0.03	0.66
t_{rise} (s)	33.16	32.15	0.10	275.40	32.75	27.51	3.00	319.80
t_{lapse} (s)	38.55	34.42	0.10	276.80	40.31	31.68	3.00	248.20
t_{gust} (s)	71.71	53.12	3.20	368.60	73.07	44.83	7.90	398.00
L_{gust} (m)	317.06	280.74	0.72	3069.66	397.07	322.32	13.73	2721.12

Based on the analysis of data from the three heights, it is evident that the gust characteristics in Nanjing's urban area differ significantly across various heights and seasons. Near-surface data (3 m) are strongly influenced by building obstructions and the urban heat island effect, resulting in higher gust intensities and larger fluctuation ranges. In contrast, at higher levels (25 m and 50 m), both wind speeds and gust events exhibit more pronounced large-scale wind field characteristics, with summer wind speeds being higher and both gust duration and spatial scale increasing.

3.1.2 Wind Direction Characteristics

The directional characteristics of wind, including prevailing directions and associated gust patterns, were analyzed for different seasons, beginning with observations at the 3-meter level. As shown in Figure 3.4, in the winter wind rose at 3 m, the wind directions are more dispersed than in summer, with pronounced columnar sectors in the northeast and southeast directions. The black columns are concentrated around the northeast, southeast, and west, indicating that during cold air intrusion periods in urban areas, the prevailing winds are typically from these directions. The red dashed lines reveal that the average gust speeds corresponding to these dominant wind directions are also relatively high—especially in the southeast direction, where the average gust speed exceeds 5 m/s. In addition, although less frequent, the northwest direction exhibits higher gust values, suggesting that urban heat islands or local shear lines during nighttime or transitional seasons may also trigger instantaneous strong winds.

In the summer wind rose at 3 m, the black columns representing the frequency of occurrence

of each wind direction are relatively concentrated, implying that near-surface wind directions are more stable. It can be observed that the frequencies are relatively high in the east and eastward sectors. The red dashed curve, outlining the average gust speed for each direction, indicates that while overall gust speeds do not vary dramatically, slightly higher gust values occur in the east and north-northwest directions. This suggests that under the combined influence of local thermal processes and the urban underlying surface in summer, winds from the east and north-northwest are more prone to producing short-term high gust speeds.

To further investigate the vertical structure of wind directionality, the analysis now focuses on the 25-meter height. In Figure 3.5, the winter wind rose at 25 m shows that the frequency of northeast winds still dominates, with a noticeable columnar sector also appearing in the westward direction; compared to the 3 m diagram, the frequency in the southeast is reduced. The red dashed line indicates that the average gust speed for westerly winds is relatively high, reaching over 5 m/s. Compared with the 3 m level, gusts at 25 m in winter exhibit a larger increment, suggesting that the tops of urban buildings and their surrounding areas are more susceptible to the downward transfer of momentum from higher altitudes, thereby forming distinct gust events. In the summer wind rose at 25 m, compared to the 3 m level, the distribution spreads from due east toward the north; however, the columnar sector shows a more pronounced tilt toward the southeast. The red dashed curve fluctuates noticeably with respect to direction, with gust speeds in most directions approaching or exceeding 4–5 m/s, and particularly higher in the southeast and due south directions. At higher levels, under the combined influence of large-scale circulation and daytime turbulence, gust speeds are more likely to reach elevated levels.

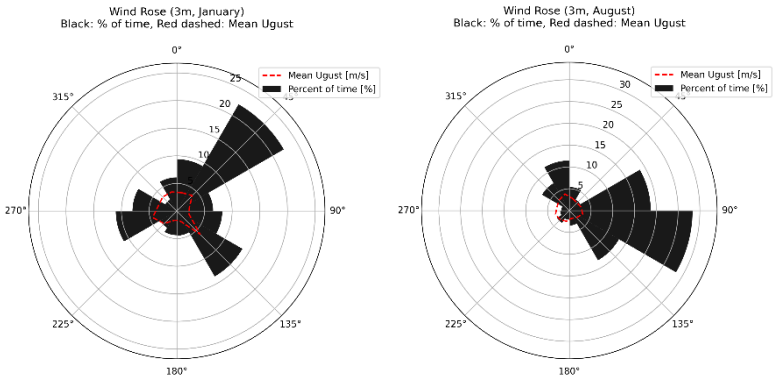

Figure 3.4 Wind rose diagrams at 3m height in January (left) and August (right) 2018

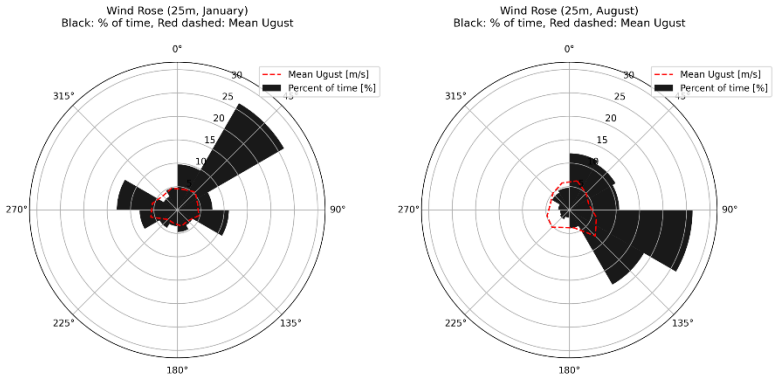

Figure 3.5 Wind rose diagrams at 25m height in January (left) and August (right) 2018

Finally, to complete the vertical profile of wind direction characteristics, the analysis extends to the 50-meter height. According to Figure 3.6, the 50 m winter wind rose indicates that northeast winds remain the predominant direction, and the black sector in the northwest extends further than at 25 m, demonstrating that under the influence of winter cold air, wind directions are highly concentrated for most periods. The red dashed curve is relatively uniform, with lower wind speeds in the southwest, suggesting that at this height, strong gusts are more common during periods of northeast or northwest wind intrusions. In the summer wind rose at 50 m, the black frequency sectors are more concentrated toward the southeast, with some distribution in the northeastern sector. The red gust dashed line shows particularly high values in the north and southeast, with the highest average gust speeds reaching up to 6 m/s or even higher, indicating that in areas above tall buildings or in nearly open spaces—where the influence of urban surface roughness is diminished—large-scale circulations and strong local convection can transport stronger momentum to this height, leading to significant short-term wind speed fluctuations.

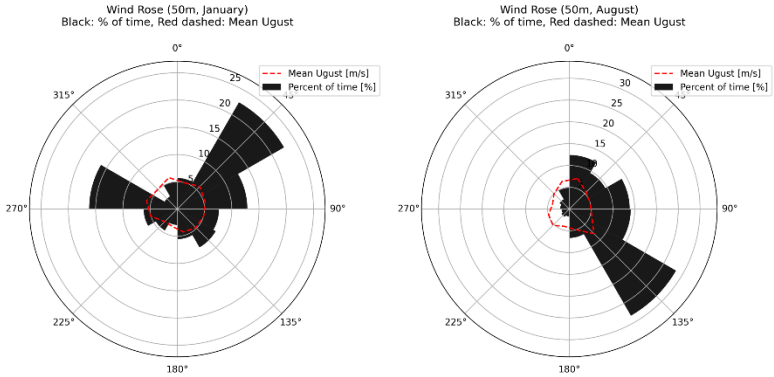

Figure 3.6 Wind rose diagrams at 50m height in January (left) and August (right) 2018

In winter, wind directions are relatively dispersed at the 3 m level, with a concentration in the northeast, southeast, and west sectors. Among these, the average gust speed in the southeast is relatively high (exceeding 5 m/s). Occasionally, high wind speeds from the northwest may be linked to urban heat island effects or local shear lines. As the height increases to 25 m and 50 m, the northeast wind remains dominant, but the directional concentration becomes stronger—especially at 50 m, where the northeast and northwest sectors are more pronounced. At higher levels (25 m and 50 m), gust speeds in the westerly direction are significantly enhanced (reaching or even exceeding 5 m/s), indicating that the tops of urban buildings are more susceptible to the downward transfer of momentum from higher altitudes.

In summer, near-surface wind directions (at 3 m) are relatively stable, predominantly from the east and eastward sectors, with only minor differences in gust speeds, though slightly higher gust values are observed in the east and north-northwest directions. As height increases (at 25 m and 50 m), there is a clear tendency for the wind to shift toward the southeast. Overall, gust speeds increase at higher altitudes, with the average gust speeds in the southeast and northern sectors at 50 m being particularly prominent—reaching as high as over 6 m/s. This suggests that open areas at higher altitudes are more easily affected by large-scale circulations and local thermal turbulence, resulting in more significant short-term wind speed fluctuations. These figures demonstrate that there is no obvious relationship between the magnitude of gusts in a given direction and the frequency of that wind direction.

3.1.3 Gust Parameter Cumulative Distribution Function Analysis

To gain a deeper statistical insight into the behavior of various wind and gust parameters, this section presents an analysis of their Cumulative Distribution Functions (CDFs) across different heights and seasons, as detailed in Figure 3.7. The analysis begins with the cumulative distribution of the mean wind speed. Figure 3.7(a) shows that at the 3-m level in January, the cumulative distribution of the mean wind speed (U_{mean}) mainly climbs within the 0–2 m/s range; near-surface mean wind speeds are generally low, though the tail can extend up to 6–8 m/s. In August, the distribution is shifted further to the left, indicating that near-surface mean wind speeds in summer are usually lower. In contrast, the curves for 25 m and 50 m are shifted to the right, with a significant increase in the mean wind speed. The differences between January and August are

mainly evident in the range above 5 m/s: at 25 m and 50 m, January shows a relatively higher occurrence of moderate-to-low wind speeds, whereas August has a higher cumulative probability in the high wind speed range. As height increases, U_{mean} generally increases—summer wind speeds at mid-to-high levels exceed those in winter, while near-surface mean wind speeds in winter are higher than in summer. This demonstrates that urban building obstructions significantly affect near-surface mean winds, and that seasonal differences are related to large-scale circulations and urban heat island processes.

Next, the focus shifts to the cumulative distribution of gust wind speed (U_gust), which is critical for assessing peak wind loads. Figure 3.7(b) displays that at the 3-m level in January, the cumulative distribution function (CDF) of gust wind speed (U_{gust}) rises steeply in the 1–4.5 m/s range, with the tail extending beyond 10 m/s before approaching 1.0, indicating that near-surface gust speeds in winter can reach relatively high levels. In August, the curve rises rapidly in the 1–3 m/s range and the tail wind speeds are significantly lower than in January, implying that strong near-surface gusts in summer are relatively rare. For the 25-m and 50-m levels, the curves shift to the right as height increases; particularly in summer, the probability of gust speeds reaching 15 m/s or higher is non-zero, suggesting that during seasons with vigorous convection, higher altitudes may experience stronger wind speeds. Thus, near-surface gusts in winter and high-level gusts in summer represent two "vulnerable" regions: the former is driven by urban roughness and cold air triggers, while the latter is influenced by large-scale wind fields and convective momentum transfer, reflecting a distinct layered structure of wind speeds within the urban boundary layer.

The gust factor (GF), representing the ratio of gust speed to mean wind speed, provides insight into the relative intensity of gusts. Figure 3.7(c) shows that most curves rapidly jump from 0 to 1.0 within a gust factor (GF) range of approximately 1.5–2.5, indicating that the vast majority of gust factors are concentrated within a relatively narrow interval. At the 3-m level, the curves for January and August are noticeably shifted to the right, with GF values reaching 3.0 or even higher before the CDF gradually approaches 1.0. This implies that near-surface gusts in both winter and summer can reach 2–3 times the mean wind speed or more. In contrast, at 25 m and 50 m, most of the cumulative probability is achieved within the 1.2–2.0 range, suggesting that with higher mean wind speeds at greater altitudes, the relative amplification of gusts is somewhat reduced. Nevertheless, in January there remains a relatively long tail at 25 m and 50 m, reflecting

the presence of extreme gust amplification events. The gust factor near the surface in winter can be significantly elevated, demonstrating that under the combined influence of urban surface roughness and cold air activity, the enhancement of gust speed relative to the mean wind is pronounced. At higher levels, the GF is mostly distributed between 1.2 and 2.0, and the summer high-level curve shifts further to the left, indicating that when large-scale winds dominate, the multiplier of gust speed relative to the mean wind is comparatively lower.

Following this, the gust amplitude, defined as the difference between the gust speed and the mean wind speed, is examined. Figure 3.7(d) illustrates that for gust amplitude within the lower range (0–2.5 m/s), most curves quickly reach a cumulative probability above 0.5, suggesting that a large proportion of gust amplitudes are relatively low. The 3-m winter curve extends considerably to the right, showing that some gust amplitudes can reach 7.5 m/s or higher. In summer, the 3-m curve is positioned furthest to the left with few significant amplitude events at the low-level, while the 25-m curve is shifted further to the right compared to the 50-m curve, indicating that in summer, the frequency of high gust amplitudes at mid-levels is greater than at high levels. The distributions of gust amplitudes for mid-to-high levels in winter do not differ much. Near-surface in winter, large-amplitude gust events are more common, whereas in summer at higher levels there is an accumulation of moderate amplitudes, reflecting the modulation of wind speed fluctuations by urban underlying surfaces and seasonal effects.

The peak factor, which quantifies the magnitude of gusts relative to the background turbulence intensity, is another key parameter investigated. Figure 3.7(e) shows that for the peak factor, most curves exhibit a steep rise in the vicinity of 2–4, indicating that urban gust peaks are generally about 2–3 times the background turbulence. The 3-m curves for January and August both display longer tails, especially the August curve, which only gradually approaches 1.0 at peak factors of 6 or higher, suggesting that near-surface gusts in summer often have relatively high intensities in terms of local turbulence. In contrast, the 25-m and 50-m curves are more concentrated in the 1.5–3.0 range with shorter tails, implying that gust peaks at higher levels do not exhibit extreme amplification relative to local turbulence. Moreover, the near-surface summer peak factors are higher than those in winter, and also exceed those at higher levels, reflecting that under the combined influence of urban surface roughness and warm air excitation, local turbulence fluctuations are more intense. At higher levels, the distribution is narrower, with peak factors

mainly concentrated between 2 and 3.

Attention then turns to the temporal characteristics of gusts, beginning with an analysis of the gust rise time (t_{rise}). Figure 3.7(f) indicates that at the 3-m level, the rise time (t_{rise}) for gusts in both seasons is highly concentrated in very short durations (0–25 s), but the tail in January extends much further (over 150 s), indicating that near-surface gusts in winter can sometimes gradually intensify and build up over a long period. In August, the distribution tends to indicate a rapid onset with a much shorter tail. At the 25-m and 50-m levels, the curves shift slightly to the right, with a larger proportion of rise times falling in the 20–60 s range. As height increases, the distribution of t_{rise} shifts toward longer durations, suggesting that the formation of gusts at higher altitudes is jointly influenced by large-scale wind fields and local turbulence, leading to a generation phase that is somewhat slower and more stable. At the same height, the rise time of gusts in winter is higher than in summer.

Complementing the rise time, the statistical distribution of gust decay time (t_{lapse}) is also explored. Figure 3.7(g) shows that at the 3-m level, in January, the decay time (t_{lapse}) exhibits a significant increase in the 10–30 s range, with the tail extending beyond 150 s, indicating that near-surface gusts in winter can sometimes decay slowly. In August, most decay times are concentrated in the 0–50 s range with a shorter tail. At the 25-m and 50-m levels, the t_{lapse} in summer shifts slightly to the right, implying that gusts at higher levels may experience a longer decay process after reaching their peak, which is associated with sustained momentum exchange due to wind shear and convective activity. Overall, the decay time distribution is similar to that of the rise time.

The overall duration of gust events (t_{gust}), encompassing both rise and decay phases, is subsequently analyzed. Figure 3.7(h) reveals that at the 3-m level, both January and August show a high concentration of gust events with short durations (0–50 s), but there remains a long tail beyond 100 s. However, the frequency of long-duration events is higher in January, indicating that near-surface gusts in winter can sometimes persist for a considerable time—a characteristic also observed at the 25-m and 50-m levels—whereas in summer, the long tail is significantly reduced, suggesting that near-surface gusts in summer tend to occur as brief bursts. As height increases, the t_{gust} curve shifts slightly to the right, signifying longer gust durations. This is related to higher large-scale wind speeds, stronger convective activity, and more intense thermal conditions.

In addition to temporal aspects, the characteristic spatial scale of gusts (L_{gust}) is investigated. Figure 3.7(i) illustrates that L_{gust}, which represents the spatial scale of gusts, ranges from small values to several hundred or even thousands of meters. At the 3-m level, the January curve rises quickly in the lower L_{gust} range (approximately 0–200 m) but maintains a certain cumulative distribution beyond 300 m, indicating that a few gusts in winter can extend over several hundred meters. In August, the distribution is generally shifted to the left with a shorter tail, suggesting that near-surface gusts in summer mostly dissipate within a smaller spatial scale. At the 25-m and 50-m levels, as height increases, the proportion of the August curve in the larger spatial scale range is higher compared to the January curve, indicating that larger-scale gust events are more likely to occur at higher altitudes in summer. Although there is also a long tail in January at higher levels, its frequency is relatively lower, suggesting that the coupling of high-altitude processes with large-scale wind fields, convection, and shear is more pronounced in summer.

Finally, the cumulative distribution of turbulence intensity (TI) is examined to characterize the overall level of local turbulence. Figure 3.7(j) shows that the turbulence intensity (TI) represents the level of local turbulence. At the 3-m level, the January curve rises rapidly in the range of 0.3–0.6, with the highest peak frequency, suggesting that high turbulence intensity values are more common near the surface in winter. In August, the curve in the high turbulence intensity range is slightly shifted to the left compared to January, while the remainder shifts to the right. This indicates that the frequency of high turbulence intensity near the surface in summer is slightly lower than in winter, but the frequency of moderate to high turbulence intensities is slightly higher than in winter. At the 25-m and 50-m levels, as height increases, TI generally shifts toward lower values (approximately 0.1–0.3). Even at 25 m and 50 m in January, there remains a certain probability of high TI, suggesting that differences in cold air or urban thermal conditions in winter can still produce strong turbulence at higher altitudes.

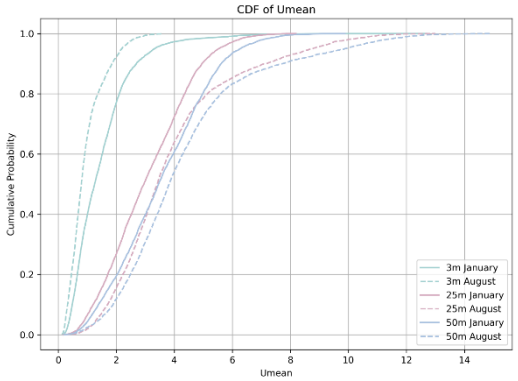
CDF of Umean
Cumulative Probability
Umean
3m January
3m August
25m January
25m August
50m January
50m August

(a)

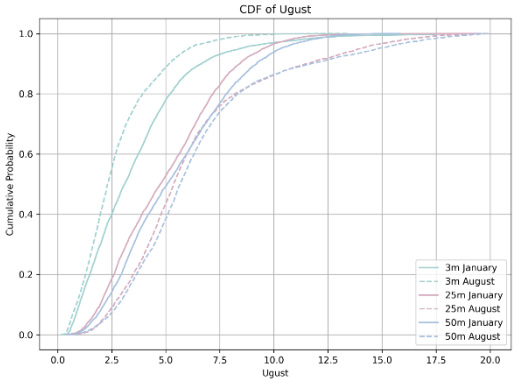
CDF of Ugust
Cumulative Probability
Ugust
3m January
3m August
25m January
25m August
50m January
50m August

(b)

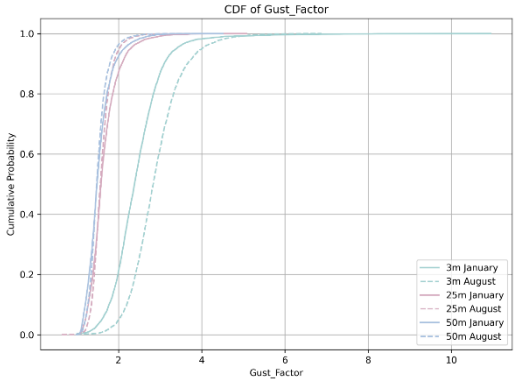
CDF of Gust_Factor
Cumulative Probability
Gust_Factor
3m January
3m August
25m January
25m August
50m January
50m August

(c)

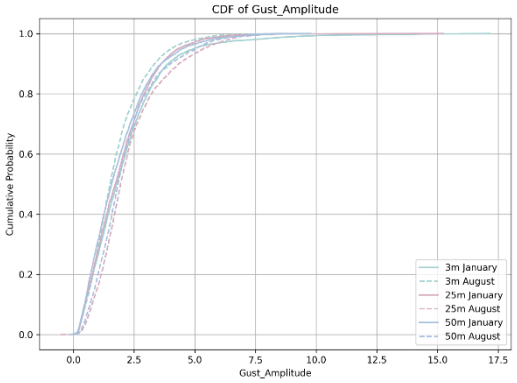
CDF of Gust_Amplitude
Cumulative Probability
Gust_Amplitude
3m January
3m August
25m January
25m August
50m January
50m August

(d)

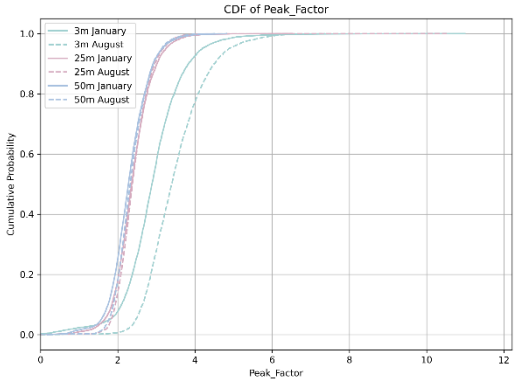
CDF of Peak_Factor
Cumulative Probability
Peak_Factor
3m January
3m August
25m January
25m August
50m January
50m August

(e)

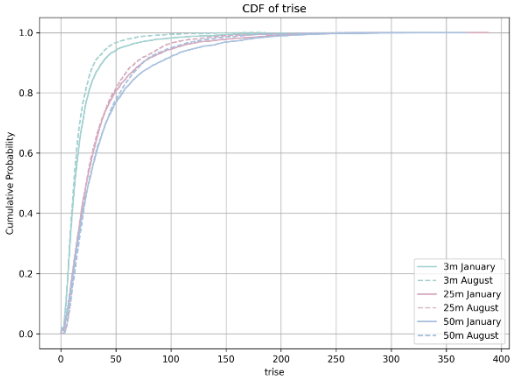
CDF of trise
Cumulative Probability
trise
3m January
3m August
25m January
25m August
50m January
50m August

(f)

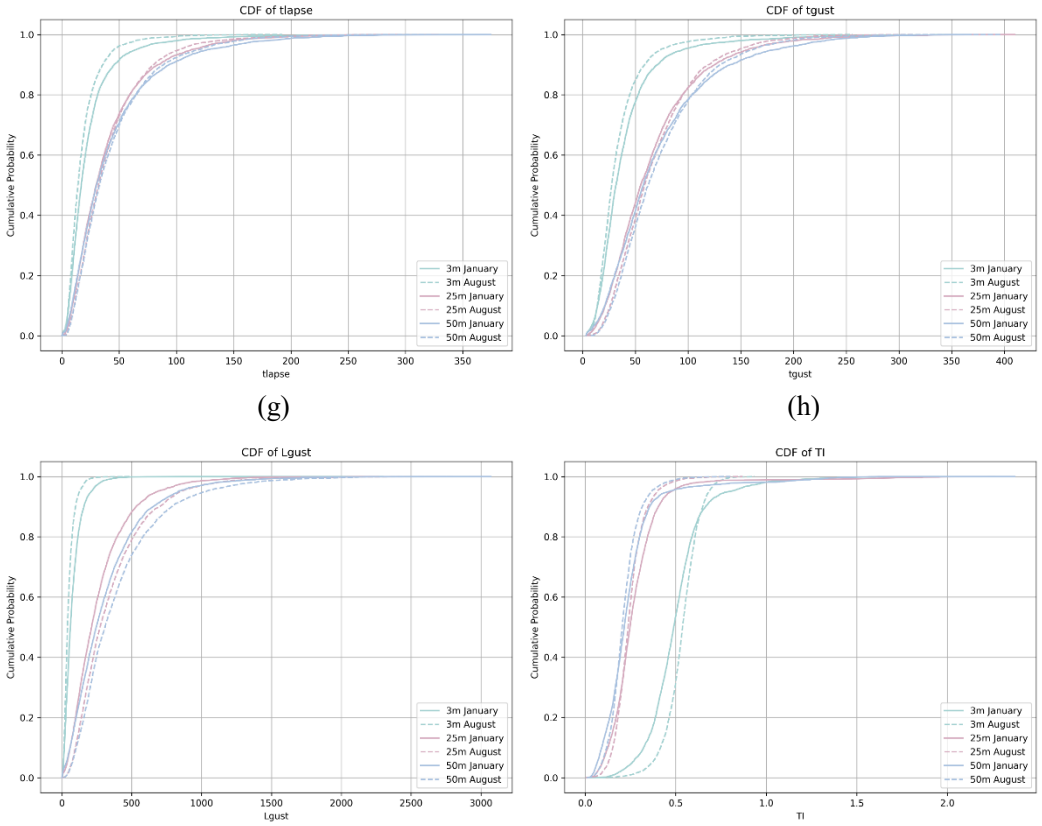

Figure 3.7 Cumulative distribution function (CDF) plots of ten gust parameters. Solid lines represent January, and dashed lines represent August. Green indicates 3 m height, purple indicates 25 m height, and blue indicates 50 m height. The subplots display: (a) 10-minute average wind speed (U_{mean}); (b) Gust wind speed (U_{gust}); (c) Gust factor (GF); (d) Gust amplitude (a_{agust}); (e) Peak factor (k_{peak}); (f) Rise time (t_{rise}); (g) Decay time (t_{lapse}); (h) Gust duration (t_{gust}); (i) Gust length scale (L_{gust}); and (j) Turbulence intensity.

3.1.4 Diurnal Variation of Gust Factor

This section delves into the diurnal variation of the gust factor, aiming to understand how its magnitude fluctuates throughout the day across different seasons and atmospheric heights. For the daily mean gust factor distribution in January shown in Figure 3.8, at the 3-m level the gust factor in winter fluctuates between 2.3 and 2.5 throughout the day. It remains relatively low from midnight to the early morning (0–10 o'clock), increases around noon, stays high between 11:00 and 16:00, and then falls again at night. This pattern indicates that near-surface gust ratios are particularly prominent at midday in winter. Although winter values are slightly lower compared to summer, they are still noticeably higher than those observed at mid-to-high levels.

At the 25-m and 50-m levels, the winter curves are consistently between 1.4 and 1.9. The diurnal variation here is characterized by a modest increase during the daytime (8:00–16:00) followed by a slight decrease at night. This behavior is likely associated with the combined effect of mechanical turbulence and the downward transfer of cold air during the day, which enhances gust fluctuations. However, due to the increased mean wind speed at these heights, the gust-to-mean wind ratio remains lower than that at the near-surface level.

In contrast, the daily mean gust factor distribution in August at the 3-m level maintains an overall range of 2.75 to 3.25 throughout the day. A peak occurs around the early morning (approximately 5:00–7:00), followed by a gradual decline, and then a significant rise again around 18:00. These high values indicate that the relative amplification of gust speed compared to the mean wind is most pronounced near the surface during the early morning and evening in summer, likely due to increased turbulence associated with urban rush-hour activities.

At the 25-m and 50-m levels in summer, the daily mean gust factor is relatively lower—around 1.4 to 1.7—and exhibits a slight increase during the day with a minor decrease at night. This reflects that, under the influence of daytime convection and enhanced vertical mixing at higher altitudes, the mean wind speeds are higher, resulting in a lower relative amplification of gusts compared to the near-surface level.

Through the analysis of the daily mean gust factor distributions in January and August shown in Figure 3.8, it is evident that at the 3-m level in winter, the gust factor reaches a high value around midday, reflecting the pronounced influence of both cold air and mechanical turbulence on near-surface gusts during the daytime. Although the overall values are slightly lower than in summer, they remain significantly higher than those at mid-to-high levels. In summer, the 3-m level exhibits a marked increase in the gust factor throughout the day, with distinct peaks during the early morning and evening rush hours, indicating that urban activities enhance both turbulence intensity and gust amplitude. At the 25-m and 50-m levels, regardless of the season, the gust factor remains within a lower range and shows only minor diurnal variations. This suggests that at higher altitudes, where the mean wind speeds are greater, the relative amplification of gusts compared to the mean wind is less pronounced, further highlighting the stratified nature of urban gust characteristics with height.

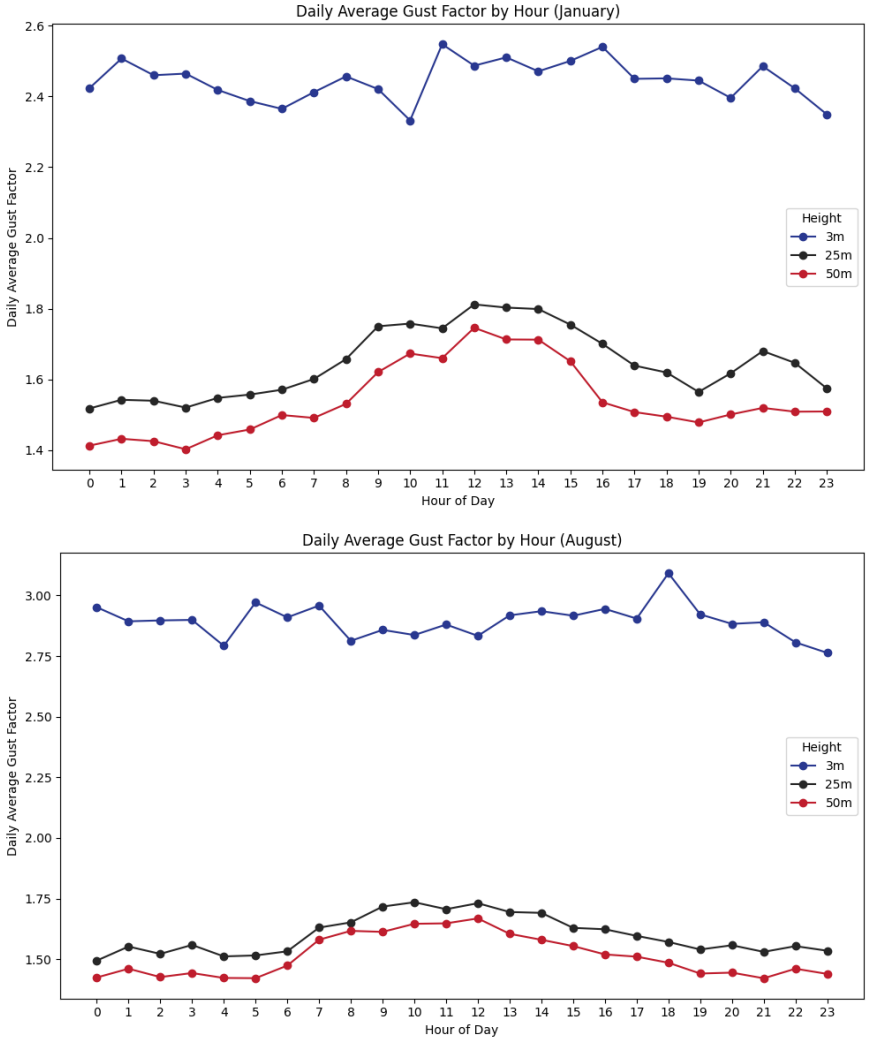

Figure 3.8 Hourly variation trend of the mean gust factor at different heights in January (top) and August (bottom) 2018

3.1.5 Inter-Level Relationships and Scatter Plot Fitting Analysis of Gusts

The focus now shifts to examining the inter-level relationships of gust amplitudes, utilizing scatter plots and linear fitting techniques to quantify the correlation and dependency between different heights during various seasons. As shown in Figure 3.9, in the scatter plot between 3 m and 25 m, the linear fit for January yields a slope of only 0.75, an intercept of 2.28, and $R^2 \approx 0.58$. Compared with summer, the scatter distribution between 3 m and 25 m in winter is more dispersed, indicating a generally weaker correlation (with R^2 dropping to 0.58). Moreover, the intercept being greater than 2 suggests that even when the 3 m wind speed is low, the gust amplitude at 25 m tends

to maintain a certain level. This implies that under the influence of cold air intrusions or large-scale circulations in winter, the gusts at 25 m do not always fluctuate synchronously with those at 3 m.

For August, the linear fit between 3 m and 25 m gives a slope of approximately 1.93, an intercept of 0.80, and $R^2 \approx 0.87$. This result indicates that in summer, when a gust occurs near the surface (3 m), the gust at 25 m is usually about twice the 3 m wind speed, and the overall correlation is high (with R^2 close to 0.9). It is inferred that under the influence of daytime convection and the urban heat island circulation, the higher level (25 m) more readily receives momentum from aloft, leading to a significant amplification of gust amplitude.

In the scatter plot between 25 m and 50 m, the January fit shows a slope of 0.99, an intercept of 0.52, and $R^2 \approx 0.85$. In winter, the two levels maintain a good consistency (with a slope close to 1), though the R^2 is slightly lower than in summer. This indicates that even at higher levels (25 m vs. 50 m), there is still a significant linear relationship in winter; however, occasionally, due to the effects of cold fronts or low-level shear, gusts at 50 m can be slightly higher than those at 25 m, resulting in some data dispersion. For August, the slope is about 1.06, the intercept 0.17, and $R^2 \approx 0.99$. This result shows that in summer, the gust amplitudes at 25 m and 50 m almost correspond one-to-one (with a very high correlation coefficient), suggesting that both levels are simultaneously regulated by large-scale circulations and local convective activity, yielding a relatively smooth wind speed profile with little vertical difference.

In the scatter plot between 3 m and 50 m, the January fit gives a slope of 0.91, an intercept of 2.21, and $R^2 \approx 0.71$. The relationship between gust amplitudes at 3 m and 50 m in winter is relatively scattered, but it exhibits a more linear trend ($R^2 = 0.71$) compared to the 3 m vs. 25 m case in January ($R^2 = 0.58$). When the 3 m wind speed is zero, gusts at 50 m can still reach approximately 2.21 m/s, suggesting that momentum at higher altitudes is more influenced by large-scale cold air and stable stratification, while near-surface winds are subject to larger fluctuations due to urban surface effects. In August, the fitted slope is about 2.01, with an intercept of 1.11 and $R^2 \approx 0.84$. Similar to the 3 m vs. 25 m summer case, the gust amplitude at 50 m is approximately twice or more that of the near-surface wind, and even when the 3 m wind speed is zero, 50 m may still exhibit gusts of around 1 m/s. This phenomenon indicates that under strong convective conditions and vertical wind shear in summer, the gust amplification effect at higher

altitudes is particularly pronounced.

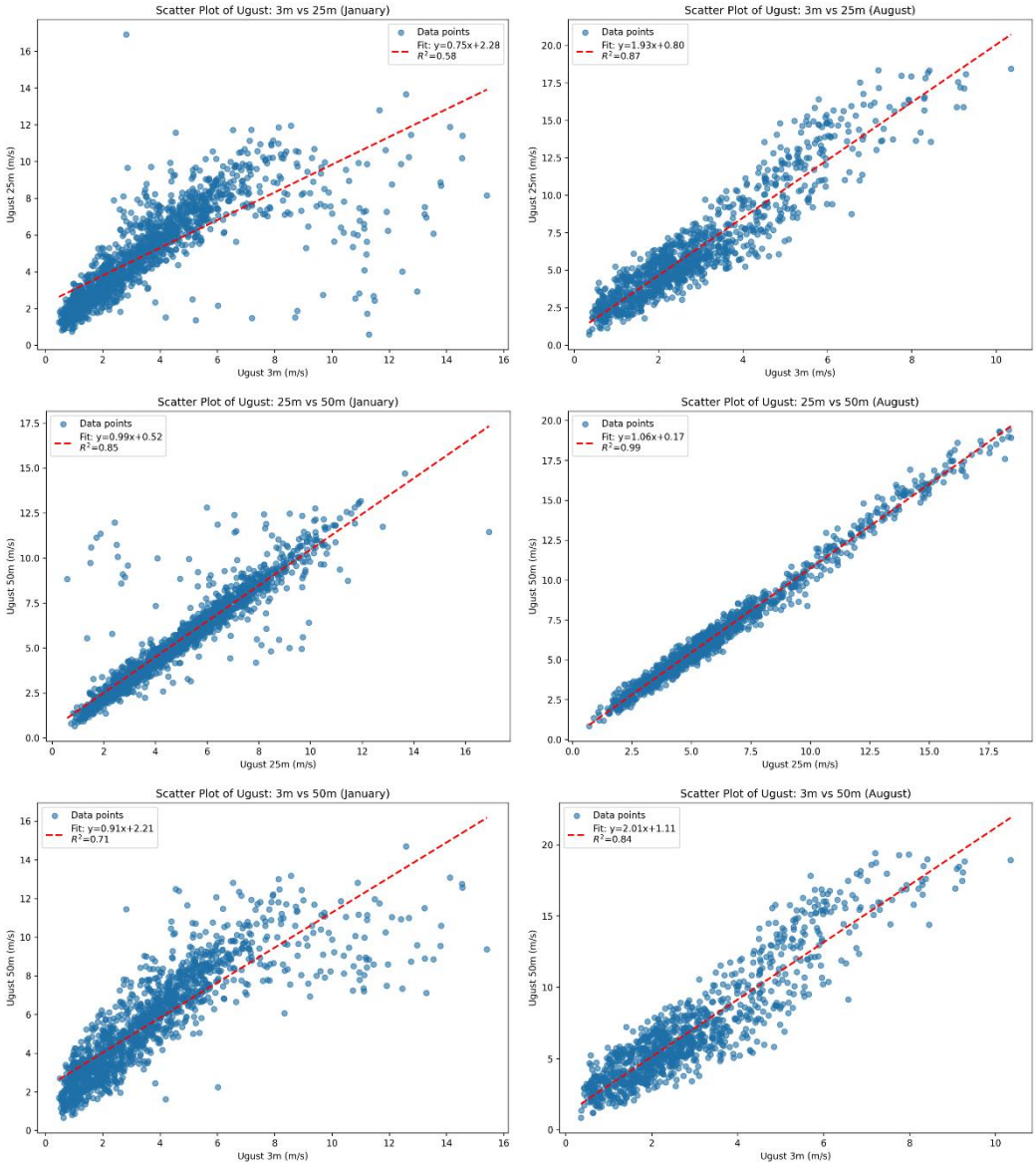

Figure 3.9 Relationship of gust wind speeds at different heights in January (left) and August (right) 2018 (Significance level tested at 0.05)

Comparing the results of the 3-m vs. 25-m and 3-m vs. 50-m scatter plots, it can be seen that as height increases, the linear fit slope in summer is generally greater than 1, indicating that the amplification effect of gusts at higher altitudes is more pronounced. In winter, although the slopes are relatively smaller, the intercepts are higher, suggesting that higher levels can still maintain a certain baseline gust amplitude. Overall, the summer (August) data show a strong correlation (with R^2 mostly above 0.8) and slopes greater than 1, emphasizing the synchronous amplification of

gusts due to convection and vertical mixing. In winter (January), the correlation is slightly weaker (with R^2 ranging from 0.58 to 0.85), and some height combinations exhibit more scatter, reflecting the uncertainties introduced by factors such as cold air activity and stable stratification. The scatter plot between 25-m and 50-m, whether in summer or winter, shows a strong linear relationship with a slope close to 1. In particular, the R^2 in summer reaches as high as 0.99, indicating a very high degree of coupling in gust amplitudes between the mid-to-high levels and revealing the relative uniformity of the wind speed profile in the upper urban boundary layer.

In summary, these scatter plots and their linear fitting results demonstrate that in the Nanjing urban boundary layer, gusts tend to be synchronously amplified with increasing height during summer, while in winter the overall correlation is slightly lower, yet higher levels still frequently maintain a high gust amplitude. This pattern is of significant importance for the wind-resistant design of tall urban buildings and the evaluation of wind energy resources, and it provides empirical evidence for further investigations into the mechanisms governing changes in the wind speed profile under different seasonal and meteorological conditions.

3.2 Statistical Analysis of Gust Correlations

3.2.1 Correlation Analysis of Gust Parameters at 3 m

The following analysis examines the correlation between gust parameters and a range of meteorological factors at the 3-meter height to identify key influencing variables during different seasons. According to Figure 3.10 and 3.11, at a height of 3 m in January, the correlation coefficients of gust speed with both the mean wind speed and gust amplitude are as high as 0.96 and 0.98, respectively, indicating that the background wind speed is the primary driving factor in gust formation. At the same time, the correlation coefficients with surface friction velocity and turbulent stress are 0.85 and 0.82, respectively, which shows that urban surface roughness and the resulting shear significantly enhance gusts. In contrast, the correlation coefficient for turbulence intensity is only 0.43, while the time-scale parameters (rise time, decay time, and duration) exhibit moderate negative correlations (approximately -0.35 to -0.37), reflecting that high wind speed gusts are often associated with shorter durations. Temperature and pressure have relatively weak correlations with gusts, with values of -0.17 and 0.10, respectively.

For August, the data show that the positive correlations of gusts with mean wind speed and

gust amplitude remain very high (0.94 and 0.98, respectively), but the correlation with turbulence intensity drops to 0.20, and the negative correlations of the time-scale parameters are slightly reduced (about -0.14 to -0.23). Temperature shows a positive correlation (0.21), and pressure is slightly negatively correlated (-0.08). Meanwhile, surface friction and turbulent stress still maintain high correlations (both at 0.80).

Overall, regardless of the season, the mean wind speed and surface shear are the key factors in the formation of near-surface gusts. However, in winter, gusts show a more pronounced dependency on turbulence intensity, and high wind speed gusts are generally accompanied by shorter durations.

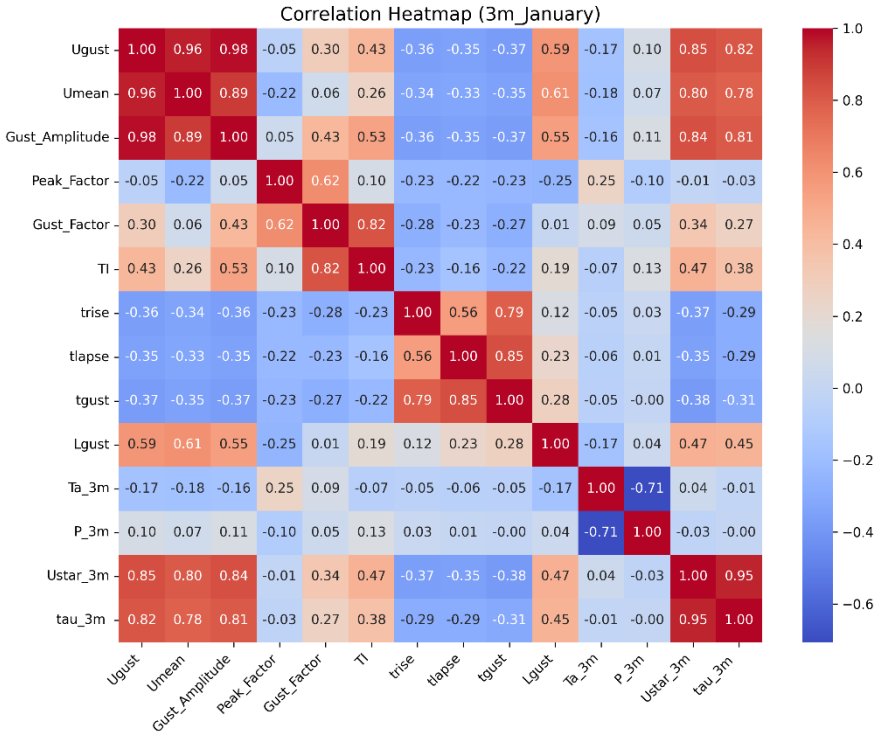

Figure 3.10 Correlation heatmap of gust parameters and other meteorological variables at 3m height in January 2018 (Significance level tested at 0.05)

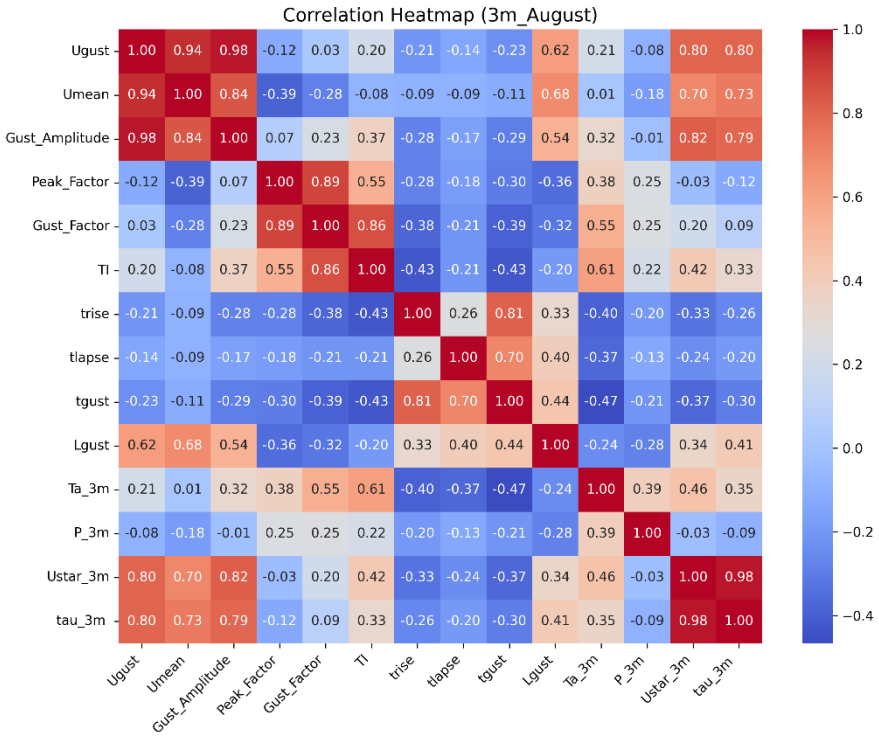

Figure 3.11 Correlation heatmap of gust parameters and other meteorological variables at 3m height in August 2018 (Significance level tested at 0.05)

3.2.2 Correlation Analysis of Gust Parameters at 25 m

Extending the correlation analysis to a higher altitude, this section investigates the relationships between gust parameters and various meteorological factors at the 25-meter level. According to Figure 3.12 and 3.13, at a height of 25 m in January, the correlation coefficients between gust speed and both the mean wind speed and gust amplitude are 0.95 and 0.93, respectively, indicating that the background wind and its fluctuations play a decisive role in gust formation. Meanwhile, the correlation coefficients with friction velocity and turbulent stress are 0.77 and 0.71, respectively, showing that surface shear also has a significant impact on enhancing gusts. The time-scale parameters (rise time, decay time, and duration) exhibit moderate negative correlations (approximately -0.40 to -0.35), reflecting that high wind speed gusts generally have shorter durations, while the correlation coefficient for gust scale is 0.45, indicating a moderate spatial extent. Temperature and pressure show relatively weak correlations with gusts, at -0.13 and 0.03, respectively.

In contrast, the August data reveal even higher correlations of gusts with mean wind speed and gust amplitude (0.98 and 0.96, respectively), whereas the correlations with Peak Factor, Gust

Factor, and turbulence intensity are almost negligible. The negative correlations of the time-scale parameters are slightly reduced (around -0.30 to -0.25), but both friction velocity and turbulent stress increase to 0.87, and atmospheric pressure exhibits a strong negative correlation (-0.57).

Overall, regardless of the season, the mean wind speed and surface shear are the primary factors influencing gusts at the 25 m level, while in summer, atmospheric pressure and time-scale parameters show distinct seasonal differences.

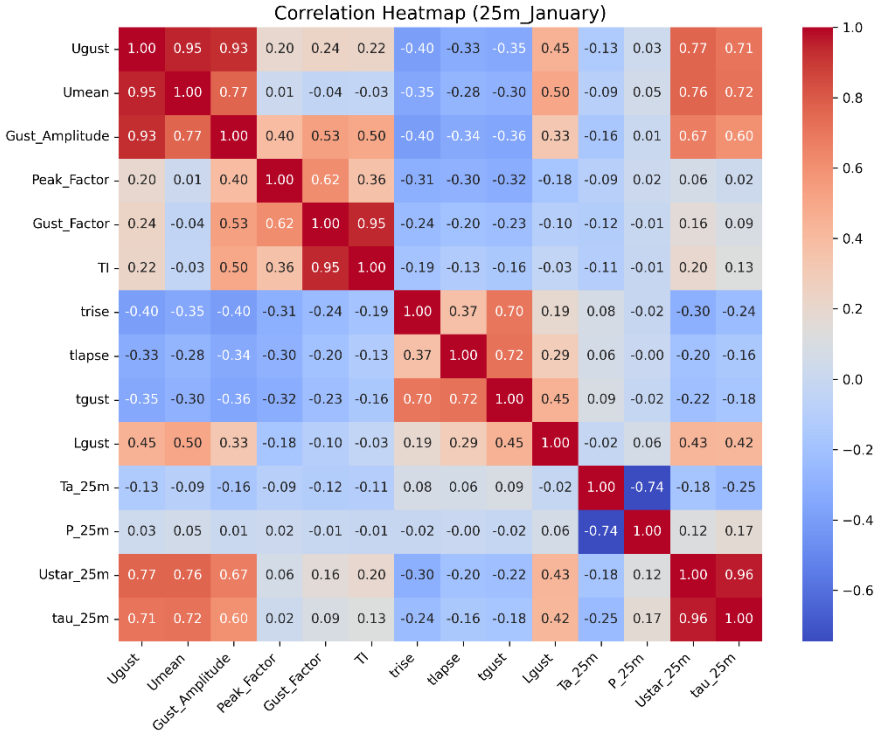

Figure 3.12 Correlation heatmap of gust parameters and other meteorological variables at 25m height in January 2018 (Significance level tested at 0.05)

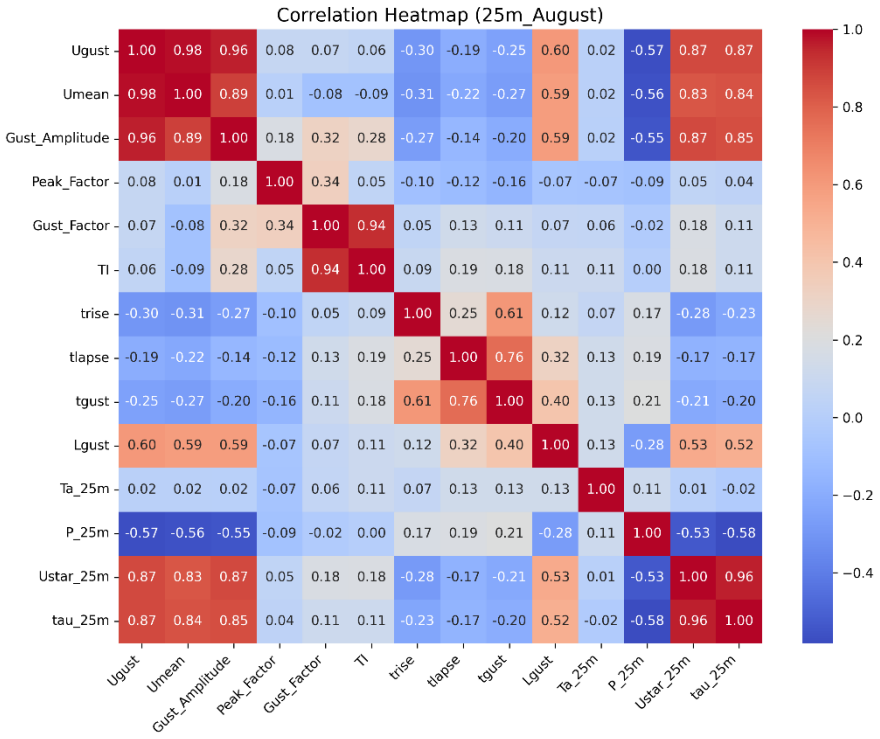

Figure 3.13 Correlation heatmap of gust parameters and other meteorological variables at 25m height in August 2018 (Significance level tested at 0.05)

3.2.3 Correlation Analysis of Gust Parameters at 50 m

Concluding the vertical examination, this section analyzes the correlations between gust parameters and various meteorological factors at the 50-meter level. Based on Figures 3.14 and 3.15, at the 50 m level in January, the correlation coefficients between gust speed and both the mean wind speed and gust amplitude are 0.96 and 0.91, respectively, demonstrating that variations in the background wind field play a decisive role in gust formation. Meanwhile, the correlations with friction velocity and turbulent stress are 0.76 and 0.66, respectively, indicating that surface shear contributes significantly to the enhancement of gusts. The time-scale parameters (rise time, decay time, and duration) all exhibit moderate negative correlations (approximately -0.32 to -0.36), which suggests that stronger gusts at higher levels are typically associated with shorter development processes. In addition, the correlations of Peak Factor, Gust Factor, and turbulence intensity with gust speed are relatively weak; temperature shows a slight negative correlation (-0.17), and pressure is almost uncorrelated (0.04).

In contrast, the August data show that the positive correlations between gust speed and both

the mean wind speed and gust amplitude are further enhanced (0.98 and 0.94, respectively), while friction velocity and turbulent stress increase to 0.86. At the same time, atmospheric pressure exhibits a significant negative correlation with gusts (-0.59), and the negative correlations of the time-scale parameters are slightly reduced (approximately -0.20 to -0.24). These results indicate that in summer, gusts at the 50 m level are more clearly influenced by large-scale wind fields and local convective activity. Overall, regardless of the season, mean wind speed and surface shear remain the primary drivers of gust formation, while under summer conditions, local pressure and time-scale indicators display distinct seasonal characteristics.

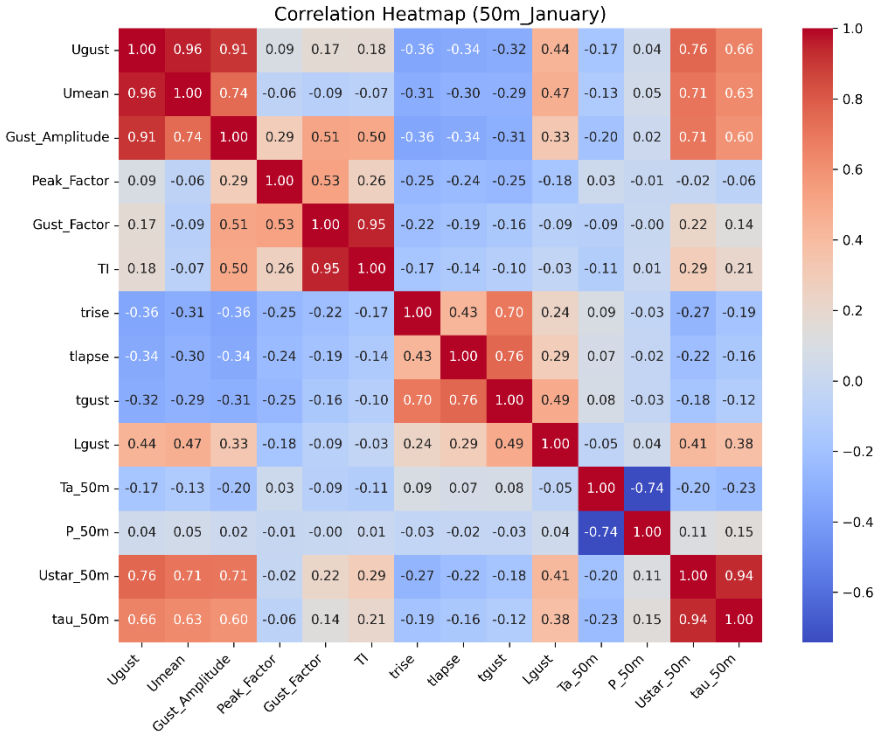

Figure 3.14 Correlation heatmap of gust parameters and other meteorological variables at 50m height in January 2018 (Significance level tested at 0.05)

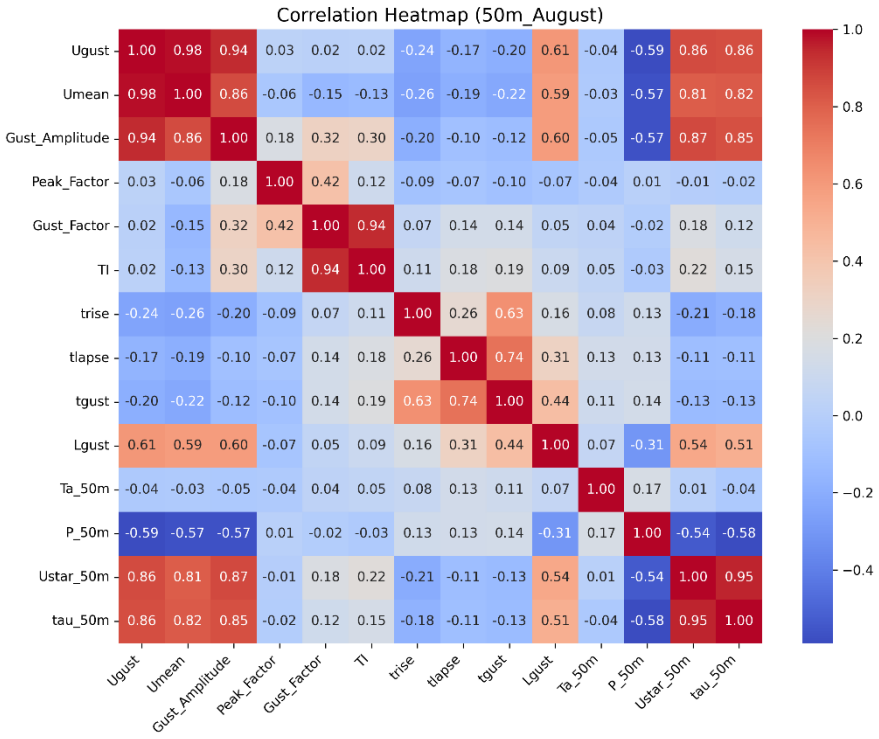

Figure 3.15 Correlation heatmap of gust parameters and other meteorological variables at 50m height in August 2018 (significance level tested at 0.05)

In summary, regardless of whether at 3 m, 25 m, or 50 m, both the mean wind speed and surface shear are key factors driving the formation of urban gusts. In winter, gusts are not only strongly coupled with the mean wind and its fluctuations, but also more dependent on turbulence intensity. Their time-scale parameters exhibit notably negative correlations, reflecting that high wind speed gusts are often accompanied by a short-lived process. In summer, under the influence of large-scale wind fields and the downward transfer of local convective momentum, gusts show an even stronger correlation with wind speed, while local atmospheric pressure exerts a negative modulatory effect on gusts. Overall, these findings reveal the synergistic role of dynamical, shear, and thermal processes in the formation of urban gusts and their seasonal differences, thereby providing robust support for further improving gust parameterization in urban boundary layer models.

4 Numerical Simulation of Gusts and Analysis of Influencing Factors in Nanjing

4.1 Validation of the Gust Model and the Design of Sensitivity Experiments

In this study, the urban boundary layer model RBLM was used to simulate the period from August 5 to 13, 2018, and the simulation results were compared with actual observational data. All the data presented in the tables represent averages over this period. To comprehensively assess the model's performance across various meteorological variables, this section selects temperature, relative humidity, and wind speed error metrics from station 58238 (located at 118.80°E, 32.00°N) and station 58336 (located at 118.51°E, 31.70°N), as well as gust-related observational data from the SORPES station (located at 119.26°E, 32.45°N), to validate the simulation outcomes.

Table 4.1 shows that the simulated temperature (T) has a mean bias of 0 °C, a normalized mean bias (NMB) of 0.00%, and a root-mean-square error (RMSE) of 2.33 °C, with a correlation coefficient of 0.79, indicating that the simulated temperature generally agrees well with the observations. In terms of relative humidity (RH), although there is a slight positive bias (MB = 0.14, NMB = 0.18%), the RMSE is 7.63% and the correlation is relatively high (R = 0.84), suggesting that the model captures the trend in humidity changes quite effectively. In contrast, the simulation of wind speed (U) shows certain deficiencies. For station 58238, the wind speed has an MB of -0.96 m/s, an NMB of -36.02%, and an RMSE of 1.85 m/s, with the correlation coefficient being only 0.50. Similarly, Table 4.2 shows that although simulated temperature and humidity at station 58336 also agree reasonably well with the observations, the wind speed has an MB of -1.01 m/s, an NMB of -32.56%, an RMSE of 1.89 m/s, and a reduced correlation coefficient of 0.44.

Table 4.1 Comparative analysis of temperature, humidity, and wind speed errors between the 58238 station and the summer case model simulation results (Significance level tested at 0.05)

Variable	MB	NMB	RMSE	R
T	0	0.00%	2.33	0.79
RH	0.14	0.18%	7.63	0.84
U	-0.96	-36.02%	1.85	0.5

Table 4.2 Comparative analysis of temperature, humidity, and wind speed errors between the 58336 station and the summer case model simulation results (Significance level tested at 0.05)

Variable	MB	NMB	RMSE	R
T	0	-0.25%	2.18	0.78
RH	-4.89	-6.23%	9.93	0.83
U	-1.01	-32.56%	1.89	0.44

These results indicate that while the model performs quite well in simulating temperature and humidity, it exhibits a noticeable negative bias in wind speed. This discrepancy in wind speed simulation may be related to local terrain features, building obstructions, and the representativeness of the observation sites.

For the simulation of gust characteristics, this study focused on comparing the performance of five different parameterization schemes at a height of 10 m, and the simulation results were compared with observational data from the SORPES station. The average observational values at the campus are: gust speed of 4.92 m/s, mean wind speed of 2.38 m/s, and a gust factor of 2.071, while the simulated mean wind speed is 3.01 m/s. As shown in Table 3, there are significant differences among the simulation results of the various schemes. The ECMWF-based scheme simulates a gust speed of 6.23 m/s and a gust factor of 2.07027, with errors of +1.31 m/s and -0.00085, respectively. In contrast, when using the TKE, TKE2, Schreur, and Nakamura schemes, both the simulated gust speeds and gust factors are significantly lower than the observed values, resulting in larger errors (for instance, the TKE scheme exhibits errors of -1.48 m/s and -0.92747, respectively). Therefore, based on both the wind speed error and gust factor error, the ECMWF scheme is able to reproduce the observed gust characteristics relatively well, with simulation results that match the observational data reasonably, although the absolute wind speed values are slightly overestimated. The other schemes, on the other hand, tend to underestimate both the gust intensity and its relative amplification.

Overall, the validation results indicate that, for conventional meteorological variables, the RBLM model performs well in simulating temperature and relative humidity—with small errors and well-matched trends—although there is a certain negative bias in wind speed simulation. Regarding the simulation of gust characteristics, although the model shows some bias in the mean wind speed (with simulated values slightly higher than the mean wind speed observed at the SORPES station), a comparative analysis of five parameterization schemes reveals that the ECMWF scheme produces gust factor results that are in good agreement with the observations.

This suggests that such a scheme can effectively capture the sudden intensification of gusts in the urban boundary layer, thereby providing reliable parameterization support for subsequent sensitivity experiments and studies on urban local effects.

Table 4.3 Data comparison analysis between SORPES station and the summer case model simulation results (10m above ground)

Scheme	Simulated Gust	Simulated Gust Factor	Gust Error	Gust Factor Error
ECMWF	6.23	2.07027	1.31	-0.00085
TKE	3.44	1.14366	-1.48	-0.92747
TKE2	3.21	1.06772	-1.71	-1.00341
Schreur	3.08	1.02373	-1.84	-1.0474
Nakamura	3.03	1.00802	-1.89	-1.0631

In summary, based on the comparative validation for the period from August 5 to 13, 2018, the RBLM model in this study demonstrates high accuracy in simulating temperature and humidity. Meanwhile, the gust model validation shows that selecting the ECMWF parameterization scheme can reasonably reproduce the relative strength of gusts observed in reality, although there is some overestimation in the absolute wind speed values. In future work, model parameters can be further optimized to account for the spatial heterogeneity of the wind field, thereby improving the overall consistency and regional applicability of the simulations.

Therefore, to study the influence of urban dynamic effects, thermodynamic effects, and the overall urban effect on gusts, three case analyses were conducted. As shown in Table 4.4, Case 1 is the control case—during the simulation, the land cover is urban, and the dynamic effects of buildings are considered. In contrast, Case 2 represents an urban land cover with the building effects removed. Case 3 represents a scenario in which the entire urban land cover is replaced with farmland, thereby also removing the building effects. Then, we subtract the simulation result of Case 1 from that of Case 2, which effectively isolates the influence of the dynamic effects from the overall urban effects. Since the overall urban effect on gusts consists of both dynamic and thermodynamic influences, subtracting the simulation result of Case 2 from that of Case 3 represents the removal of the thermodynamic effects. Finally, subtracting the simulation result of Case 1 from that of Case 3 yields the impact of removing the overall urban effects.

Table 4.4 Configuration of sensitivity experiments in the numerical model.

Case	Land Surface Type	Presence of Buildings
Case1	Urban	Yes
Case2	Urban	No
Case3	Non-urban	No

4.2 Analysis and Discussion of Gust Simulation Results

4.2.1 Spatial Distribution Characteristics

This section analyzes the spatial distribution characteristics of key meteorological variables across Nanjing and its surrounding areas during a specific summer period to elucidate the influence of urban morphology and underlying surfaces. Examining the wind field components first, the spatial variability of gust wind speed is detailed.Figures 4.1 and 4.2 present the spatial distribution characteristics of various meteorological variables over Nanjing and its surrounding areas during the period from August 5 to 13, 2018. These variables include gust wind speed, mean wind speed, gust factor, air temperature, surface temperature, relative humidity (RH), and turbulence kinetic energy (TKE). The figures provide insights into the relationships between urban morphology and meteorological elements, as well as the effects of urban underlying surfaces. The black dot indicates the location of the SORPES station.

Examining the wind field components first, the spatial variability of gust wind speed is detailed. Figure 4.1(a) shows that gust wind speeds in the Nanjing region exhibit significant spatial variability: in the urban center, where buildings are densely clustered, gust wind speeds are relatively low, generally around 6–7 m/s, whereas higher gust wind speeds occur in the urban periphery and more open areas (such as flat terrains with high vegetation cover in the suburbs), with maximum values reaching nearly 9.5–10 m/s. In the southwest and certain eastern local areas, gust values are relatively high, which may be associated with local terrain channels and wind corridor effects. The SORPES station, marked by a black circle in the figure, is located in the eastern part of the urban area; its relatively low gust values are consistent with the surrounding urban characteristics, indicating that the urban underlying surface has a significant suppressive effect on gust wind speeds—primarily due to the reduction in mean wind speed, which in turn lowers the overall gust speed.

Complementing the gust data, the spatial patterns of mean wind speed are also investigated.

Figure 4.1(b) illustrates the spatial distribution of mean wind speed over Nanjing during the same period. It can be seen that, due to the combined effects of dense urban structures, high surface roughness, and the urban heat island effect, the city center forms a low wind speed area (approximately 1.5 m/s), while higher wind speeds are observed at the urban margins and in suburban areas, creating a clear gradient.

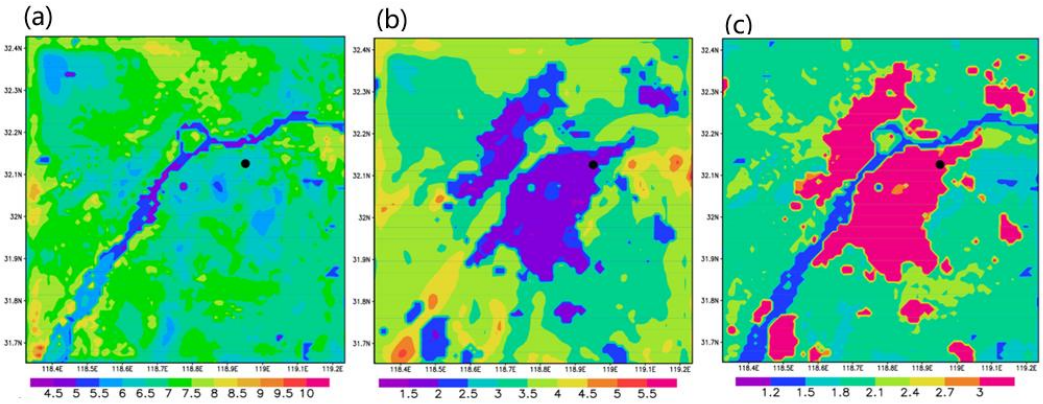

Figure 4.1 Spatial distribution characteristics of simulated meteorological elements in Nanjing from August 5 to August 13, 2018: (a) gust wind speed (m/s); (b) mean wind speed (m/s); (c) gust factor

To understand the relationship between gusts and mean wind, the distribution of the gust factor is analyzed. Figure 4.1(c) shows the spatial distribution of the gust factor (defined as the ratio of gust wind speed to mean wind speed). Overall, the gust factor is markedly higher in the urban center and in some densely built-up areas, reaching values of around 2.7–3 or more, indicating that although the mean wind speed is suppressed, local gust fluctuations are relatively enhanced. In contrast, in open or heavily vegetated suburban areas, the gust factor is mainly concentrated between 1.2 and 2.0. This distribution reveals the important role of urban structure in regulating local wind speed fluctuations and the formation of sudden, strong wind events.

Beyond wind characteristics, the spatial analysis extends to thermal properties, humidity, and turbulence kinetic energy. Figure 4.2(a) shows the spatial distribution of near-surface air temperature. Overall, due to the urban heat island effect and high building density, temperatures in the city center are higher, primarily ranging from 29.0 to 29.4 °C; whereas in the surrounding suburban and hilly areas, where surface conditions are better, temperatures are slightly lower, around 28.2–28.8 °C. Figure 4.2(b) depicts the spatial distribution of surface temperature, which exhibits a clear gradient with higher temperatures in the city center and lower temperatures in the

periphery. In the urban center, surface temperatures are generally above 30 °C, with some areas reaching 31–32 °C, while in suburban areas and near water bodies, surface temperatures mostly range between 24 and 28 °C. This pattern reflects the effects of urban surface heat accumulation and the differential influences of land and water on surface temperature. Figure 4.2(c) illustrates the spatial distribution of near-surface relative humidity. Overall, the southern and southwestern parts of the city exhibit relatively low relative humidity, approximately 71–75%, whereas the eastern and parts of the city center show higher relative humidity, reaching about 78–82%. Figure 4.2(d) presents the spatial distribution of turbulence kinetic energy (TKE). It can be seen that TKE values are higher in the city center, ranging from approximately 0.15 to 0.3, indicating that dense high-rise buildings and anthropogenic heat emissions significantly enhance turbulence in the urban boundary layer. In contrast, in suburban and more open areas, TKE values are generally lower, only in the range of 0.05–0.1.

In summary, Figures 4.1 and 4.2 comprehensively present the spatial distribution characteristics of gusts, mean wind speed, gust factor, air temperature, surface temperature, relative humidity, and turbulence kinetic energy in the Nanjing region during the period from August 5 to 13, 2018. Overall, the urban center, due to dense buildings, high surface roughness, and the urban heat island effect, exhibits relatively low mean and gust wind speeds, but the gust factor and TKE are significantly enhanced, while both air and surface temperatures are elevated. In contrast, suburban and open areas show higher wind speeds, lower gust factors, and relatively lower temperatures. These results clearly reflect the combined regulatory effects of surface characteristics and local thermal and dynamic processes on the wind field structure and thermal environment in urban areas, thereby providing a solid empirical basis for further discussion of gust characteristics and their influencing factors.

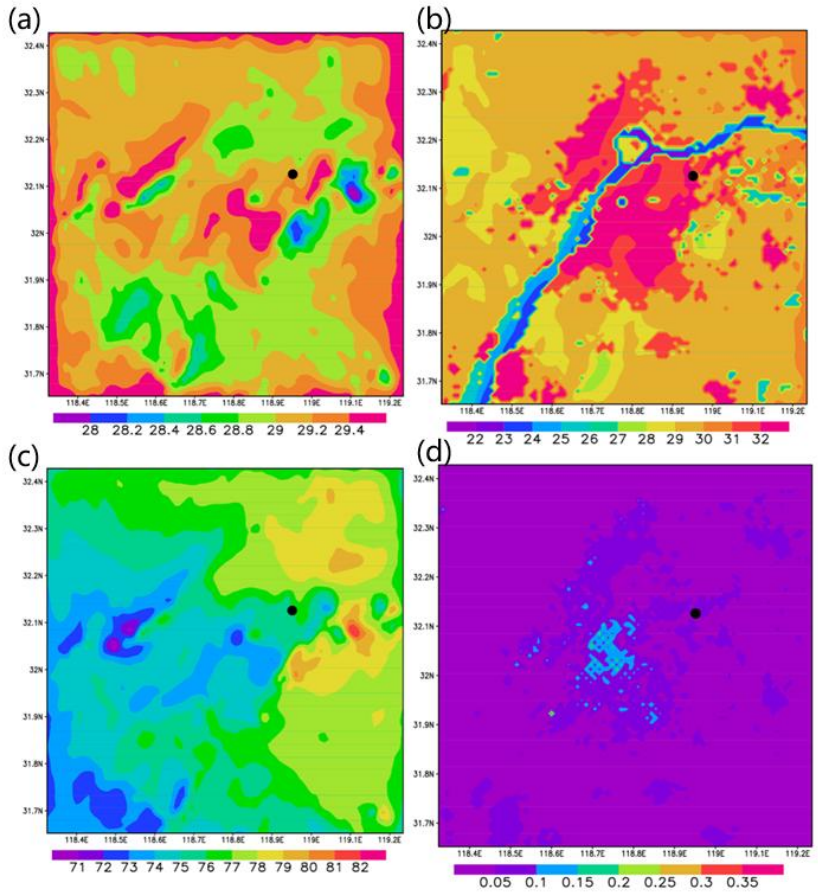

Figure 4.2 Spatial distribution characteristics of simulated meteorological elements in Nanjing from August 5 to August 13, 2018: (a) air temperature (℃); (b) surface temperature (℃); (c) relative humidity (%); (d) turbulent kinetic energy (J/kg)

4.2.2 Temporal Distribution Characteristics

This section focuses on the temporal distribution characteristics, specifically the diurnal variations, of key meteorological variables within the Nanjing urban environment during the same summer period, aiming to reveal the interplay of urban surface properties and thermal processes. Figures 4.3(a)–(d) display the hourly variations of the average gust wind speed, mean wind speed, gust factor, and turbulence kinetic energy (TKE) in the Nanjing region during the period from August 5 to August 13, 2018. By comparing the diurnal patterns of these variables, we can gain a deeper understanding of how urban underlying surface properties and thermal processes jointly shape the wind field structure and turbulent activity during Nanjing's summer.

The diurnal pattern of gust wind speed is first examined to understand its daily cycle. Figure

4.3(a) shows that during the early morning hours (01:00–05:00), the gust wind speed is relatively low at about 5 m/s; subsequently, from early morning to late morning (06:00–11:00), it slowly increases, and in the afternoon (12:00–15:00) it rises rapidly, reaching its daily peak of approximately 9.5–10 m/s between 16:00 and 18:00. In the evening and night (19:00–24:00), the gust wind speed gradually decreases and tends to return to low values by late night. This diurnal variation is mainly controlled by the evolution of the boundary layer height and the urban heat island effect: at night, radiative cooling and the high surface roughness of the city suppress near-surface turbulence, resulting in lower gust speeds; during the day, enhanced solar radiation increases convective mixing, causing gust speeds to climb rapidly in the afternoon to their highest levels; and as the surface cools in the evening and at night, the weakening of turbulent activity leads to a decline in gust speed.

Following this, the hourly variations of mean wind speed are analyzed to compare its diurnal cycle with that of gust speed. Figure 4.3(b) illustrates that the mean wind speed is only about 2.4–2.7 m/s during the early morning (01:00–05:00), then begins to rise at around 06:00, exceeding 3.5 m/s by midday (11:00–13:00), and reaching a peak of about 4.3–4.5 m/s in the afternoon (14:00–17:00). From the evening to night (18:00–22:00), the mean wind speed gradually declines to approximately 3.0 m/s. Compared with the gust wind speed, the peak in mean wind speed occurs slightly earlier, but is still concentrated during the period of most active convection and urban heat island effect in the afternoon to early evening. At night and in the early morning, due to the combined effects of radiative cooling and stable stratification over the urban surface, near-surface wind speeds remain low; during the day, as the ground heats up, enhanced turbulent mixing causes the mean wind speed to rise, creating a clear diurnal cycle.

The diurnal behavior of the gust factor is then investigated to assess the daily changes in the relative intensity of gusts. Figure 4.3(c) shows the diurnal variation of the gust factor (the ratio of gust wind speed to mean wind speed). Overall, the gust factor remains relatively stable at about 2.1–2.2 during the early hours (01:00–06:00), then rises rapidly in the afternoon (15:00–19:00) to reach a daily peak of approximately 2.45 around 19:00, before slightly decreasing yet remaining around 2.25. This pattern indicates that, although the mean wind speed also increases in the afternoon, the instantaneous wind speed fluctuations become more pronounced, leading to a surge in the gust factor during this period. Even though the gust factor decreases somewhat at night due

to surface cooling and weakened turbulence, it still remains at a certain level, reflecting the persistent influence of urban building clusters and thermal processes on wind speed variability.

Finally, the diurnal cycle of turbulence kinetic energy (TKE) is explored to understand the daily evolution of turbulent activity. Figure 4.3(d) displays the spatial distribution of TKE. TKE is relatively low during the night and early morning (00:00–06:00), typically below 0.01 m^2/s^2; it then rises rapidly after early morning (07:00–08:00), reaching a peak (approximately 0.09–0.10 m^2/s^2) in the afternoon (12:00–15:00), and subsequently drops significantly in the early evening (17:00–19:00) before settling at lower levels again at night. From a dynamical and thermal perspective, the diurnal variation of TKE is closely related to the evolution of the boundary layer height and the urban heat island effect: stable stratification at night weakens turbulence intensity, while increased solar radiation in the morning heats the surface, intensifying convective mixing and turbulent activity, which ultimately culminates in the highest TKE in the afternoon; as the surface cools again at night, turbulent activity decays and TKE correspondingly decreases.

In summary, Figures 4.3(a)–(d) illustrate that, during the period from August 5 to August 13, 2018, the average wind speed, gust factor, and TKE in the Nanjing region exhibit significant diurnal variations. The stable stratification during the night and early morning leads to low wind speeds and turbulence intensity; during the day—especially from the afternoon to early evening—the enhancement of the urban heat island effect and increased instability cause rapid increases in gust wind speed, mean wind speed, and TKE, with the gust factor also peaking during this period. The roughness of the urban surface and associated thermal processes play critical roles in modulating the diurnal cycles of these variables, thereby providing empirical support for further analysis of the causes and influencing mechanisms of urban gust characteristics.

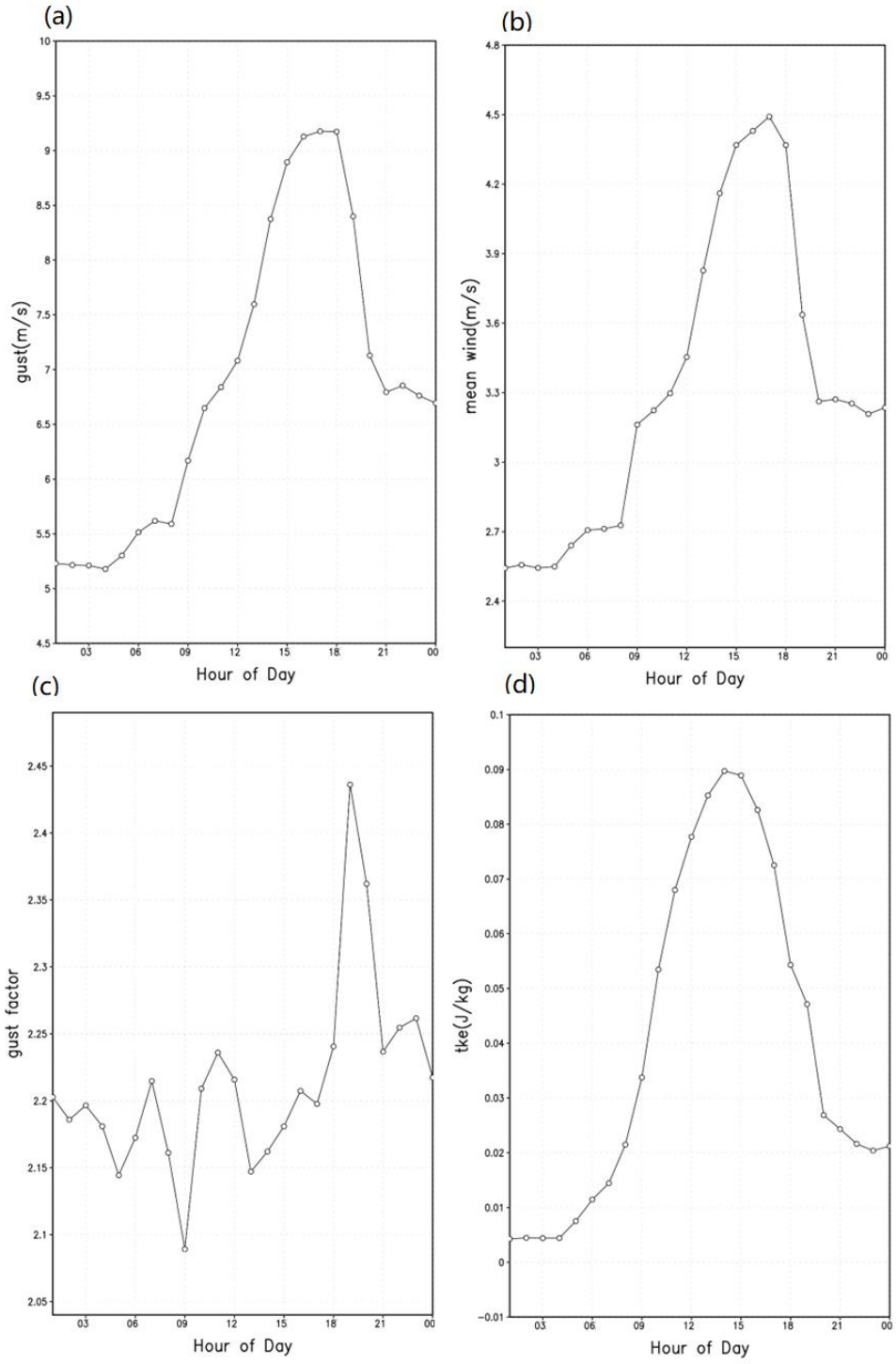

Figure 4.3 Hourly variation of simulated gust wind speed (a), mean wind speed (b), gust factor (c), and turbulent kinetic energy (d) in the Nanjing region from August 5 to August 13, 2018

4.3 Impact of Urban Environment on Gust Characteristics

4.3.1 Influence of Urban Building Dynamics on Gust Characteristics

To investigate the influence of urban buildings on the gust characteristics and related meteorological variables in the Nanjing region, this study designed two scenarios—"with buildings" and "without buildings"—and computed the difference fields between the two. Figures 4.4 and 4.5 respectively show the spatial distributions of the differences (without buildings minus with buildings) in gust wind speed, mean wind speed, gust factor, air temperature, surface temperature, relative humidity, and turbulence kinetic energy (TKE). By comparing these differences, the key role of urban buildings in either dampening or enhancing gusts, as well as in modulating local thermal processes and turbulent activity, can be directly assessed.

Focusing first on the wind field, the impact of buildings on gust wind speed is examined through the difference fields. Figure 4.4(a) shows that after removing buildings, gust wind speeds in urban areas—especially in the city center—increase by between 0.2 and 1.0 m/s, with the highest increases in the center reaching around 0.8–1.0 m/s. This indicates that, under the "with buildings" scenario, urban structures significantly reduce instantaneous wind speeds; the high roughness due to dense building clusters has a marked blocking effect on gust formation. In contrast, the differences in more peripheral or open areas are relatively small, suggesting that building density has a limited impact on gusts in suburban areas.

Similarly, the influence of urban structures on mean wind speed is assessed by analyzing the differences between the two scenarios. Figure 4.4(b) shows that, similar to gust wind speed, the mean wind speed in the city also generally increases after buildings are removed, with maximum differences reaching about 0.35–0.4 m/s; in suburban or relatively open regions, the increase is lower, around 0.05 m/s. Under the "with buildings" scenario, the height and density of buildings exert a strong drag on the near-surface wind field, thereby suppressing mean wind speed; once the buildings are removed, the wind speed in the city center increases markedly, demonstrating the prominent role of high building density and roughness in reducing urban wind speeds.

The analysis then turns to how buildings affect the gust factor, which indicates changes in the relative intensity of gusts. Figure 4.4(c) shows that the gust factor (the ratio of gust wind speed to mean wind speed) exhibits negative differences in most urban areas, with the maximum decrease in the city center reaching up to 0.18; in some peripheral urban areas, the values even

increase slightly, though the increase is relatively minor. This means that after removing buildings, although both gust and mean wind speeds increase in urban areas, the increase in mean wind speed is more pronounced, resulting in an overall decrease in the gust factor. Under the “with buildings” scenario, urban structures tend to enhance turbulence and local disturbances, thereby elevating the amplification of instantaneous wind speed relative to the mean wind speed. In a few areas on the outskirts of the city center, a slight positive difference is observed, indicating that there the increase in gust speed slightly exceeds that of the mean wind speed when buildings are removed.

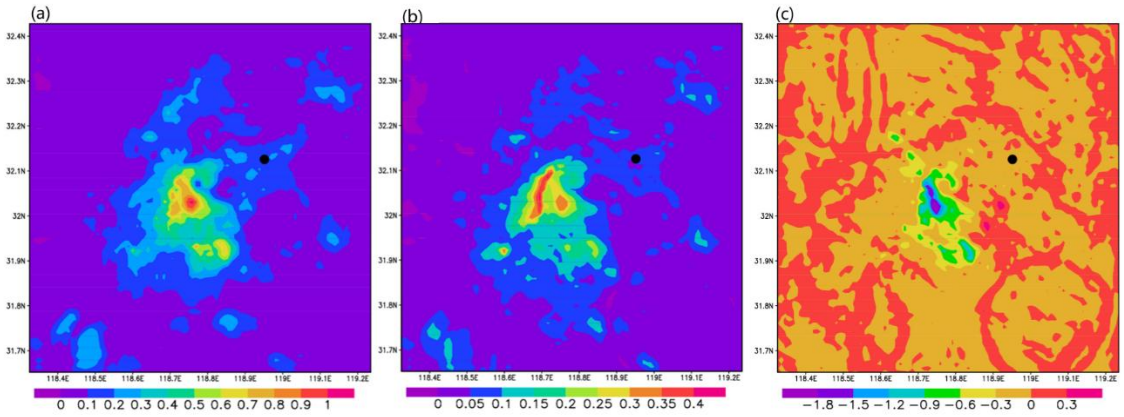

Figure 4.4 Spatial distribution characteristics of the differences in simulated meteorological elements in Nanjing between the "No-Building" and "With-Building" scenarios ("No-Building" − "With-Building") from August 5 to August 13, 2018: (a) gust wind speed (m/s); (b) mean wind speed (m/s); (c) gust factor ($\times 10^{-1}$)

Beyond wind characteristics, the thermal impact of buildings is explored, beginning with the differences in air temperature. Figure 4.5(a) shows that the temperature differences are generally distributed between -0.06 and +0.12 °C. In the city center, the differences are negative, indicating that after the buildings are removed, the air temperature decreases by about 0–0.09 °C; whereas in the peripheral areas, there are slight positive differences (up to about +0.10–+0.12 °C), suggesting a slight warming in those regions after the removal of buildings. This implies that in the central area, buildings contribute to higher local temperatures by storing heat and blocking heat loss, so that removing them facilitates heat diffusion and leads to a temperature drop, while in the peripheral areas, the reshaping of the wind field and thermal circulation may result in a slight temperature increase.

The influence on surface temperature is also a key aspect of the urban thermal environment affected by buildings. Figure 4.5(b) shows that after removing buildings, the surface temperature

in urban areas mostly decreases by about 0–0.1 °C, whereas in some peripheral areas it slightly increases by 0–0.06 °C. Dense urban buildings in the city center, under the “with buildings” scenario, tend to accumulate solar radiation and experience insufficient heat loss at night, resulting in higher surface temperatures; once these buildings are removed, the decrease in surface roughness and improved ventilation enhance heat dissipation in the center, leading to a reduction in surface temperature. Conversely, in some transitional zones, the removal of buildings leads to a re-distribution of the wind field or heat, causing a slight increase in surface temperature. Overall, buildings reinforce the urban heat island effect in the central area, which is alleviated when they are removed.

Changes in relative humidity due to the presence of urban structures are then considered. Figure 4.5(c) shows that the differences in near-surface relative humidity (RH) exhibit a complex pattern of both positive and negative values, ranging from approximately -0.5 to +0.3. In some parts of the city center, RH increases slightly (by 0–0.3), possibly because the decrease in air and surface temperatures alters local moisture transport and evaporation characteristics; whereas in the urban periphery, there are distinct negative differences (0 to -0.5), indicating that the micro-circulation created by the building pattern is disrupted or that moisture is transported elsewhere, resulting in reduced RH.

Finally, the impact of buildings on turbulence kinetic energy (TKE) is investigated to understand changes in turbulent activity. Figure 4.5(d) shows that the vast majority of urban areas and their surroundings exhibit negative differences in TKE, mostly within 0–0.1 J/kg, indicating that turbulence intensity is significantly reduced after the removal of buildings. Under the “with buildings” scenario, dense high-rises enhance turbulence through increased surface roughness, shear, and local convection; when the buildings are removed, near-surface disturbances are markedly reduced. In peripheral and open areas, the differences are smaller, showing that the low building density in these regions means that their contribution to turbulence generation is limited.

A systematic comparison of the difference distributions in Figures 4.4 and 4.5 shows that urban buildings play a crucial role in suppressing both the mean wind speed and instantaneous wind speed (gusts) in the urban area, while to some extent enhancing the gust factor and turbulence intensity. At the same time, urban building clusters exert a dual regulatory effect on the urban thermal environment: air and surface temperatures in the central area are significantly elevated

(forming a “heat island” effect), whereas some peripheral areas may exhibit the opposite change. As for relative humidity, its behavior varies across different regions, indicating that the complex coupling among building patterns, local wind fields, and moisture transport warrants further investigation.

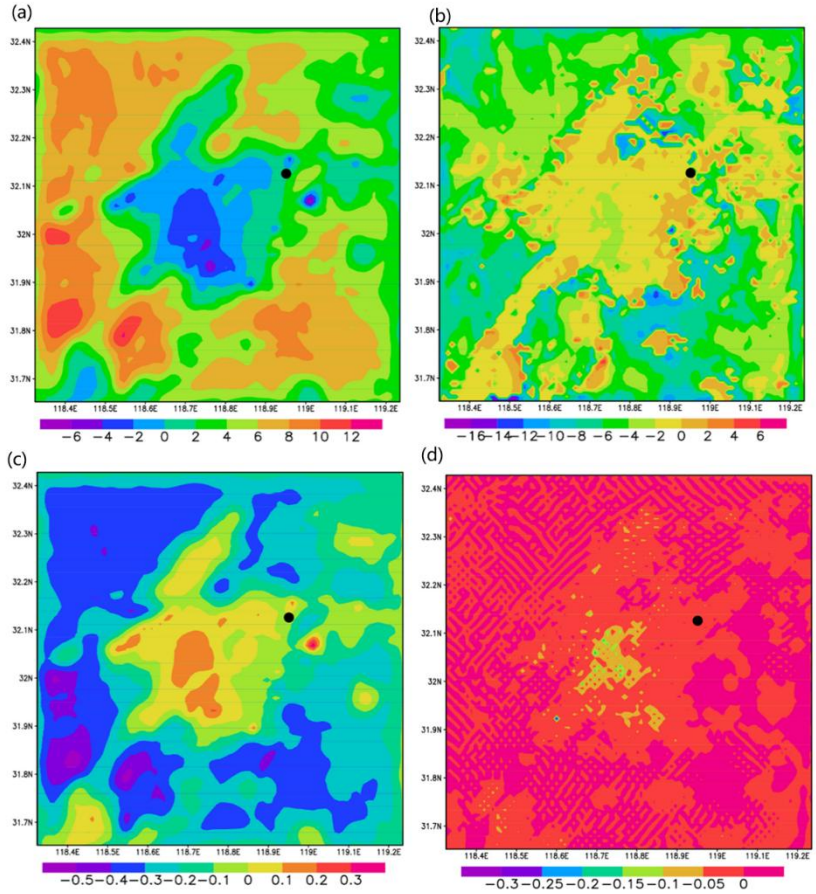

Figure 4.5 Spatial distribution characteristics of the differences in simulated meteorological elements in Nanjing between the "No-Building" and "With-Building" scenarios ("No-Building" − "With-Building") from August 5 to August 13, 2018: (a) air temperature (×10⁻²°C); (b) surface temperature (×10⁻²°C); (c) relative humidity (%); (d) turbulent kinetic energy (J/kg)

The results of this sensitivity experiment indicate that after the removal of buildings, both gust and mean wind speeds in the city center generally increase, whereas the gust factor and TKE generally decrease; air and surface temperatures in the central urban area drop by a certain amount, while some peripheral areas may experience a slight increase. These findings demonstrate that urban buildings significantly influence the weakening of wind speeds, the enhancement of turbulent disturbances, the exacerbation of the urban heat island effect, and the regulation of local

humidity, making them important factors in shaping the structure of the urban boundary layer and the characteristics of gusts.

To further explore the regulatory effects of urban buildings on gusts and related variables over time, this section compares the hourly differences (calculated as “without buildings” minus “with buildings”) under two scenarios for gust wind speed, mean wind speed, gust factor, and turbulence kinetic energy (TKE). Figures 4.6(a)–(d) present the hourly difference curves for these four variables, respectively.

Examining these temporal differences, the hourly variation in the impact on gust wind speed is first detailed. Figure 4.6(a) shows the hourly variation in gust wind speed differences. The differences are essentially positive, with values near 0 at midnight. Starting from the early morning, the difference gradually increases and reaches high values of 0.10–0.12 m/s during the afternoon to early evening (12:00–21:00); during the day, although there are slight fluctuations, the difference remains above 0.07 m/s. From a dynamical perspective, the stable stratification during the night and early morning suppresses turbulence and the enhancement of instantaneous wind speed, resulting in limited differences between the “with buildings” and “without buildings” cases; in contrast, during the day and evening, when convection is more active, the absence of building-induced blockage significantly reduces near-surface roughness, allowing enhanced momentum transfer and thus a more pronounced increase in gust wind speed. The overall positive difference indicates that, when buildings are removed, the gust wind speed is higher at all hours compared to the original scenario, once again confirming the significant weakening effect of dense urban high-rises on instantaneous strong winds.

Next, the diurnal pattern of differences in mean wind speed between the two scenarios is considered. Figure 4.6(b) presents the hourly differences in mean wind speed between the two scenarios. Starting from 01:00, the difference quickly rises to about 0.03–0.06 m/s, with peak values (around 0.06 m/s) occurring during certain periods (e.g., around 18:00). Although the difference slightly decreases at night, it remains positive. This indicates that during the day and evening, the drag effect of buildings on mean wind speed is most significant; when buildings are removed, the near-surface wind field becomes considerably more open, resulting in a larger increase in mean wind speed. At night, due to the generally weaker wind and turbulence, the influence of buildings is relatively limited. This diurnal pattern is consistent with the differences

observed in gust wind speed, again highlighting the role of urban buildings in weakening the urban wind field during the day through high roughness and thermal processes.

The influence of buildings on the gust factor throughout the day is then explored by analyzing its hourly differences. Figure 4.6(c) shows the hourly variations in the difference of the gust factor (the ratio of gust wind speed to mean wind speed). Overall, the differences are predominantly negative throughout the day, around -0.01 to 0, with the oscillation amplitude gradually diminishing and turning positive around 22:00, reaching a short-lived peak of approximately +0.006. This phenomenon can be explained as follows: under the "with buildings" scenario, although the mean wind speed is suppressed, the buildings enhance the incremental increase of instantaneous wind speed relative to the mean, resulting in a higher gust factor; once the buildings are removed, the greater increase in mean wind speed causes the gust factor to decrease slightly during most hours. However, in the early evening, local dynamic and thermal conditions may shift, resulting in a relatively more pronounced increase in instantaneous wind speed or a slower increase in mean wind speed, so that in the "without buildings" scenario the gust factor briefly exceeds that of the "with buildings" case. Overall, the magnitude of the differences is small (within ±0.01), indicating that although urban buildings consistently influence the gust factor, this effect is moderated on a temporal scale by boundary layer processes and the urban heat island effect.

Finally, the temporal changes in turbulence kinetic energy (TKE) due to the presence of buildings are assessed through their hourly differences. Figure 4.6(d) displays the hourly differences in TKE between the two scenarios, which are all negative (ranging from -0.01 to 0 m^2/s^2), indicating that TKE is generally lower in the "without buildings" case compared to the original scenario. During the early hours (01:00–07:00), the differences are relatively small; from early morning to the afternoon (08:00–15:00), the differences become markedly negative, reaching a minimum of about -0.012 J/kg, and then slightly rebound in the early evening while still remaining negative. This finding is consistent with the conclusion that during the day, dense urban buildings significantly enhance turbulence through increased surface roughness, shear, and local thermal disturbances; when the buildings are removed, the substantial reduction in roughness leads to a decrease in near-surface shear and convective mixing, resulting in a pronounced decay in TKE.

In summary, the diurnal difference analysis in Figures 4.6(a)–(d) indicates that after the

removal of buildings, both the gust wind speed and mean wind speed in the urban center and observation areas increase during most hours, particularly during the day and evening; in contrast, the gust factor and TKE generally decrease during most hours. This underscores the important role that urban buildings play in “suppressing wind speeds while enhancing relative fluctuations and turbulent activity.” The relatively smaller differences during the night and early morning reflect that under conditions of stable stratification and generally weak wind, the impact of buildings is diminished. These temporal results are consistent with the spatial difference analysis discussed earlier, further corroborating the key role of urban buildings in shaping urban gust characteristics and their environmental impacts.

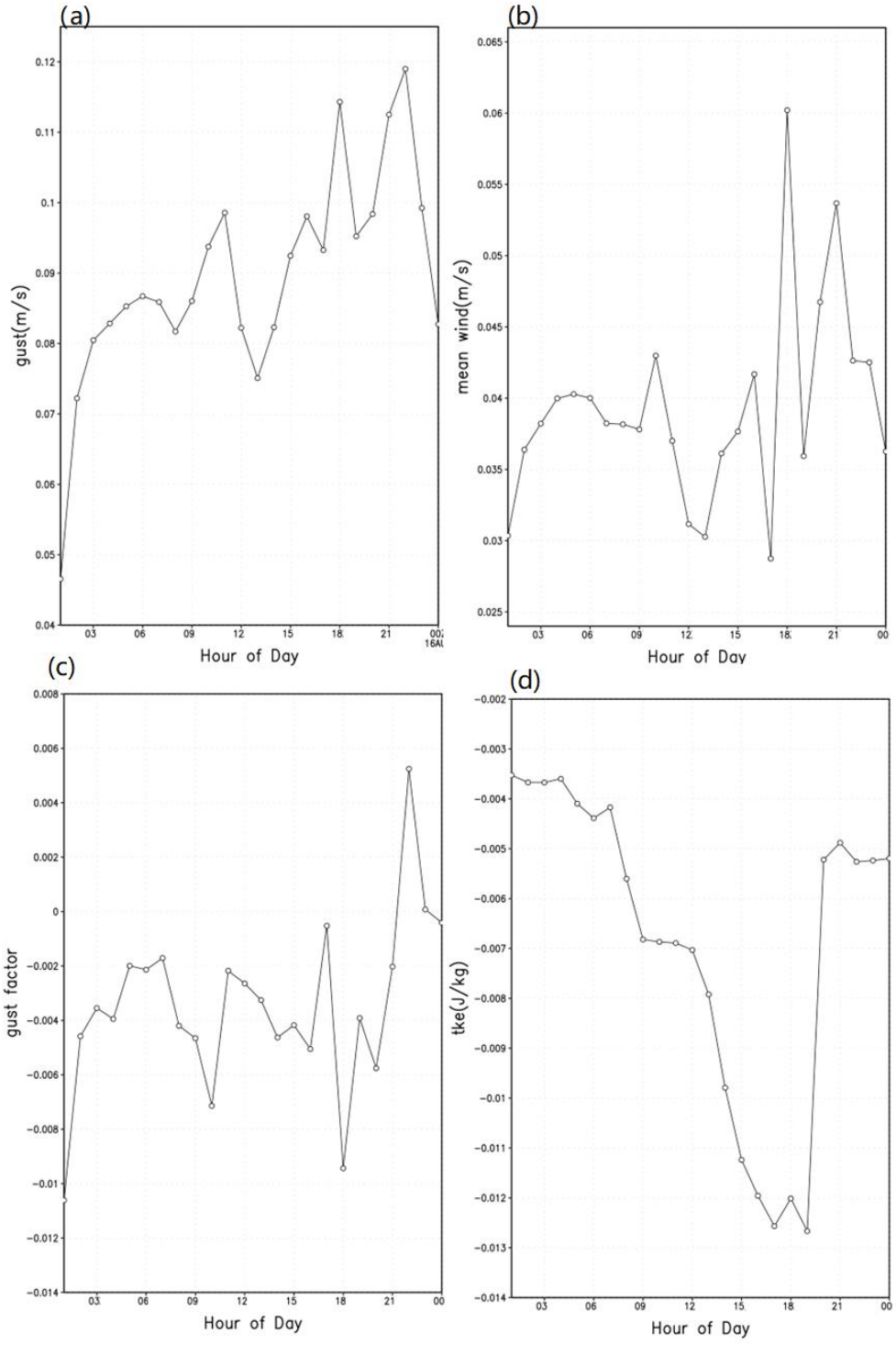

Figure 4.6 Hourly variation of the differences between the "No-Building" and "With-Building" scenarios ("No-Building" − "With-Building") for simulated gust wind speed (a), mean wind speed (b), gust factor (c), and turbulent kinetic energy (d) in the Nanjing region from August 5 to August 13, 2018

4.3.2 The Impact of Urban Thermodynamic Effects on Gust Characteristics

Because urban gusts are primarily influenced by dynamic and thermodynamic effects, this study investigates the impact of urban thermodynamic effects on gusts by subtracting the "urban without buildings" case from the "no urban" case. In principle, the influence of thermodynamic effects on gusts is obtained by subtracting the case that removes comprehensive urban effects from the case that removes only dynamic effects.

Examining the spatial impact of these thermodynamic effects, the changes induced in gust wind speed are first considered. Figure 4.7(a) illustrates the impact of pure thermodynamic effects on gust wind speed over Nanjing from August 5 to 13, 2018, obtained by subtracting the "With City, No Buildings" scenario from the "No City" scenario (negative values indicate that thermodynamic effects enhance wind speed). Spatially, the greatest differences occur in the central urban area, with values between –1.6 and –0.8 m/s. Moving outward, the effect weakens gradually: at the urban fringe and inner suburbs, differences lie mostly between –0.8 and –0.2 m/s; beyond the study domain in open areas, values approach zero or even show slight positive values, indicating minimal thermodynamic influence there. Urban thermodynamic effects amplify boundary-layer instability and turbulent activity, markedly increasing gust strength in the city core and tapering off toward open regions.

The influence of urban thermodynamic effects on the spatial distribution of mean wind speed is then analyzed. Figure 4.7(b) shows the mean wind speed difference for the same subtraction. In the central city, differences are generally positive, ranging from 0.9 to 1.8 m/s and locally reaching up to 2.1 m/s, which implies that retaining thermodynamic effects ("With City, No Buildings") significantly suppresses mean wind speed. Toward the urban edge and suburbs, the difference decreases to near zero or slight negative values (around –0.3 m/s), suggesting that thermodynamic effects have little to no suppressive impact—and may even slightly enhance—mean wind speed in these open areas. By strengthening boundary-layer instability and vertical heat transport, urban thermodynamic effects reduce mean wind speed most in the city center, with their influence diminishing outward and becoming neutral in the suburbs.

Subsequently, the way urban thermodynamic effects alter the gust factor across the study area is investigated. Figure 4.7(c) presents the gust factor difference after subtraction, predominantly negative, indicating that urban thermodynamic effects substantially increase the gust factor. In the

central city, values cluster between –1.8 and –0.9, meaning the gust factor there rises by 0.9–1.8; in some hotspots, differences exceed –2.0, corresponding to increases over 2.0. Toward the urban fringe and inner suburbs, differences approach –0.3, showing a reduced enhancement; in open areas and at the domain boundary, values converge on zero, indicating that thermodynamic effects on gust factor are nearly absent outside the urban core. Urban thermodynamic effects thus amplify relative gust intensity in the city center by reinforcing boundary-layer instability, with their impact fading toward the suburbs.

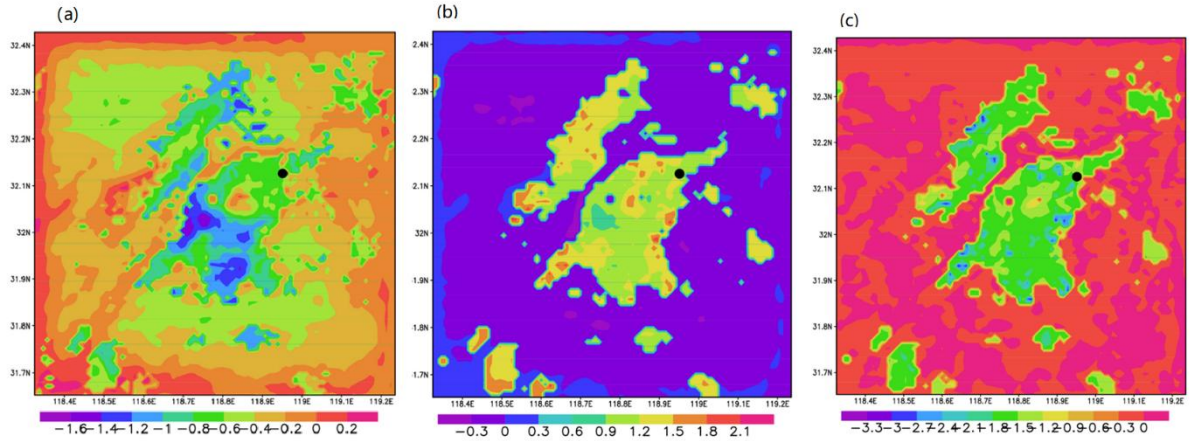

Figure 4.7 Spatial Distribution Characteristics of the Differences in Simulated Meteorological Elements for the Nanjing Region Between the “No Urban” Case and the “Urban Without Buildings” Case for August 5–13, 2018: (a) Gust wind speed (m/s); (b) Mean wind speed (m/s); (c) Gust factor.

Turning to thermal impacts, the modulation of surface air temperature by urban thermodynamic effects is now detailed. Figure 4.8(a) shows the difference obtained by subtracting the “With City, No Buildings” case from the “No City” case, revealing how urban thermodynamic effects modulate surface air temperature. Overall, most of the urban area exhibits negative values, indicating that when anthropogenic heat sources are retained (“With City, No Buildings”), thermodynamic effects generally raise surface temperature. The largest temperature differences, between –1.2 and –0.8 °C, occur in the city core, implying that the urban heat island there can increase air temperature by 0.8–1.2 °C. Moving outward, this warming effect gradually weakens, with values around –0.5 to –0.3 °C at the urban fringe; beyond the study domain and in distant suburbs, differences approach zero, suggesting that in open areas the thermodynamic influence is

minimal or dissipated by ventilation corridors. Urban thermodynamic effects elevate temperatures in the city center by enhancing surface and boundary-layer heat storage and instability, then taper off with distance.

The analysis continues with the impact of these effects on surface temperature, a key indicator of the urban heat island. Figure 4.8(b) maps the same subtraction applied to surface temperature, again yielding mostly negative values and thus confirming a significant urban warming. In the central urban area, differences range from –3.5 to –5 °C, meaning that with anthropogenic heat the surface there is about 3.5–5 °C warmer than in a completely "No City" scenario. Toward the suburbs, the warming decreases to within –1 °C or even near zero, indicating that the thermodynamic effect on surface temperature essentially vanishes in outlying areas. Artificial surfaces and anthropogenic heat release heighten heat storage and boundary-layer instability, producing the strongest heat-island warming in the urban core and diminishing outward.

The influence of urban thermodynamic processes on near-surface relative humidity is also explored. Figure 4.8(c) depicts relative-humidity differences from the "No City" minus "With City, No Buildings" case, showing predominantly positive values. This indicates that urban thermodynamic effects reduce air humidity in and around the city center. In the core area, relative-humidity drops by about 3–5.5 percentage points under anthropogenic heating. Moving toward the edge of the city, this decrease falls to 2–3 percent, and in far-flung open areas it is below 1 percent, demonstrating a rapid decline in humidity impact with distance. By raising surface and boundary-layer temperatures and enhancing evaporation and vertical mixing, urban thermodynamic effects markedly lower relative humidity in the core before weakening outward.

For the spatial analysis, the impact of urban thermodynamic effects on turbulence kinetic energy is also assessed. Figure 4.8(d) presents turbulence-kinetic-energy (TKE) differences after subtracting "With City, No Buildings" from "No City," which are mostly positive. This shows that, with anthropogenic heating retained, thermodynamic effects actually suppress boundary-layer turbulence. The largest increases—between 0.03 and 0.15 J kg^{-1}—are concentrated near the city center, meaning that removing thermodynamic effects would boost TKE there by roughly 0.03–0.15 J kg^{-1}. Toward the urban edge, differences quickly fall below 0.03 J kg^{-1} and approach zero in the suburbs, indicating that the suppression of turbulence by heating is confined to the urban core. Urban thermodynamic effects thus reinforce boundary-layer stability, locally inhibiting

turbulent energy mainly in the city center and fading outward.

To elucidate the temporal dynamics of these urban thermodynamic impacts, their hourly variations on key wind and turbulence parameters are now examined. Figure 4.9 shows the hourly differences between the “No City” and “With City, No Buildings” scenarios for simulated gust wind speed (a), mean wind speed (b), gust factor (c), and turbulence kinetic energy (d) over Nanjing from August 5 to 13, 2018, in order to reveal the diurnal pattern of urban thermodynamic effects.

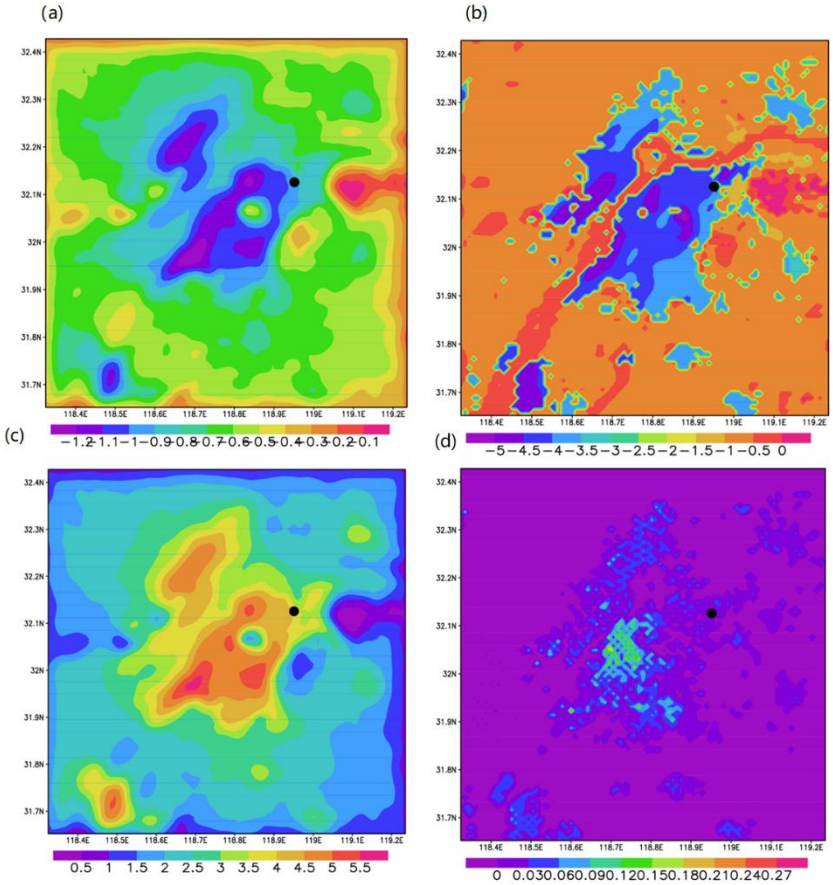

Figure 4.8 Spatial distribution of the differences in simulated meteorological variables over Nanjing from August 5 to 13, 2018, between the “No City” and “With City, No Buildings” scenarios ("No City " − " With City, No Buildings "): (a) air temperature (℃); (b) surface temperature (℃); (c) relative humidity (%); (d) turbulence kinetic energy (J/kg).

Focusing first on gust wind speed, the diurnal cycle of its alteration by thermodynamic effects

is detailed. In Figure 4.9(a), the “No City” minus “With City, No Buildings” gust speed difference remains negative throughout, indicating that thermodynamic effects always enhance gusts. This enhancement varies by hour: from 01:00 to 08:00 the difference is small (around –0.1 to –0.2 m/s); at 09:00 it jumps to about –0.6 m/s; around noon it falls back to –0.3 m/s, then strengthens again between 12:00 and 14:00; from 15:00 to 17:00 it weakens to –0.4 to –0.7 m/s; it peaks at –0.88 m/s between 18:00 and 19:00; from 20:00 to 21:00 it drops sharply to about –0.05 m/s; and between 22:00 and midnight it stabilizes at roughly –0.1 m/s. This pattern reflects the urban heat island’s effect in destabilizing the boundary layer most strongly in the afternoon, with weaker enhancement overnight and in the early morning.

Next, the hourly influence of urban thermodynamic processes on mean wind speed is analyzed. Figure 4.9(b) plots the hourly mean wind speed differences. Most values are positive, showing that thermodynamic effects generally suppress mean winds, though slight enhancement occurs at times. Specifically, at 01:00 the difference is about 0.17 m/s; it slowly falls to 0.13 m/s by 04:00; rises again to about 0.18 m/s by 07:00; then plunges between 08:00 and 09:00 to –0.01 m/s, indicating a brief mean‑wind enhancement; from 10:00 to 18:00 it remains positive, oscillating between 0.05 and 0.24 m/s; at 19:00 it briefly dips to –0.07 m/s, the day’s minimum; between 18:00 and 23:00 it peaks at 0.26–0.29 m/s, showing strongest suppression in the evening; and by midnight it drops back to around 0.15 m/s. This diurnal cycle suggests that heating suppresses mean winds most effectively at dusk and that vertical mixing or local circulations partly offset this suppression during transition periods.

The investigation continues with the daily pattern of changes in the gust factor due to these thermodynamic effects. In Figure 4.9(c), the gust factor difference is negative at all hours, indicating a continuous amplification of gust factor by thermodynamic effects, though with clear fluctuations: at 01:00 the difference is about –0.27; it deepens to –0.28 to –0.31 between 02:00 and 07:00; weakens to around –0.21 at 08:00; rises to –0.36 at 10:00; oscillates between –0.28 and –0.36 from 11:00 to 19:00; peaks at –0.46 at 20:00; and returns to –0.27 by midnight. Thus, daytime and early evening heating amplify gust factor most effectively, while enhancements are smaller in the morning and late at night.

Finally, the diurnal variation of turbulence kinetic energy (TKE) as influenced by urban thermodynamic effects is explored. Figure 4.9(d) presents the turbulence kinetic energy (TKE)

differences, which exhibit two distinct trends over 24 hours. From 01:00 to 08:00, the difference is slightly positive (about 0.0018–0.003 J/kg), meaning that removing urban heat slightly increases TKE at night and early morning. After sunrise, between 09:00 and 10:00, the difference rapidly becomes negative, reaching a minimum of –0.008 J/kg around 10:00, indicating strong TKE suppression by thermodynamic effects in the late morning. From 11:00 to 18:00, it climbs back above zero and peaks near 0.009 J/kg, showing midday enhancement; however, between 09:00 and 13:00 the negative values confirm that heating intensifies turbulence then. From 14:00 through the night, aside from a small dip at 19:00, differences remain positive and large in the evening, indicating that heating again suppresses TKE in the afternoon and night. This cycle reveals that thermodynamic effects vary by daypart: they suppress turbulence in the morning, afternoon, and night, with the strongest suppression at night, and briefly enhance it around noon.

By subtracting the "With City, No Buildings" scenario from "No City," this study successfully isolates urban thermodynamic effects on gusts and related meteorological elements over Nanjing. Spatially, these effects peak in the city core—gust speeds increase by 0.8–1.6 m/s, gust factor rises by 0.9–1.8, and mean winds are suppressed by 0.9–2.1 m/s; surface temperature and air temperature climb by about 3.5–5.0 °C and 0.8–1.2 °C, respectively; relative humidity falls by 3–5.5 percentage points; and TKE is locally reduced by 0.03–0.15 J/kg. All of these enhancements or suppressions decay outward, approaching zero in open suburbs.

Temporally, the enhancement of gust speed and suppression of mean wind both exhibit clear diurnal cycles: gust enhancement is strongest in daytime and weakest at night and dawn (–0.1 to –0.2 m/s); mean‐wind suppression peaks at 0.25–0.3 m/s at night, with brief enhancement near 09:00 and 19:00; gust factor follows a similar pattern; and TKE is suppressed in the morning and evening but briefly enhanced at midday. These results demonstrate that urban thermodynamic effects, by increasing boundary‐layer instability and vertical mixing, produce a strong‐center, weak‐edge heat‐island–gust coupling in space and intensify gust events, increase gust factors, and weaken mean winds and turbulence energy in space and time following the daily cycle of the urban heat island.

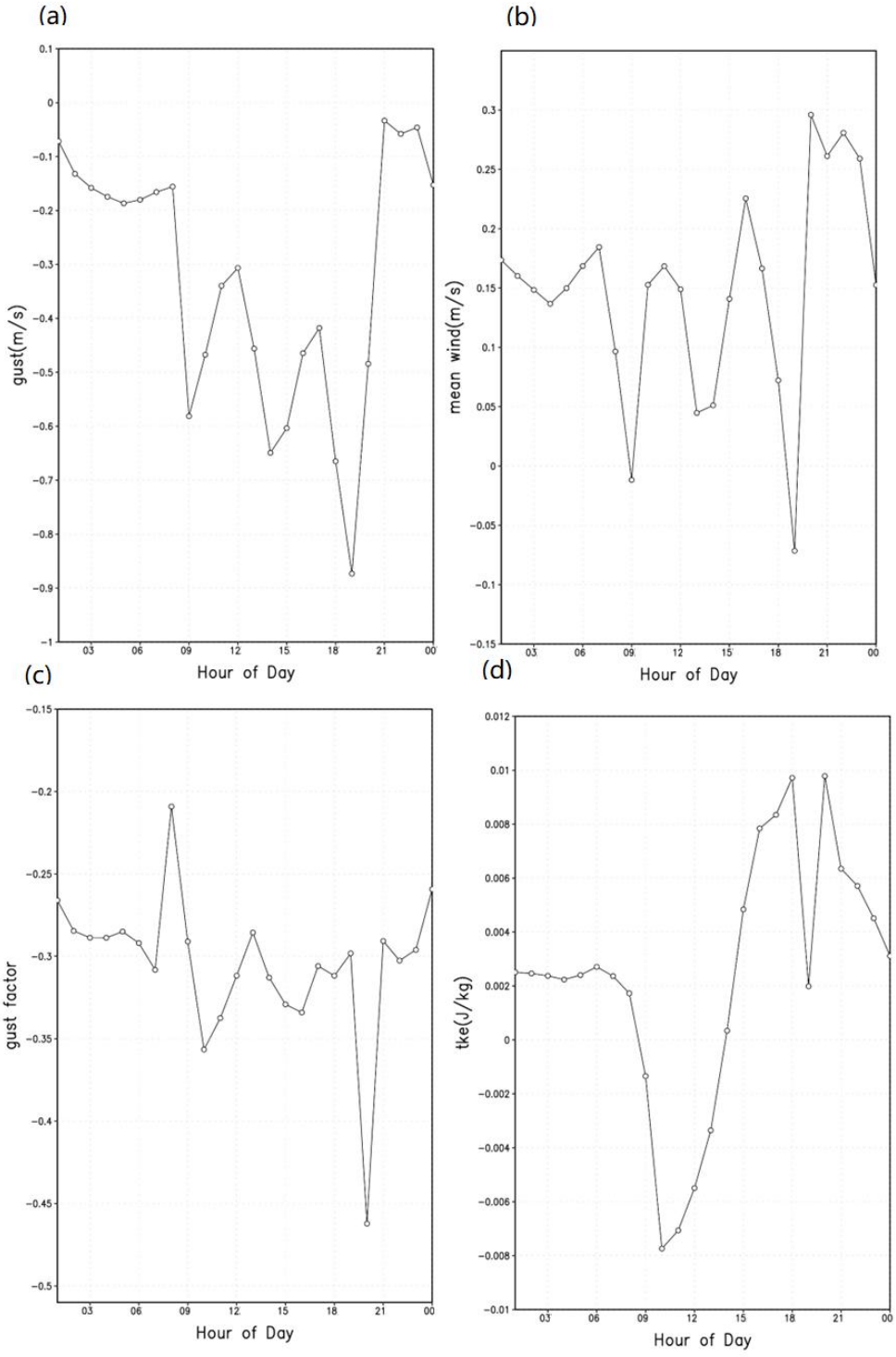

Figure 4.9 Hourly variations of the differences between the “No City” and “With City, No Buildings” scenarios("No City " − " With City, No Buildings ") for simulated gust wind speed (a), mean wind speed (b), gust factor (c), and turbulence kinetic energy (d) over Nanjing from August 5 to 13, 2018.

4.3.3 Impact of Integrated Urban Effects on Gust Characteristics

Based on the difference distribution results shown in Figures 4.10 and 4.11, this section compares the changes in gust wind speed, mean wind speed, gust factor, air temperature, surface temperature, relative humidity, and turbulence kinetic energy (TKE) between two scenarios—"with city" and "without city"—in the Nanjing region. The aim is to reveal, from a spatial perspective, the multifaceted regulatory effects of urban underlying surfaces on the local wind field and thermal environment.

The analysis of these integrated urban effects begins with their impact on the spatial distribution of gust wind speed. Figure 4.10(a) shows that when the city is removed, the gust wind speeds in the urban area are significantly lower compared to the "with city" scenario (by about -0.4 to -1.2 m/s), whereas a few peripheral or open areas exhibit slight positive differences (around 0 to +0.4 m/s). The negative differences in the city center indicate that the previously dense buildings and urban heat island effect have, to some extent, amplified instantaneous wind speeds; once the city is removed, the absence of building gaps and turbulence generation leads to a reduction in gust intensity.

Next, the influence of the complete urban environment on mean wind speed is examined across the study area. As shown in Figure 4.10(b), under the "without city" scenario, the mean wind speed in the central urban area shows a positive difference of about 0.9–1.5 m/s, while in the peripheral or relatively open areas, there are negative differences ranging from 0 to -0.3 m/s. This means that the influence of the urban underlying surface on the mean wind is not a simple "weakening" or "strengthening" but is coupled with local terrain, channeling effects, and the urban heat island circulation. The significant positive difference in the city center suggests that in the "with city" scenario, the dense building configuration or local heat island effect may have substantially impeded wind speeds; once the city is removed, the reduction or disappearance of such resistance leads to a more unobstructed near-surface wind field and a notable increase in mean wind speed. Conversely, the negative difference in the peripheral areas indicates that the original urban layout played a role in guiding or enhancing the wind field in these areas; when the city is removed, this effect disappears and wind speeds decrease.

The overall effect of the city on the gust factor is then investigated to understand changes in relative gust intensity. Figure 4.10(c) displays the hourly differences in the gust factor (the ratio

of gust wind speed to mean wind speed) under the “without city” scenario. It can be seen that in the city center, the differences are clearly negative, ranging roughly from -1.8 to -1, indicating that the presence of urban buildings, through local turbulence generation and channeling effects, significantly enhanced instantaneous wind speeds and thereby resulted in a higher gust factor under the “with city” scenario. In contrast, in the urban periphery and open areas, the differences are much smaller, only about -0.2, and in some areas even approach zero or show slightly positive values. This suggests that in these regions, the impact of urban buildings on the gust factor is weak, so that removing the city does not significantly change the ratio of instantaneous wind speed to mean wind speed in the wind field. Overall, the results of Figure 4.10(c) reflect the evident contribution of the city to enhancing gusts in the central area; when the city is removed, the gust factor in the center decreases markedly, while its influence in the periphery is much smaller, exhibiting a relatively smooth spatial and temporal distribution.

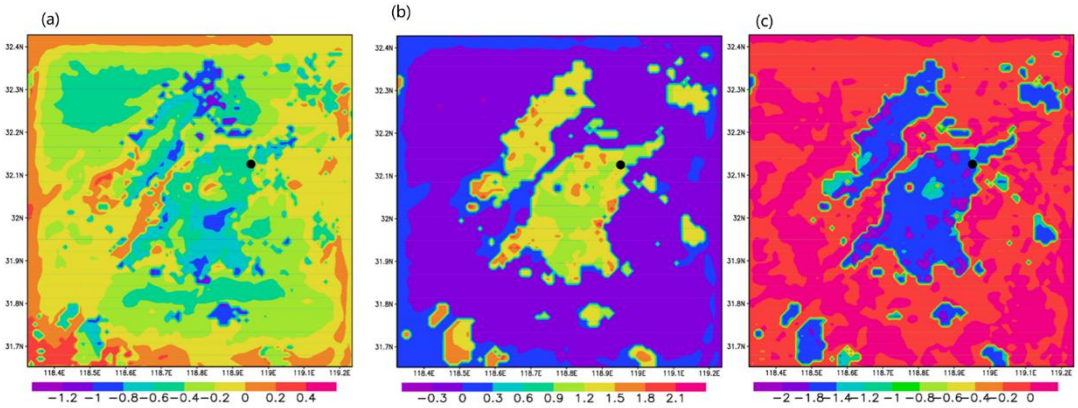

Figure 4.10 Spatial distribution characteristics of the differences in simulated meteorological elements in Nanjing between the "No urban" and "Urban" scenarios ("No urban" − "Urban") from August 5 to August 13, 2018: (a) gust wind speed (m/s); (b) mean wind speed (m/s); (c) gust factor

Turning to thermal characteristics, the integrated urban impact on air temperature is now detailed. Figure 4.11(a) shows that in the “without city” scenario, air temperatures in most urban areas decrease significantly compared to the “with city” scenario (by about -0.7 to -1.3 °C), while in a few peripheral areas the cooling is smaller (approximately -0.6 to -0.2 °C). In the “with city” scenario, the urban heat island effect causes the central area to accumulate heat; once the city is removed, the dense building structure and associated heat storage effects vanish, leading to a pronounced drop in air temperature, with less impact in the peripheral areas.

The study continues by assessing how the presence of the city influences surface temperatures. Figure 4.11(b) illustrates that, under the "without city" scenario, surface temperatures in the urban center decrease substantially, with reductions reaching 3–5 °C, whereas the effect in the outskirts or suburban areas is relatively minor. This spatial pattern is closely linked to the urban heat island effect: when the city is present, densely built areas are more prone to heat accumulation and insufficient nocturnal heat loss; without the city, the land surface becomes more natural, enabling rapid heat dissipation and a significant drop in surface temperature.

The integrated effect of the urban environment on near-surface relative humidity is subsequently explored. Figure 4.11(c) shows that the differences in relative humidity (RH) reveal a marked positive shift in the urban center and surrounding areas (about +3–+5%), indicating that RH generally increases after the city is removed; in peripheral regions, the differences are smaller (around +0.5–+2%). Under the "with city" condition, the urban heat island effect and the blockage imposed by tall buildings tend to lower RH; when urban structures are removed, the drop in temperature and the enhanced retention or convergence of moisture in the near-surface layer lead to a noticeable increase in RH, highlighting the city's suppressive effect on the moisture environment.

Finally, the overall urban impact on turbulence kinetic energy (TKE) is analyzed to gauge changes in turbulent activity. Figure 4.11(d) demonstrates that after removing the city, turbulence kinetic energy (TKE) generally decreases slightly across most areas (by about 0–0.03 J/kg), although a few central areas show a slight increase (0–0.03 J/kg). In the "with city" scenario, high building density and the urban heat island effect enhance local turbulence; when these are removed, the corresponding dynamic and thermal disturbances weaken, resulting in lower TKE, although in some central areas, a re-distribution of the wind field can cause a minor increase.

Based on the difference analysis in Figures 4.10 and 4.11, it can be seen that urban buildings and the urban heat island effect exert a dual regulatory influence on the local wind field and thermal environment. Under the "with city" scenario, buildings increase surface roughness and trigger local turbulence, leading to significantly higher gust wind speeds and gust factors in the urban center. At the same time, a pronounced heat island effect is generated, which raises both air and surface temperatures and suppresses relative humidity. Conversely, when the city is removed, the underlying surface becomes more natural; mean wind speeds increase in some areas, while

instantaneous wind speeds, gust factors, and turbulent activity generally decrease, resulting in a marked drop in both air and surface temperatures and an increase in relative humidity. This series of changes clearly demonstrates that urban structures play a pivotal role in shaping the complex, multi-scale urban wind field and thermal environment, offering important guidance for improving urban weather forecasts and optimizing the urban wind environment.

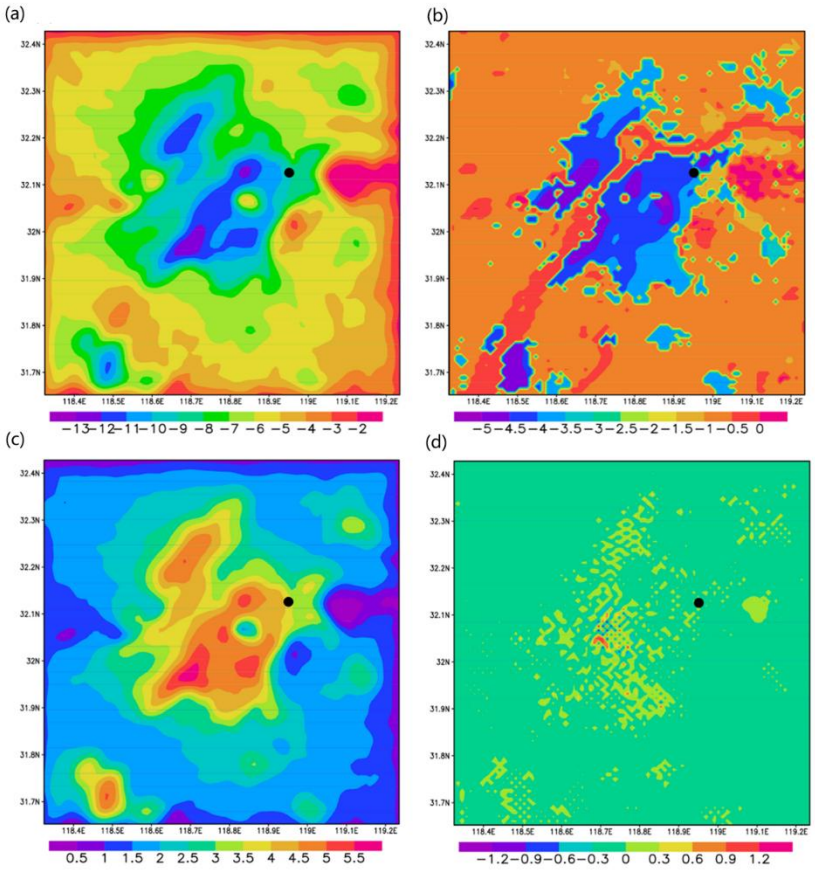

Figure 4.11 Spatial distribution characteristics of the differences in simulated meteorological elements in Nanjing between the "No urban" and "Urban" scenarios ("No urban" − "Urban") from August 5 to August 13, 2018: (a) air temperature (×10^{-1} ℃); (b) surface temperature (℃); (c) relative humidity (%); (d) turbulent kinetic energy (×10^{-1} J/kg)

Based on the difference results in Figures 4.12(a)–(d), a comparison of the hourly evolution of gust wind speed, mean wind speed, gust factor, and turbulence kinetic energy (TKE) under the “without city” and “with city” scenarios is conducted, with the aim of clarifying, on a temporal scale, the integrated influence of urban morphology on the local wind field and turbulence

processes.

Delving into these temporal impacts, the hourly differences observed in gust wind speed when considering the integrated urban effect are first analyzed. Figure 4.12(a) shows that the hourly differences in gust wind speed (calculated as “without city” minus “with city”) are mostly negative, with values reaching as low as -0.8 m/s, indicating that in the “without city” scenario the gusts are clearly lower than in the “with city” case; only duringnight periods do small positive differences (around +0.1 m/s) appear. Physically, urban buildings and the heat island effect during the day and early evening can enhance turbulence and mechanical shear, leading to a significant amplification of instantaneous wind speed; when the city is removed, although the overall roughness is reduced, the lack of building-induced turbulence generation causes gust levels to be lower for most hours. At night or in the early morning, when turbulent activity is weak, the differences between the two scenarios are relatively limited or briefly reverse.

The analysis then considers the diurnal pattern of changes in mean wind speed resulting from the overall urban presence. Figure 4.12(b) indicates that the hourly differences in mean wind speed between the “without city” and “with city” scenarios range roughly from -0.05 to +0.35 m/s. From midnight to early morning, the differences mostly remain around +0.1–0.2 m/s, occasionally approaching zero; during the afternoon to early evening the differences rapidly widen, reaching up to approximately +0.35 m/s, and then stabilize at night. This suggests that during the day and early evening, the suppressive effect of the urban surface on mean wind speed is more pronounced—when the city is removed, the reduced near-surface resistance allows wind to more easily reach the ground, resulting in a significantly higher mean wind speed compared to the “with city” scenario.

Subsequently, the hourly influence of the integrated urban environment on the gust factor is examined. Figure 4.12(c) displays the hourly differences in the gust factor (i.e., the ratio of gust wind speed to mean wind speed), which are mostly negative, ranging between -0.15 and -0.50. In other words, for most hours the gust factor in the “without city” scenario is clearly lower than in the “with city” case. Urban buildings and the heat island effect tend to enhance the increment of instantaneous wind speed relative to the mean (through channeling or turbulence amplification), thereby increasing the gust factor. When the city is removed, even if the mean wind speed increases during some periods, the absence of the building-induced “amplification” causes the

gust factor to decrease overall, indicating that urban morphology plays a significant role in supporting the relative amplification of instantaneous wind speed compared to the mean.

Finally, the temporal variations in turbulence kinetic energy (TKE) due to the combined effects of the city are explored. Figure 4.12(d) shows that the hourly differences in TKE between the "without city" and "with city" scenarios mostly range between -0.018 and +0.006 m^2/s^2. From early morning to afternoon, the differences are significantly negative—reaching a minimum of about -0.015 m^2/s^2—indicating that the "with city" scenario enhances turbulent intensity during the day. In the early evening and night, the differences may briefly turn positive, suggesting that in the absence of the city, wind field redistribution or a greater background momentum transfer might slightly increase TKE. Overall, the high surface roughness and heat island effect associated with urban buildings significantly enhance daytime turbulence; when the city is removed, the TKE levels generally decrease, although in some central areas they may increase slightly due to changes in the wind field.

In summary, the results in Figures 4.12(a)–(d) indicate that, on a diurnal scale, the "without city" versus "with city" differences are consistent with the previous spatial analysis. Due to the turbulence generated by urban morphology, gust wind speeds during the day and early evening are higher in the "with city" scenario, resulting in significant negative differences when the city is removed. In contrast, mean wind speeds show positive differences, as they are significantly higher without the urban blockage. The gust factor is mostly lower in the "without city" scenario, demonstrating the important role of urban form in enhancing the relative magnitude of instantaneous wind fluctuations. Additionally, TKE is increased during the day by the presence of the city and decreases when the city is removed, although slight reversals may occur at night. These sensitivity experiment results further demonstrate that urban buildings and the heat island effect exert multiple influences at different times of day: they can both enhance daytime turbulence and gusts while under certain conditions suppress overall wind speeds. When the city is removed, the underlying surface becomes flatter and free of the heat island effect, leading to a significant increase in mean wind speed, but with reduced peaks in gusts and turbulent activity.

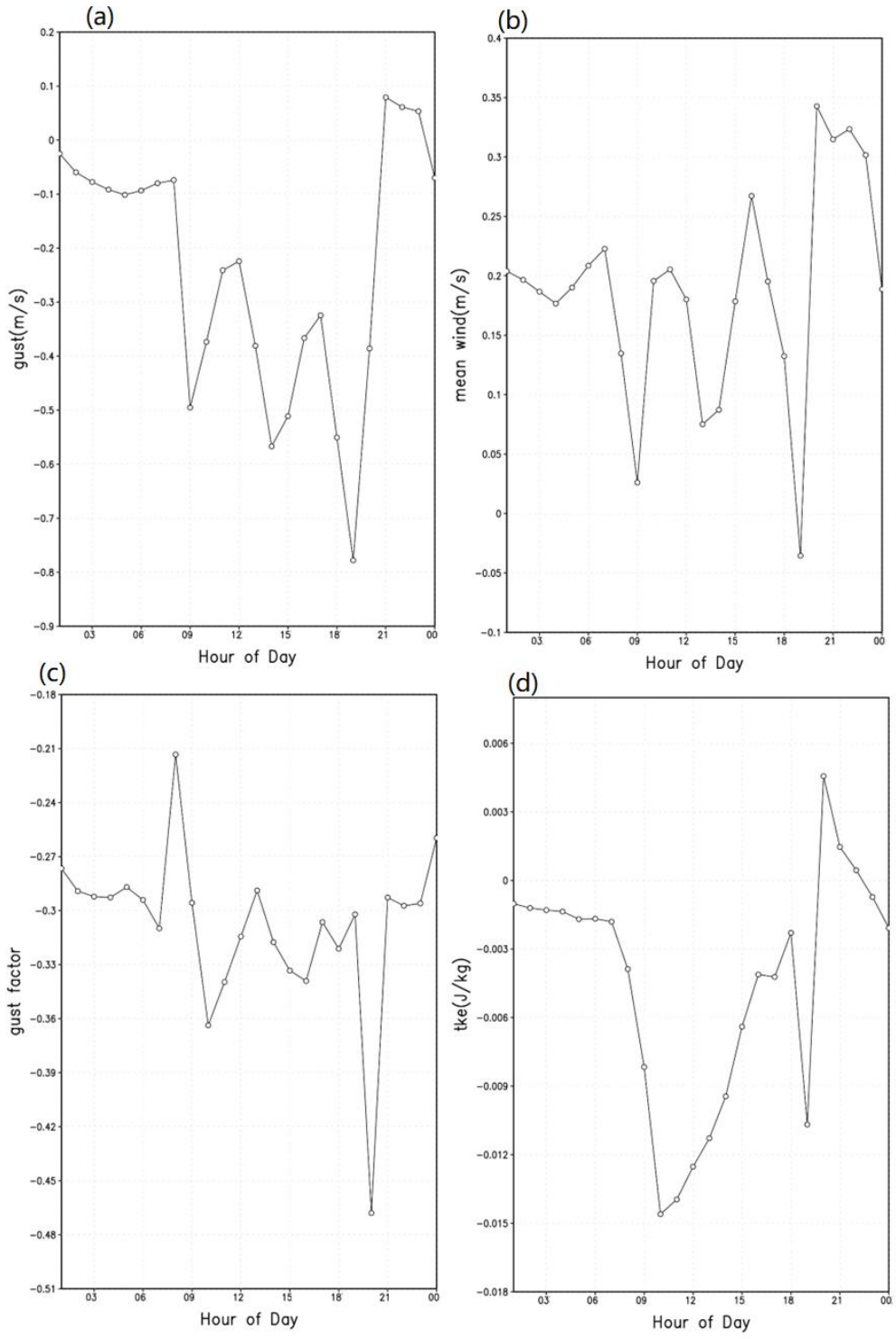

Figure 4.12 Hourly variation of the differences between the "No urban" and "Urban" scenarios ("No urban" − "Urban") for simulated gust wind speed (a), mean wind speed (b), gust factor (c), and turbulent kinetic energy (d) in the Nanjing region from August 5 to August 13, 2018

5 Conclusion and Outlook

5.1 Conclusions

In this study, ultrasonic data from the tower at the Nanjing University Station for Observing Regional Processes of the Earth System (SORPES) were analyzed to examine the statistical characteristics of urban gusts. Moreover, the RBLM model coupled with a gust module was employed to investigate the impacts of urban dynamic effects, thermodynamic effects, and overall urban effects on gusts. The main conclusions are as follows:

(1) Near-Surface Gust Characteristics: In winter, due to the combined effects of dense urban buildings and cold air invasions, the average wind speed, gust wind speed, amplitude, gust factor, and duration are all higher than in summer, with pronounced tail effects in extreme events. At a height of 3 m, the winter average wind speed is about 0.5 m/s higher than in summer, and the probability of wind speeds exceeding 2 m/s is significantly higher in winter. The average gust wind speed in winter is approximately 0.87 m/s higher than in summer (around 3.65 m/s in winter versus 2.78 m/s in summer), and there are more extreme events with gust wind speeds over 10 m/s in winter. Among the near-surface extreme events in winter, a relatively high proportion have amplitudes greater than 7.5 m/s, indicating stronger gust variability in winter. The gust factor (GF) at 3 m is mainly concentrated between 1.5 and 2.5, but in winter, about 20% of near-surface gusts have a GF exceeding 2.5 with a pronounced tail effect, suggesting that near-surface gust intensities often reach 2–3 times or even higher than the average wind speed; additionally, the winter GF at 3 m is about 0.37 higher than in summer. Most peak factors at 3 m are distributed between 2 and 4; however, in summer, approximately 20% of near-surface events have peak factors exceeding 4—significantly higher than in winter—reflecting that the intensity of extreme instantaneous gusts is stronger in summer. Moreover, winter gust durations are about 6–7 seconds longer than in summer, with approximately 5% of 3 m events in winter lasting over 100 seconds compared to less than 5% in summer, indicating longer gust durations in winter. The average spatial scale of gusts at 3 m in winter is about 32.46 m larger than in summer, and the winter distribution exhibits a longer tail, indicating stronger heterogeneity.

(2) Middle and Upper-Level Gust Characteristics: At higher levels in summer, both the average wind speed and extreme gust wind speed are higher, while the gust factor is relatively lower; however, the spatial scale and duration of gusts are significantly increased, indicating a

notable influence of large-scale circulation and local thermal convection on high-level gusts. In summer, the cumulative wind speed distribution shifts to the right, and the probability of wind speeds exceeding 8 m/s is over 10% higher than in winter, showing that high-level wind speeds are stronger and more strongly controlled by the large-scale wind field. At 25 m and 50 m, summer gust wind speeds are about 1 m/s higher than in winter, and the probability of gust wind speeds exceeding 10 m/s at higher levels is significantly increased, indicating that extreme gusts are more likely at higher altitudes. At 25 m, the proportion of events with amplitudes over 5 m/s is noticeably higher than at 50 m, reflecting more pronounced wind speed fluctuations in the mid-levels. In both 25 m and 50 m layers, the GF is mainly concentrated between 1.2 and 2.0, with less than 10% of events exceeding 2.0, indicating a smaller relative increase in gusts over the average wind speed at higher levels. Peak factors at these levels are concentrated between 1.5 and 4.0, with a weaker tail effect, suggesting that the intensity of extreme instantaneous gusts is relatively stable. In summer, the average gust time scales at 25 m and 50 m are approximately 68 seconds and 73 seconds, respectively, and both the rise and decay durations increase with height, reflecting that high-level gusts are more persistently affected by large-scale momentum exchange and thermal convection. Moreover, the average spatial scale of gusts in summer at these heights is roughly 80 m larger than in winter, with more than 20% of mid-to-high-level gust events in summer having spatial scales exceeding 500 m, compared to only about 10% in winter, indicating a more pronounced spatial expansion of high-level gusts under the influence of large-scale circulation in summer.

(3) Diurnal Variations of the Gust Factor: Analysis of the diurnal variation in Nanjing shows that the near-surface layer is most affected by the urban underlying surface, with the gust factor being significantly higher than at middle and upper levels. In winter, the near-surface gust factor reaches a high value of around 2.5 between 11:00 and 16:00, whereas in summer, it increases significantly during the morning and evening peak hours (approximately 5:00–7:00 and around 18:00). At higher levels, the gust factor remains relatively stable but is consistently higher during the daytime than at night, indicating that the enhanced average wind speeds during the day result in a relatively lower ratio of gust wind speed to average wind speed, and that the more active daytime boundary layer at middle and upper levels increases the gust factor by about 0.1–0.2.

(4) Scatter Plot Fitting Analysis: Scatter plot fitting reveals that, within the same season, the

correlation between near-surface and middle/upper-level gusts is relatively low, while the correlation between middle and upper levels is high. In summer, the synchronization of gust amplitudes across different heights is strong, with a clear linear relationship (R^2 mostly above 0.8); in winter, there is greater uncertainty (R^2 = 0.58–0.85), though the higher levels still maintain a certain baseline gust speed. This suggests that the variation of urban gusts with height in Nanjing is jointly influenced by seasonal large-scale circulation, local turbulence, and surface roughness.

(5) Correlation Analysis of Gust Parameters: The analysis shows that surface shear (represented by friction velocity and turbulent stress) is consistently a key factor driving urban gusts, with correlation coefficients as high as approximately 0.66–0.85, and the correlations are higher near the surface than at middle and upper levels. In winter, gusts are closely related to turbulence intensity (with correlations up to 0.43 near the surface). In summer, gusts are more influenced by the large-scale wind field and local convective processes, with air pressure exhibiting a pronounced negative correlation—reaching around -0.6 at middle and upper levels—reflecting seasonal differences in the dynamical, shear, and thermal processes in gust formation.

(6) Urban Building Dynamics: The dynamic effects of urban buildings significantly influence gust characteristics. When buildings are removed, gust wind speeds in the urban center increase by 0.2–1.0 m/s, and average wind speeds increase by 0.35–0.4 m/s—substantially greater than in suburban areas—indicating that urban clusters have a notable suppressive effect on wind speeds. Additionally, the gust factor in the urban center decreases (by as much as 0–0.18), with slight increases (0–0.03) in some peripheral areas. Turbulence intensity in the urban center decreases, and the urban heat island effect weakens, with air and surface temperatures decreasing by 0.06–0.12℃, demonstrating the complex regulatory effects of buildings on gust fluctuations and the thermal environment.

(7) Urban thermodynamic effects exert a pronounced influence on gust characteristics. In this study, we isolated these effects by subtracting the “With City, No Buildings” scenario from the “No City” scenario, thereby revealing their impact on gusts and related meteorological variables over Nanjing. Without the thermodynamic influence, gust speeds in the city core decrease by 0.8–1.6 m/s, mean wind speeds increase by 0.9–1.8 m/s, and gust factors decline by 0.9–1.8. Concurrently, surface temperature and near-surface air temperature in the core fall by 3.5–5.0 °C and 0.8–1.2 °C, respectively, while relative humidity rises by 3–5.5 %. Turbulence kinetic energy,

however, locally increases by 0.03–0.15 J/kg in the urban center. All of these enhancements or suppressions diminish with distance from the city center, approaching zero in suburban or open areas.

(8) Removal of the Entire Urban Area: When the urban area is completely removed, the widespread gust wind speeds in the urban area significantly decrease by 0.4–1.2 m/s, while a few peripheral or open areas exhibit a slight positive change (0 to 0.4 m/s). However, the average wind speed increases significantly by about 0.9–1.5 m/s. Meanwhile, the gust factor notably decreases—dropping by approximately 1.8 to 1 in the city center—and turbulence intensity also decreases markedly, indicating that existing urban buildings significantly enhance instantaneous wind speeds through local turbulence excitation and channeling effects. In the urban area, air and surface temperatures decrease significantly, relative humidity increases markedly, and turbulence intensity decreases, demonstrating that urban areas play a central role in regulating local wind field structures and the thermal environment.

(9) The urban thermodynamic enhancement of gusts outweighs the dynamical suppression.

5.2 Innovations of This Study

The innovations of this study are mainly reflected in two aspects:

(1) Ultrasonic observational data were used to analyze the gust characteristics of Nanjing, revealing clear seasonal variations and changes with height in urban gust behavior. Correlation analysis further indicated that friction velocity and turbulent stress are the primary driving factors of urban gusts.

(2) An urban boundary layer model (RBLM) with an integrated gust module was developed and used to investigate the influence of urban features on gusts, examining both dynamic and thermodynamic effects. The findings show that building dynamic effects suppress both gust and mean wind speeds while increasing the gust factor, whereas thermodynamic effects enhance gust wind speeds. Furthermore, the urban thermodynamic effects are greater than the dynamic effects.

5.3 Outlook

This study has achieved certain results in revealing the characteristics of urban gusts in the Nanjing area and their influencing factors; however, several issues merit further investigation:

(1) The available observational data on urban gusts remains relatively limited. Future efforts should further strengthen long-term and systematic observations in different urban areas to improve the statistical analysis of the spatiotemporal characteristics of gusts. The current study only focused on a summer case for gust simulation, which has certain limitations. Future work could include additional studies on winter cases.

(2) The model used in this study has certain limitations in depicting the fine-scale urban structure. In the future, the development of high-resolution numerical simulation methods is recommended to more accurately describe the influence of complex urban structures on gusts. The mechanisms by which gusts affect pollutant dispersion are not yet fully understood. Future research could further conduct high-resolution simulations incorporating chemical processes to deeply analyze the chemical and physical response mechanisms of different types of pollutants under the influence of gusts.

References

Ao, X., Yue, C., Yang, X., Deng, L., & Huang, W. (2022). Urbanization effects on rainfall processes induced by land falling Typhoon Lekima (2019) over the Shanghai metropolitan area. Journal of Hydrometeorology, 23, 1075–1093.

Ashcroft, J. (1994). The relationship between the gust ratio, terrain roughness, gust duration and the hourly mean wind speed. Journal of Wind Engineering and Industrial Aerodynamics, 53, 331–355.

Barthelmie, R. J., Doubrawa, P., Wang, H., Giroux, G., & Pryor, S. C. (2016). Effects of an escarpment on flow parameters of relevance to wind turbines. Wind Energy, 19, 2271–2286.

Beljaars, A. C. M. (1987). The influence of sampling and filtering on measured wind gusts. Journal of Atmospheric and Oceanic Technology, 4, 613–626.

Berg, J., Mann, J., Bechmann, A., Courtney, M., & Jørgensen, H. E. (2011). The Bolund Experiment, Part I: Flow over a steep, three-dimensional hill. Boundary-Layer Meteorology, 141, 219–243.

Blocken, B., Janssen, W. D., & van Hooff, T. (2012). CFD simulation for pedestrian wind comfort and wind safety in urban areas: General decision framework and case study. Journal of Wind Engineering and Industrial Aerodynamics, 104–106, 377–388.

Born, K., Ludwig, P., & Pinto, J. G. (2012). Wind gust estimation for Mid-European winter storms: Towards a probabilistic view. Tellus A, 64, 17471. https://doi.org/10.3402/tellusa.v64i0.17471

Bradbury, W., Deaves, D., Hunt, J., Kershaw, R., Nakamura, K., Hardman, M., & Bearman, P. (1994). The importance of convective gusts. Meteorological Applications, 1, 365–378.

Brasseur, O. (2001). Development and application of a physical approach to estimating wind gusts. Monthly Weather Review, 129, 5–25.

Butler, B. W., Wagenbrenner, N. S., Forthofer, J. M., et al. (2015). High-resolution observations of the near-surface wind field over an isolated mountain and in a steep river canyon. Atmospheric Chemistry and Physics, 15, 3785–3801.

Chen, Y., Jiang, W. M., Zhang, N., He, X. F., & Zhou, R. W. (2009). Numerical simulation of the anthropogenic heat effect on urban boundary layer structure. Theoretical and Applied Climatology, 97, 123–134.

Clifton, A., Daniels, M., & Lehning, M. (2014). Effect of winds in a mountain pass on turbine performance. Wind Energy, 17, 1543–1562.

Durran, D. R. (1990). Mountain waves and downslope winds. In Atmospheric Processes over Complex Terrain (pp. 59–81). Boston, MA: American Meteorological Society.

ECMWF. (2021). IFS Documentation CY47R3—Part IV: Physical Processes. European Center for Medium-Range Weather Forecasts. https://doi.org/10.21957/eyrpir4vj

Earl, N., Dorling, S., Starks, M., & Finch, R. (2017). Subsynoptic-scale features associated with extreme surface gusts in UK extratropical cyclone events. Geophysical Research Letters, 44, 3932–3940.

Grubišić, V., Doyle, J. D., Kuettner, J., Dirks, R., Cohn, S. A., … & Czyzyk, S. (2008). The Terrain-Induced Rotor Experiment: A field campaign overview including observational highlights. Bulletin of the American Meteorological Society, 89, 1513–1533.

Gutierrez, A., & Fovell, R. G. (2018). A new gust parameterization for weather prediction models. Journal of Wind Engineering and Industrial Aerodynamics, 177, 45–59.

Hasager, C. B., Nielsen, N. W., Jensen, N. O., Boegh, E., Christensen, J. H., … & Soegaard, H. (2003). Effective roughness calculated from satellite-derived land cover maps and hedge information used in a weather forecasting model. Boundary-Layer Meteorology, 109, 227–254.

Hirose, C., Nomichi, T., & Ikegaya, N. (2022). Distributions of gust and peak factors at a pedestrian level in a simplified urban canopy obtained by particle image velocimetry. Building and Environment, 222, 109350.

Hertenstein, R. F., & Kuettner, J. P. (2005). Rotor types associated with steep lee topography: Influence of the wind profile. Tellus A, 57, 117–135.

He XF, Jiang WM, Chen Y, et al. Numerical simulation of the impacts of anthropogenic heat on the structure of the urban boundary layer. Chinese J. Geophys. (in Chinese), 2007, 50(1): 74～82

He Xiaofeng, Jiang Weimei, Zhou Rongwei. 2009. Development of a single-layer urban canopy model and numerical experiments [J]. Chinese Journal of Atmospheric Sciences (in Chinese), 33 (5): 981 - 993.

Hu, W., Letson, F., Barthelmie, R. J., & Pryor, S. C. (2018). Wind gust characterization at wind

turbine relevant heights in moderately complex terrain. Journal of Applied Meteorology and Climatology, 57, 1459–1476.

Jubayer, C. M., & Hangan, H. (2018). A hybrid approach for evaluating wind flow over a complex terrain. Journal of Wind Engineering and Industrial Aerodynamics, 175, 65–76.

Kawamura, S., Kimoto, E., Fukushima, T., & Taniike, Y. (1988). Environmental wind characteristics around the base of a tall building—a comparison between model test and full scale experiment. Journal of Wind Engineering and Industrial Aerodynamics, 28, 149–168.

Kanda, M., Inagaki, A., Miyamoto, T., Gryschka, M., & Raasch, S. (2013). A new aerodynamic parametrization for real urban surfaces. Boundary-Layer Meteorology, 148(2), 357–377.

Kurbatova, M., Rubinstein, K., Gubenko, I., & Kurbatov, G. (2018). Comparison of seven wind gust parameterizations over the European part of Russia. Advances in Science Research, 15, 251–255.

Liao, J. B., Wang, T. J., Jiang, Z. Q., Zhuang, B. L., Xie, M., Yin, C. Q., Wang, X. M., Zhu, J. L., Fu, Y., & Zhang, Y. (2015). WRF/Chem modeling of the impacts of urban expansion on regional climate and air pollutants in the Yangtze River Delta, China. Atmospheric Environment, 106, 204–214.

Li, W., Mak, C. M., Cai, C., Fu, Y., … & Niu, J. (2024). Wind tunnel measurement of pedestrian-level gust wind flow and comfort around irregular lift-up buildings within simplified urban arrays. Building and Environment, 256, 111487.

Lin, C.-Y., Chen, F., Huang, J.-C., Chen, W.-C., Liou, Y.-A., Chen, W.-N., & Liu, S.-C. (2008). Urban heat island effect and its impact on boundary layer development and land–sea circulation over northern Taiwan. Atmospheric Environment, 42, 5635–5649.

Liu, G., Wang, X., Wu, Q., Fang, D., Wu, Z., Liu, H., & Lyu, M. (2023). Effect of urbanization on gust wind speed in summer over an urban area in Eastern China. Environmental Research Letters, 18, 074025.

Liu, J., Niu, J., Mak, C. M., & Xia, Q. (2017). Detached eddy simulation of pedestrian-level wind and gust around an elevated building. Building and Environment, 125, 168–179.

Markowski, P. M., & Dotzek, N. (2011). A numerical study of the effects of orography on supercells. Atmospheric Research, 100, 457–478.

Murakami, S., Uehara, K., & Komine, H. (1979). Amplification of wind speed at ground level due

to construction of high-rise building in urban area. Journal of Wind Engineering and Industrial Aerodynamics, 4, 357–370.

Nakamura, K., Kershaw, R., & Gait, N. (1996). Prediction of near-surface gusts generated by deep convection. Meteorological Applications, 3, 157–167.

Oke, T. R. (1982). The energetic basis of the urban heat island. Quarterly Journal of the Royal Meteorological Society, 108, 1–24.

Onol, A. O., & Yesilyurt, S. (2017). Effects of wind gusts on a vertical axis wind turbine with high solidity. Journal of Wind Engineering and Industrial Aerodynamics, 162, 1–11.

Rakib, M. I., Evans, S. P., & Clausen, P. D. (2020). Measured gust events in the urban environment: A comparison with the IEC standard. Renewable Energy, 146, 1134–1142.

Rucker, M., Banta, R. M., & Steyn, D. G. (2008). Along-valley structure of daytime thermally driven flows in the Wipp Valley. Journal of Applied Meteorology and Climatology, 47, 733–751.

Roth, M. (2000). Review of atmospheric turbulence over cities. Quarterly Journal of the Royal Meteorological Society, 126, 941–990.

Ryu, Y.-H., Baik, J.-J., & Lee, S.-H. (2013). Effects of anthropogenic heat on ozone air quality in a megacity. Atmospheric Environment, 80, 20–30.

Schreur, B. W., & Geertsema, G. (2008). Theory for a TKE based parameterization of wind gusts. HIRLAM Newsletter, 54, 177–188.

Shi, Y., Zeng, Q. C., Liu, L., Cheng, X. L., & Hu, F. (2022). Important role of turbulent wind gust and its coherent structure in the rapid removal of urban air pollution. Environmental Research Communications, 4, 075001. https://doi.org/10.1088/2515-7620/ac7c5f

Sheridan, P. (2011). Review of techniques and research for gust forecasting parameterization (Forecasting Research Technical Report No. 570). UK Met Office, Exeter.

Sheridan, P. (2018). Current gust forecasting techniques, developments and challenges. Advances in Science Research, 15, 159–172.

Solari, G. (2014). Emerging issues and new frameworks for wind loading on structures in mixed climates. Wind and Structures, 19, 295–320.

Suomi, I., Vihma, T., Gryning, S.-E., & Fortelius, C. (2013). Wind-gust parametrizations at heights relevant for wind energy. Quarterly Journal of the Royal Meteorological Society, 139(675),

1298–1310.

Suomi, I., & Vihma, T. (2018). Wind gust measurement techniques – from traditional anemometry to new possibilities. Sensors, 18(4), 1300.

Suomi, I. (2017). Wind gusts in the atmospheric boundary layer [Doctoral dissertation, University of Helsinki]. http://hdl.handle.net/10138/215229

Tao, W., Liu, J., Ban-Weiss, G. A., Zhang, L., Zhang, J., Yi, K., & Tao, S. (2017). Potential impacts of urban land expansion on Asian airborne pollutant outflows. Journal of Geophysical Research: Atmospheres, 122, 7646–7663.

Toja-Silva, F., Peralta, C., Lopez-Garcia, O., Navarro, J., & Cruz, I. (2015). Roof region dependent wind potential assessment with different RANS turbulence models. Journal of Wind Engineering and Industrial Aerodynamics, 142, 258–271.

Wagenbrenner, N. S., Forthofer, J. M., Lamb, B. K., Shannon, K. S., & Butler, B. W. (2016). Downscaling surface wind predictions from numerical weather prediction models in complex terrain with WindNinja. Atmospheric Chemistry and Physics, 16, 5229–5241.

Wang, X. Y., Miao, S., Liu, H., Sun, J., Zhang, N., & Zou, J. (2019). Assessing the impact of urban hydrological processes on the summertime urban climate in Nanjing using the WRF model. Journal of Geophysical Research: Atmospheres, 124, 12683–12707.

Wang, X. M., Liao, J., Zhang, J., Shen, C., Chen, W., Xia, B., & Wang, T. (2014). A numeric study of regional climate change induced by urban expansion in the Pearl River Delta, China. Journal of Applied Meteorology and Climatology, 53, 346–362.

World Meteorological Organization. (2014). Guide to Meteorological Instruments and Methods of Observations (8th ed.). Geneva, Switzerland: World Meteorological Organization.

Wieringa, J. (1973). Gust factors over open water and built-up country. Boundary-Layer Meteorology, 3, 424–441.

Wieringa, J. (1992). Updating the Davenport roughness classification. Journal of Wind Engineering and Industrial Aerodynamics, 41, 357–368.

Xu Min, Jiang Weimei, Ji Chongping, et al. 2002. Numerical modeling and verification of structures of the boundary layer over Beijing area [J]. Journal of Applied Meteorological Science (in Chinese), 13(S1): 61-68.

Yan Zijing, Liu Hongnian. 2024. Study on the meteorological and environmental effects of Lake

Taihu based on the urban boundary layer model coupling lake model [J]. Journal of the Meteorological Sciences (in Chinese), 44(1): 176-188.

Yang, J., Liu, H., & Sun, J. (2018). Evaluation and application of an online coupled modeling system to assess the interaction between urban vegetation and air quality. Aerosol and Air Quality Research, 18, 693–710.

Yang, J., Liu, H., Sun, J., Zhu, Y., Wang, X., Xiong, Z., & Jiang, W. (2015). Further development of the regional boundary layer model to study the impacts of greenery on the urban thermal environment. Journal of Applied Meteorology and Climatology, 54, 137–152.

Zhao, W., Zhang, N., Sun, J., & Zou, J. (2013). Evaluation and parameter sensitivity study of a single-layer urban canopy model with measurements in Nanjing, China. Journal of Hydrometeorology, 15, 1078–1090.

Zhang, W., Villarini, G., Vecchi, G. A., & Smith, J. A. (2018). Urbanization exacerbated the rainfall and flooding caused by Hurricane Harvey in Houston. Nature, 563, 384–388.

Acknowledgements

As the years have passed, I have increasingly felt how swiftly time flies. It always seems as though I had just begun my journey at Nanjing University, yet now my master's studies are drawing to a close.

First and foremost, I must thank my advisor, Professor Liu Hongnian, for his invaluable guidance throughout my two years of study. When I first entered the program, my abilities were rather limited, and Professor Liu set up a learning plan tailored for me. As my studies progressed, his meticulous guidance—whether it was about operating and modifying models or writing code—proved to be both patient and indispensable. Through both my academic work and daily life, I have learned many valuable lessons from him. I consider myself extremely fortunate to be his student, and I sincerely wish him good health and a happy family.

I would also like to express my gratitude to every member of our research group, whose precious suggestions and advice have greatly contributed to my work. I am thankful for every senior and fellow in the group for their constant support and assistance. My thanks also go to the administrative staff and all the lecturers at the college, as well as every classmate who has helped me along the way. I am deeply grateful to all the friends who have cared for and accompanied me. I also thank Nanjing University.

In addition, I must thank my girlfriend, whose care and encouragement have been invaluable to me. Her excellence continually inspires me, and her companionship fills my life with happiness and joy.

Finally, I am forever grateful to my parents for their selfless support throughout my life. Their unwavering support has enabled me to overcome many challenges in my academic journey, and they will always be my strongest pillar.